Synthesis, Characterization and Properties of Electrochemically Active Dendrimers

Joseph Chung-Yin Lam

林仲賢

A Thesis Submitted in Partial Fulfilment of the Requirements for the Degree of Master of Philosophy

In

Chemistry

October 2000


香港中文大學
圖書館系統
28 JUN 2001
UNIVERSITY
LIBRARY SYSTEM
THE CHINESE UNIVERSITY OF HONG KONG

Contents

	Pages
Contents	i
Acknowledgements	ii
Abstract	iii
Abbreviations	v
Chapter I. Introduction	
(1) General background of dendrimers	1
(2) Electrochemically active dendrimers	2
(3) Electrochemically active dendrimers as models for studying the redox behaviour of complex proteins	11
Chapter II. Synthesis and Characterization	
(1) Structure of the electrochemically active dendrimers	16
(2) Retrosynthetic analysis	17
(3) Synthesis	18
(4) Structural Characterization	26
(5) Conclusion	33
Chapter III. Physical and Electrochemical Properties	
(1) Physical appearance and solubility properties	34
(2) Cyclic voltammetry studies	34
Chapter IV. Summary	40
Chapter V. Experimental	41
References	62
Spectra	65

Acknowledgements

I would like to express my sincere thanks to my supervisor, Prof. H. F. Chow, for his invaluable advice and patient guidance during the course of my research and the preparation of this thesis. Thanks are also given to Prof. H. K. Lee for his advice and technical assistance in performing cyclic voltammetric studies, and Mr. K. W. Kwong for recording mass spectra.

I would like to give thank to graduates and research assistants in Labs. 257C and 258 for their assistance, helpful discussion and encouragement throughout the past two years. Special thanks are given to Dr. Chi-Wai Wan for his guidance and training in experimental technique.

June, 2000

Joseph Chung-Yin Lam

Department of Chemistry

The Chinese University of Hong Kong

Abstract

Metallodendrimers with a metal ion holding two dendritic subunits together were synthesized. The dendritic subunit is a polyether-based dendrimer with a 2,2':6', 2"-terpyridine core serving as a tridentate coordinating ligand. These target molecules were prepared by an accelerated approach of convergent scheme in which the growth was propagated from the surface to the core. Dendritic ligands of the zeroth to second generations were synthesized and they were coordinated to an iron(II) ion to form bis-complexes of various generations.

All these dendritic ligands and the electrochemically active dendrimers were characterized by ^{1}H, ^{13}C NMR, mass spectrometry and elemental analysis. The dendrimers synthesized prepared were used to investigate the effect of electron relays on the redox behaviour of metallodendrimers.

摘要

我們合成了由金屬離子將兩個樹形單元結合在一起的一類具有電化學活性的樹形分子。樹形單元是具有三配位 2,2':6,2"-三聯吡啶核的聚醚類樹形分子，這些分子是利用由表及裡的收斂法製備的。我們合成了以零代到二代的樹形配體，它們與二價鐵離子配位形成了相應的雙復合體。

所有這些樹形配體以及具有電化學活性的樹形分子都經 ^{1}H NMR, ^{13}C NMR, 質譜以及元素分析加以表徵。而且，這些具有電化學活性的樹形分子被用來研究電子弛豫對於金屬樹形分子氧化還原行爲的影響。

Abbreviations

18-C-6	18-crown-6	M	mole per liter
Anal.	Analytically	Me	methyl
Ar	aromatic	MHz	megahertz
Bn	benzyl	min	minute(s)
br	broad (NMR)	mM	millimoles per liter
b.p.	boiling point	mmol	millimole(s)
^{t}Bu	*tert*-butyl	mol	mole(s)
°C	degree Celsius	m.p.	melting point
d	doublet (NMR)	M.S.	mass spectrometry
DMSO	dimethylsulfoxide	*m/z*	mass to charge ratio
EI	electron impact	NMR	nuclear magnetic
equiv.	Equivalent		resonance
EtOAc	ethyl acetate	ppm	parts per million
Et_2O	diethyl ether	q	quartet (NMR)
FAB	fast atom bombardment	quin	quintet (NMR)
g	gram(s)	s	singlet (NMR)
h	hour(s)	t	triplet (NMR)
Hz	hertz	TBAT	tetrabutylammonium
J	coupling constant (NMR)		tetrafluoroborate
L-SIMS	liquid secondary ion	terpy	2,2':6',2"-terpyridine
	mass spectroscopy	THF	tetrahydrofuran
m	multiplet (NMR)	TMS	tetramethylsilane

Chapter I. Introduction

1. General background of dendrimers

Dendrimer, in contrast to linear polymer, has a highly branched fractal-like structure typified by multiple of untangled chain-ends and surface functional groups with similar microenvironment (Figure 1).[1] More importantly, the structural-property relationship of dendrimers can be rationalized accurately because of their structural homogeneity and regularity. Because of their relatively large molecular size and topology, the chemical and physical properties of dendrimers are usually different from those of small molecules even though the same functional groups are present.

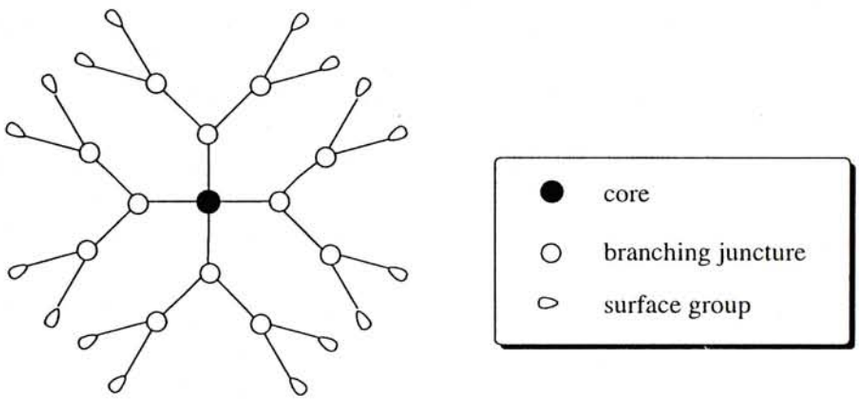

Figure 1. The schematic structure of a dendrimer.

Recently, research direction focus on dendrimer chemistry has switched to the exploration of the practical usefulness of functional dendritic molecules.[2] Therefore, functionalization of dendrimers has taken preference over the simplified version of synthesizing large dendrimers for their own sake. Today, dendritic molecules containing discrete functional groups can be prepared by careful planning of the synthetic route, and the potential applications of functional dendrimers have been found not only in the material industries, but also in various medical and pharmaceutical areas.

This thesis is concerned with the study of the various factors that affect the electrochemical properties of dendrimers. In the following sections, we will begin with a review on some of the electrochemically active dendrimers. In the subsequent section,

we define the objectives of our research. Chapter 2 reports the detail of our research strategy and the experimental findings of our work.

2. Electrochemically active dendrimers

The term "electrochemically active dendrimers" is used to describe dendritic molecules that contain one or more redox centers and therefore exhibit some kind of activity under oxidative or reductive conditions.[3] Amongst the various electrochemically active dendrimers, they can be arbitrarily divided into three groups (Figure 2): (i) those where the redox center(s) is situated at the surface of the dendritic sector; (ii) those where the redox center(s) is located in the interior of the dendrimer, *i.e.*, the redox center is buried within the dendritic envelop; and (iii) those having more than one kind of electrochemically redox centers. Since it is impossible to provide a detail account of the various electrochemically active dendrimers here, we will focus our attention on two particular classes, namely, ferrocenyl-based and metal–bis(terpy)-based dendrimers, which are the main targets in this project.

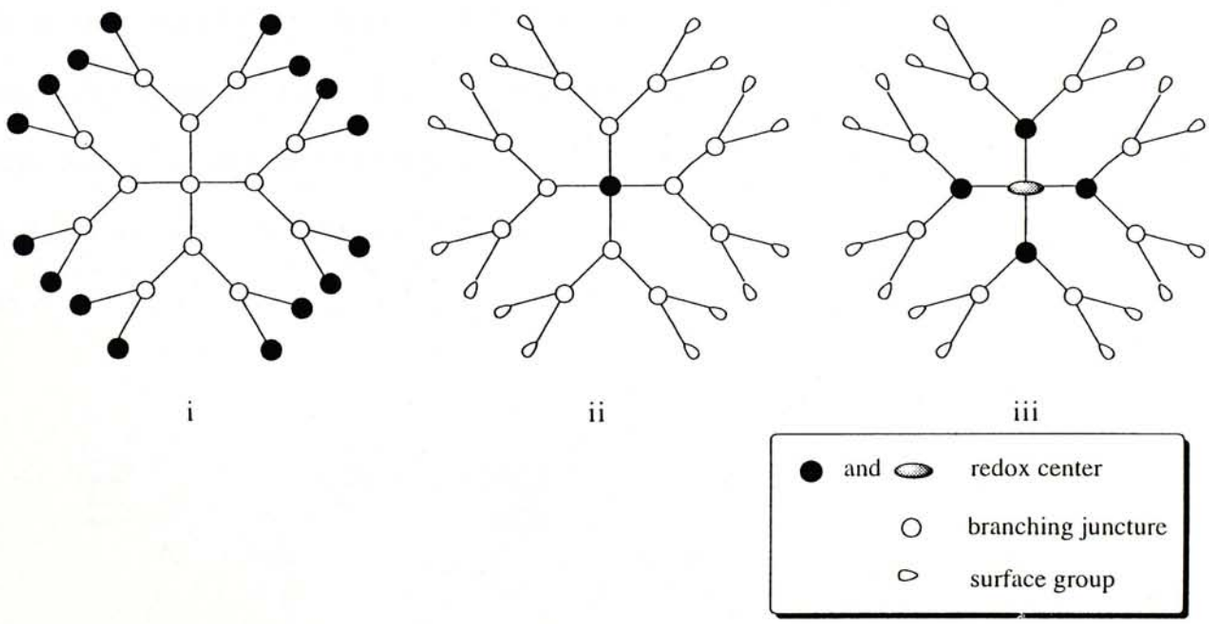

Figure 2. Electrochemically active dendrimer with: (i) redox center at the surface; (ii) redox center at the interior; (iii) more than one electrochemically different redox center.

(i) Ferrocenyl or metal–bis(terpy)-based dendrimers with redox center(s) at the surface of dendrimer

Ferrocenyl and metal– bis(terpy)-based dendrimers are by far the most commonly encountered types of electrochemically active dendrimers and examples of which could be dated back to the early nineties.[4] A series of poly(propylenediamine) dendrimers **1–3** terminated with ferrocenyl groups was synthesized by Cuadrado and co-workers.[5] Based on the ^{1}H-NMR study, significant interbranch H-bonding interactions were noted for the higher generation species. Due to the hydrophobic nature of dendrimers **1–3**, they are not soluble in aqueous media, but their aqueous solubility could be greatly enhanced in the presence of β-cyclodextrin (β-CD). This was due to the formation of inclusion CD–ferrocene complexes.

The redox properties of the dendrimers **1–3** were studied by cyclic voltammetry (CV). All ferrocenyl moieties attached on the surface behaved independently and were oxidized at the same redox potential. Interestingly, differential redox behavior was observed for the different generation dendrimers when the experiment was conducted in the presence of β-CD. Hence, for the G2-dendrimer **2**, only one voltammetric wave was noted in the presence of β-CD, indicating that all the surface ferrocenyl residues were equivalent and were bound by β-CD. In contrast, the electrochemical behavior of the G3-dendrimer **3** solubilized by β-CD exhibited two different voltammetric waves; the

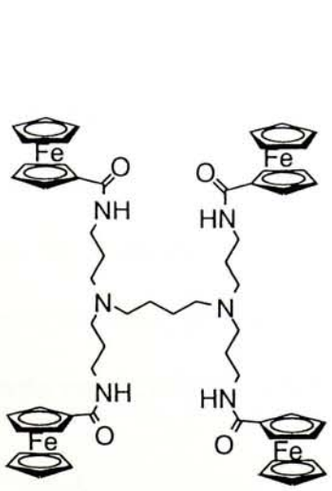

1

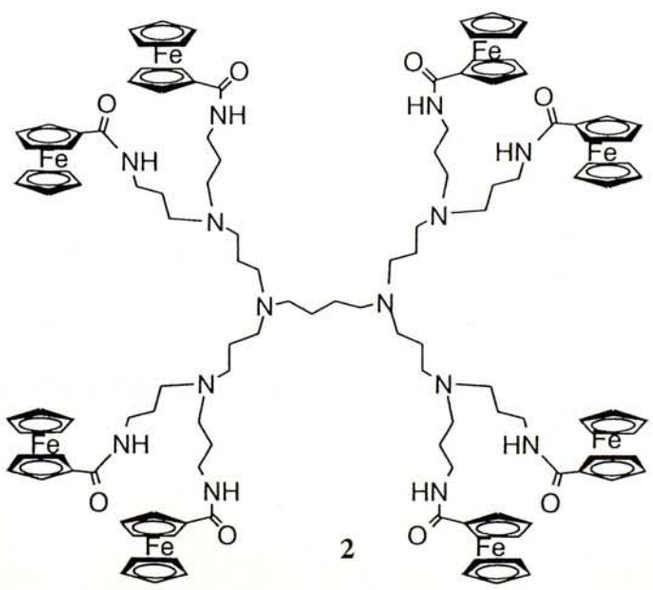

2

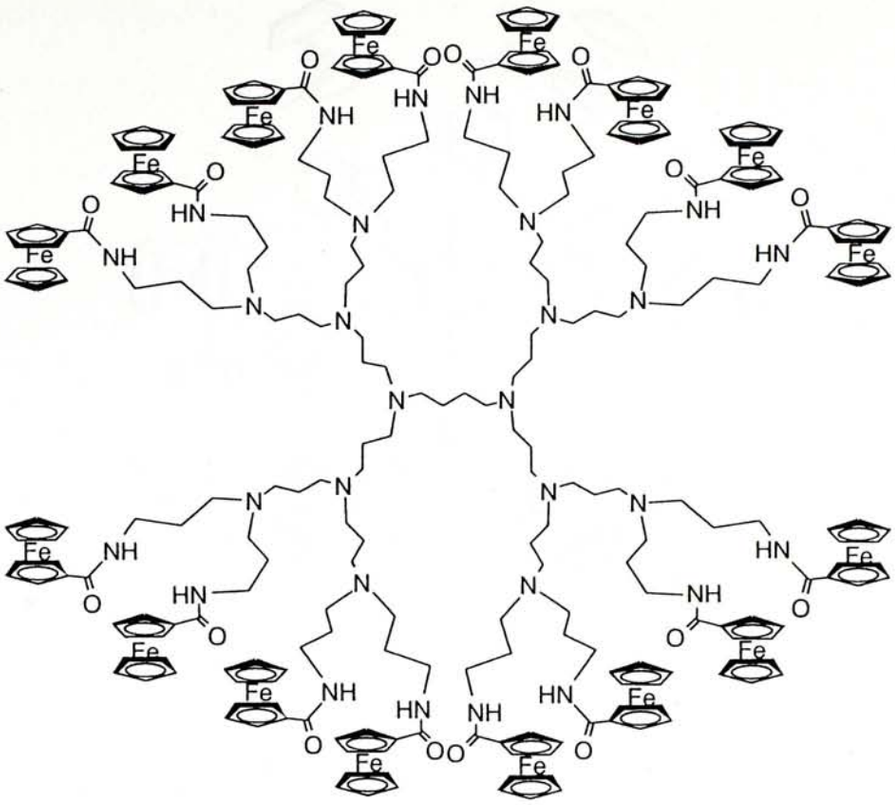

one at a less-positive potential (+0.38 V *vs* SCE) corresponded to the redox process of uncomplexed ferrocene residues while the more anodic wave (+0.51 V *vs* SCE) resulted from the oxidation of the β-CD-complexed ferrocene subunits. Further additions of β-CD to this solution did not change the voltammetric behavior, suggesting that the uncomplexed ferrocene residues were not accessible due to the substantial steric congestion at the surface of dendrimer **3**. This report also demonstrated that the redox potential of dendrimers could be moderated by the surrounding environment.

Another group of dendrimers having multiple ferrocenyl surface groups was reported by Astruc.[6] Such systems with several redox centers are excellent candidates for use as multi-electron redox catalysts. Cyclic voltammetry studies of compound **4**

3

was investigated, only one oxidation wave was observed (+0.78 V vs SCE). Thus, the six ferrocenyl moieties were electrochemically equivalent.

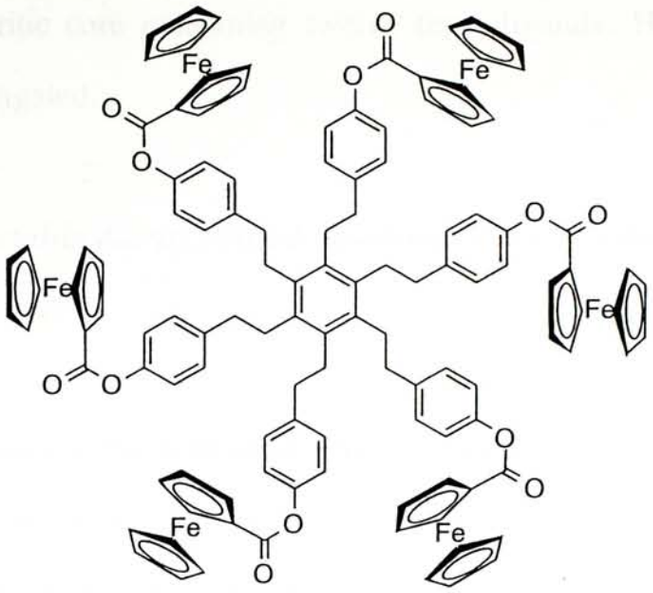

4

Electrochemically active dendrimers having metal–bis(terpy) units on the dendrimer surface had also been reported. For example, the dodecaruthenium heteroleptic bis(terpy) complex **5** was synthesized by Newkome and Constable.[7] This red crystalline complex was prepared by coupling of (terpy)$RuCl_3$ (12 equiv.) to a

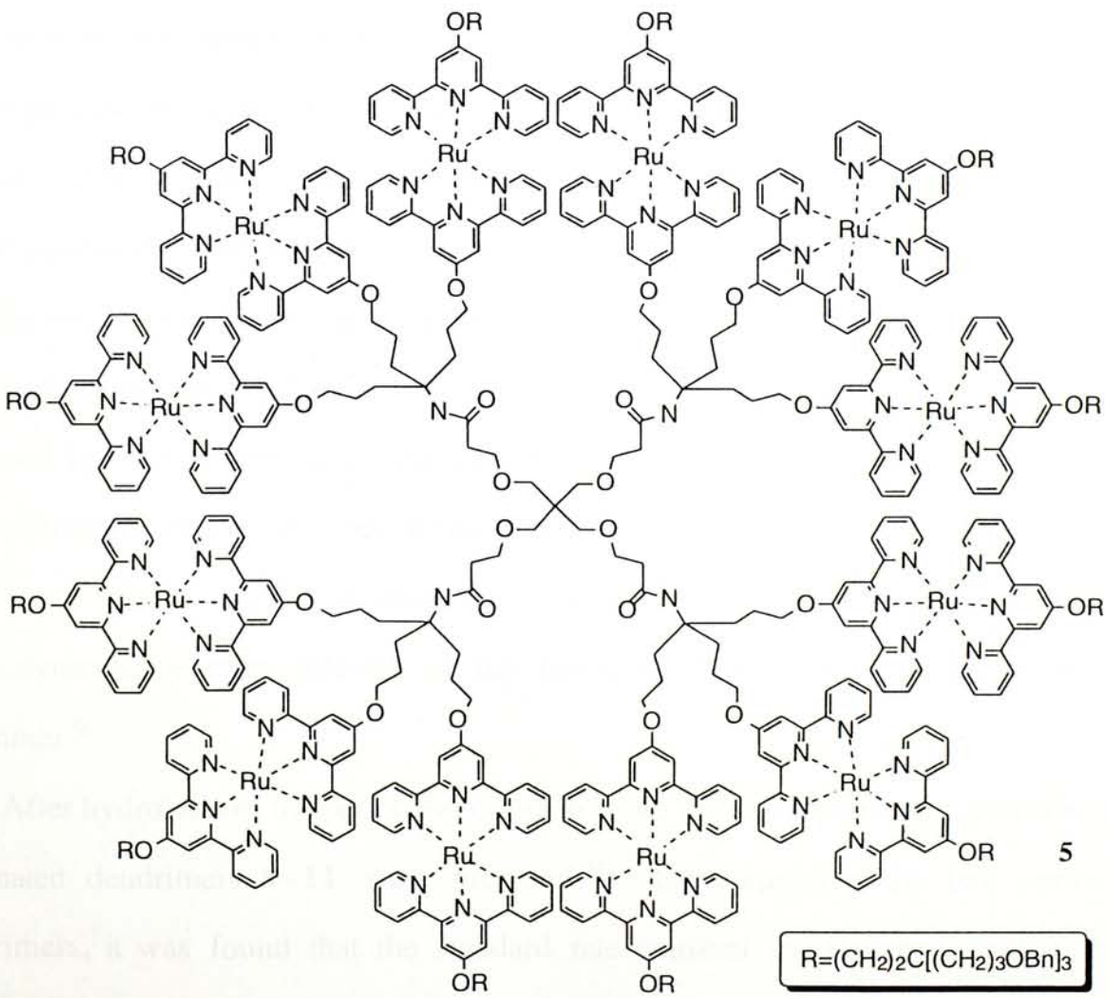

5

polyamido-based dendritic core containing twelve terpy-ligands. However, its redox property was not investigated.

(ii) Ferrocenyl or metal-bis(terpy)-based dendrimers with redox center(s) in the interior of dendrimer

The redox behavior for this type of dendritic molecules is usually different from that of the dendrimers described in the previous section. Since the redox center(s) is buried within the dendritic matrix, variation of the electrochemical properties between different generations can easily be observed. Furthermore, the effect of dendrimerization and the surface/interior environment on the redox properties can also be monitored.

An example of electrochemically active dendrimer with a ferrocenyl functionality located at the focal point was reported by Kaifer.[8] The G0–G2 generations of dendrimers **6–8** were prepared by attaching a ferrocene carboxylic acid moiety to the focal point amino functionality of a series of polyamide dendrons terminated with ester surface groups. As expected, the anodic electrochemistry was characterized by the one-electron oxidation of the ferrocene nucleus. This electrochemical process was fast for the G0 generation dendrimer **6** with a reasonably fast heterogeneous electron transfer rate constant. However, the values quickly decreased for G1 and G2 dendrimers **7** and **8**. Furthermore, the half-wave potentials ($E_{1/2}$) for the ferrocene oxidation also decreased by 90 mV with increasing molecular mass of the dendrimer, which reflected the stabilization of the oxidized ferrocenium nucleus by the dendritic environment relative to the solvent medium. Therefore, ferrocene oxidation became thermodynamically more difficult as the ferrocene subunit was buried inside the dendrimer.[9]

After hydrolysis of the peripheral esters in **6–8**, the corresponding carboxylic acid terminated dendrimers **9–11** were prepared.[10] By comparing the two series of dendrimers, it was found that the standard rate constant for heterogeneous electron transfer in aqueous medium were similar for the corresponding generation of dendrimer.

It was suggested that although compounds **9–11** had a more extended structure, solvation of the carboxylic acid groups by water molecules may hinder the electron transfer process; while the presence of the bulky *tert*-butyl groups in compounds **6–8** may compensate such effect. Moreover, the $E_{1/2}$ value for the oxidation of compounds **9–11** increased by 30 mV as the generation increased. This trend was exactly opposite to that observed for the oxidation of compounds **6–8**. It was because the oxidized forms of water-soluble dendrimers **9–11** are relatively easier for hydration than those of compounds **6–8**. As the generation increased, the ferrocene was surrounded by more dendrimer branches which interfered the hydration of the ferrocene moiety, resulting in a destabilization of the ferrocenium ion, which was reflected in the positive shift in $E_{1/2}$ value.

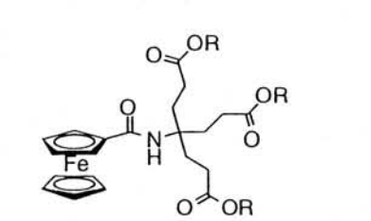

6 R=*tert*-butyl
9 R=H

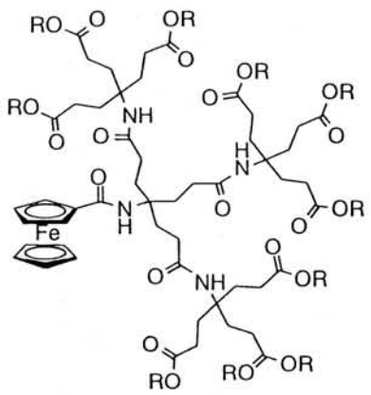

7 R=*tert*-butyl
10 R=H

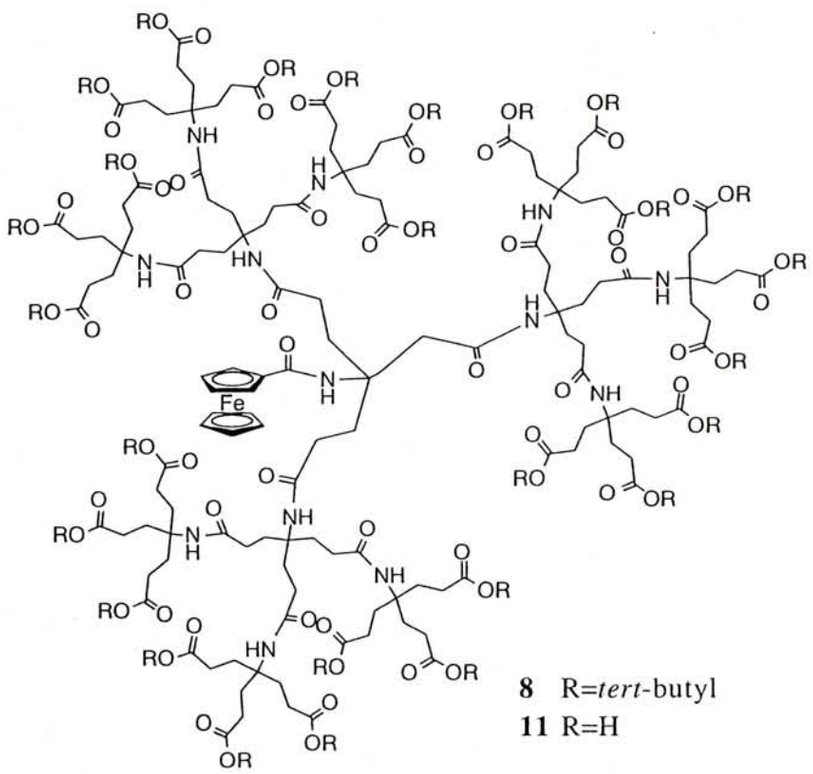

8 R=*tert*-butyl
11 R=H

Another series of dendrimers having electrochemically active functionality located near the central core was that reported by Newkome.[11] Such molecules **12–14** were constructed by having a single Ru(II) atom linking two terpy-based dendritic ligands within a polyamide envelope. The Ru–bis(terpy) redox-active center of these complexes was probed by cyclic voltammetry. The Ru(II)/Ru(III) and the terpy-based redox couples

were chemically reversible for the lower generation compound **12**. However, drastic irreversible behavior became evident for the more sterically congested G3 complex **13** and completely irreversible behavior was clearly seen for **14**.

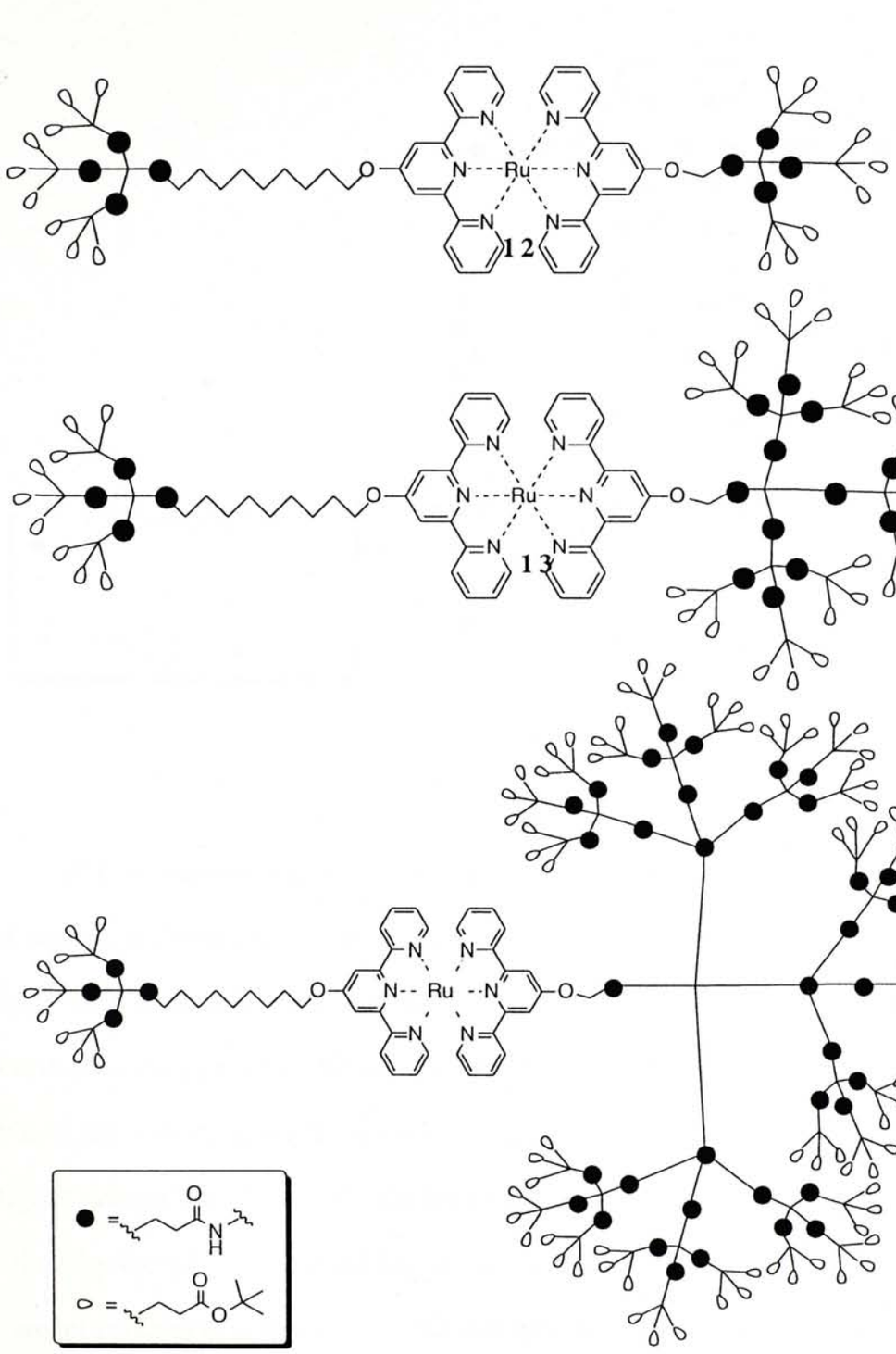

Newkome's finding was similar to that discovered by our own research group in 1996.[12] A series of Fe(II)–bis(terpy)-based polyether dendrimers **15**–**17** containing a central Fe(II) ion was synthesized, and their redox properties was studied by CV. Reversibility of the redox reaction decreased gradually towards the higher generation, as the peak separation are greatly increased with increasing generation (from 50 to 120

mV). The finding indicated that the dendritic sectors acted as an "insulating scaffold" for the redox center. Therefore, electron transfer processes were more hindered as the generation was higher.

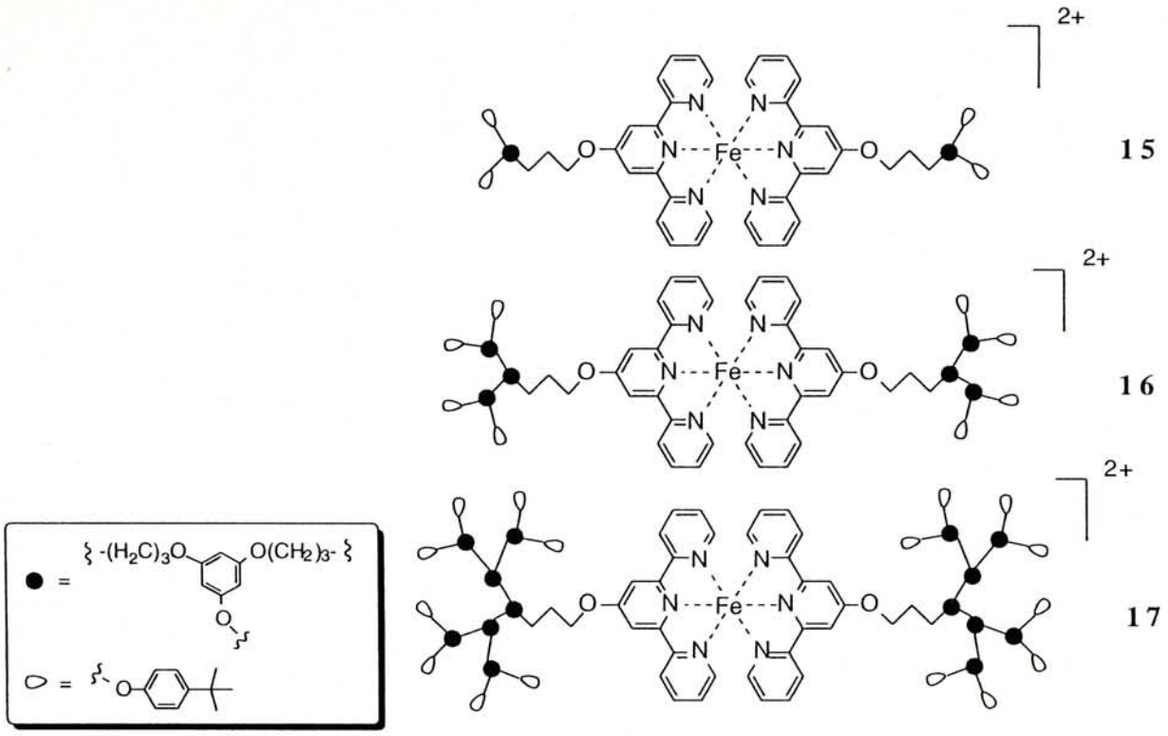

All the examples stated above involved dendritic molecules having a certain degree of structural flexibility. A recent example of electrochemically active dendrimer with a rigid structure was reported by Kimura.[13] The cyclic voltammetry of a G2 Ru(II)–bis–(terpy) metallodendrimer **18** was investigated, and the result was similar to that of the non-rigid dendrimer, *i.e.*, the potential separation was larger for complexes of higher generation. It can be concluded that the redox behavior of the dendrimer can be varied by the size of the dendritic sectors surrounding the redox center, since the electron transfer process is dependent on the distance between the redox center and the electrode surface.

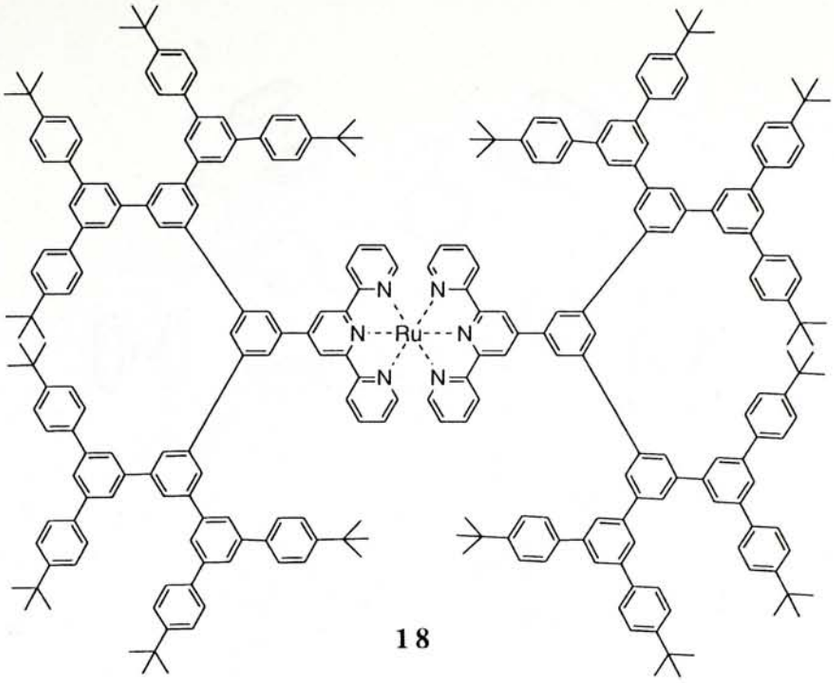

18

(iii) Ferrocenyl- and metal–terpy-based dendrimers with multiple, electrochemically different redox centers

The presence of multiple, yet electrochemically different redox centers in a single dendritic molecule illustrates the potential interactions of the various redox centers. To probe the possible interactions of two electrochemically active centers, Astruc described the preparation and CV study of a G1 hepta-iron derivative **19**.[6] This compound was structurally very similar to compound **4** described earlier, but possessed an additional central $[FeCp(arene)]^+$ unit locating at the central core.

Comparison of the CV behavior of compounds **4** and **19** indicated that the redox potential of the six peripheral ferrocene units in compound **19** was perturbed to +0.88 V (+0.78 V in compound **4**) due to the presence of the central iron moiety. The result suggested that the central and surface iron centers were interacting with each other. However, this kind of interaction appeared to be dependent on the structural environment around the metal vicinities. Thus, the redox potentials of the peripheral ferrocene units in both compounds **20** and **21** had the same value (+0.44 V), despite the presence of an additional $[FeCp(arene)]^+$ moiety in the latter compound.

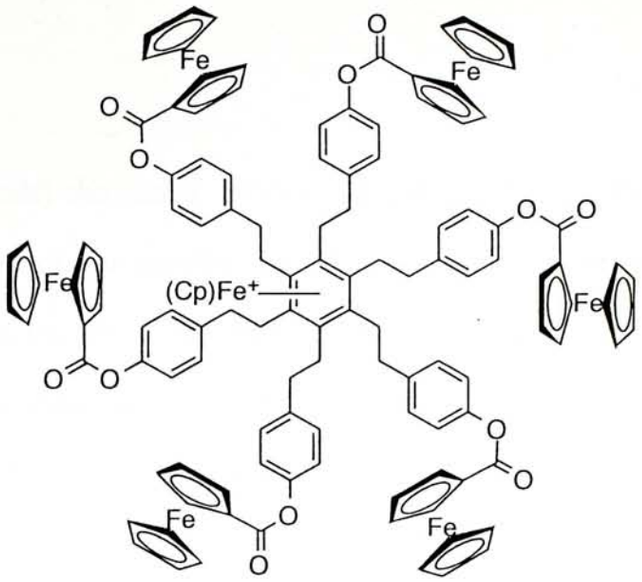

19

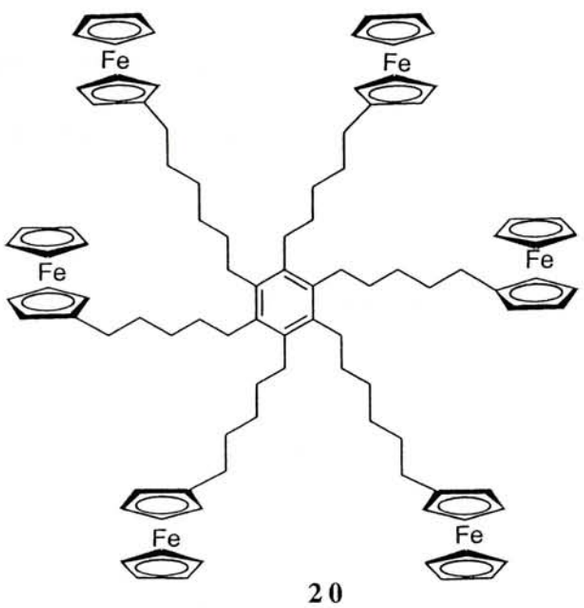

20

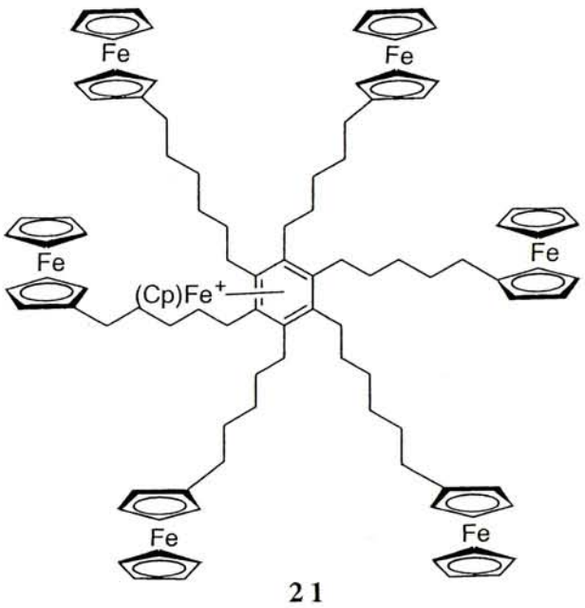

21

3. Electrochemically active dendrimers as models for studying the redox behavior of complex proteins

It has recently been proposed that dendrimers can mimic some aspects of protein behavior.[14] The three dimensional environment within a protein can be successfully simulated by carefully selecting the functionality groups used to construct the dendritic model. Among the various protein functions, the electron transfer process is of particular interest due to many of the important biological processes are controlled by

redox proteins such as cytochromes in oxidative phosphorylation and ferredoxins in nitrogen fixation.

In a study to model the redox process of cytochrome *c*, Diederich reported the construction of a series of Zn porphyrins **22**–**24** embedded in dendritic envelope.[15] Electrochemical studies on the lower generation porphyrins **22** and **23** revealed two reversible one-electron reduction processes while experiments conducted on the G3 compound **24** showed a less well defined wave for a single irreversible reduction process. In addition, the first reduction potential of the zinc porphyrin unit became more negative with increasing dendrimer generation. This trend can be explained by the increasingly electron-rich microenvironment created by the dendritic branches around the porphyrin core and hence electron addition becomes energetically more difficult for the higher generation dendritic porphyrins.

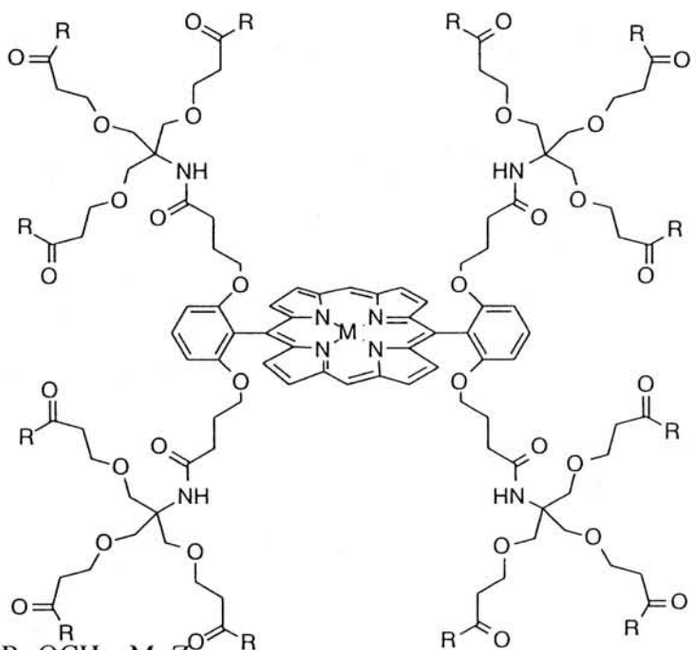

22 R=OCH_3, M=Zn

23 R=$NHC(CH_2OCH_2CH_2CO_2CH_3)_3$, M=Zn

24 R=$NHC[CH_2OCH_2CH_2NHCO(CH_2OCH_2CH_2CO_2CH_3)_3]_3$, M=Zn

25 R=$OCH_2CH_2OCH_2CH_2OCH_2CH_2OCH_3$, M=FeCl

26 R=$NHC(OCH_2CH_2OCH_2CH_2OCH_2CH_2OCH_3)_3$, M=FeCl

When the ester moieties on the surface of the porphyrins **22** and **23** were replaced by water soluble triethyleneglycol monomethyl groups, and the Zn(II) metal center was also converted into [Fe(III)Cl],[16] the resulting porphyrins **25** and **26** became water

soluble. Their CV behavior was then studied in aqueous media. Both compounds exhibited two reduction processes, Fe(III) → Fe(II) and Fe(II) → Fe(I). Because of the more dense structure of **26** than **25**, the reduction potential of Fe(III) of **26** was shifted to more positive value (+420 mV) as compared to that of **25**. Hence, the environmental polarity strongly influences the potential of redox reactions occurring at the heme metal center. Moreover, in aqueous media, the more densely packed dendritic branches of **26** impeded aqueous solvation of the iron porphyrin. As a result of reduction in contact between the heme and the external solvent, the highly charged oxidized form was destabilized.

Other than the solvent effect, the nature of addition ligation center also has profound influence on the redox properties. For example, when an imidazole was added to the axial position of the heme Fe(III) centers of **25** and **26**, their redox behavior was greatly changed and the redox potential experienced approximately 1V positive shift anodically.[17]

Gorman synthesized a series of 4 iron-4 sulfur cluster dendrimers to mimic the redox behavior of ferredoxins in a protein which has an important role in nitrogen fixation.[18] The compounds were prepared by attaching a series of polyether dendrons onto a 4-Fe-4-S cluster central core (one of the dendrimers is shown as compound **27**). Similar to the findings reported earlier, as the generation of dendrimer increased, the tendency for the reduction of Fe(III) became lower. The peak separation also increased with the increasing generation.

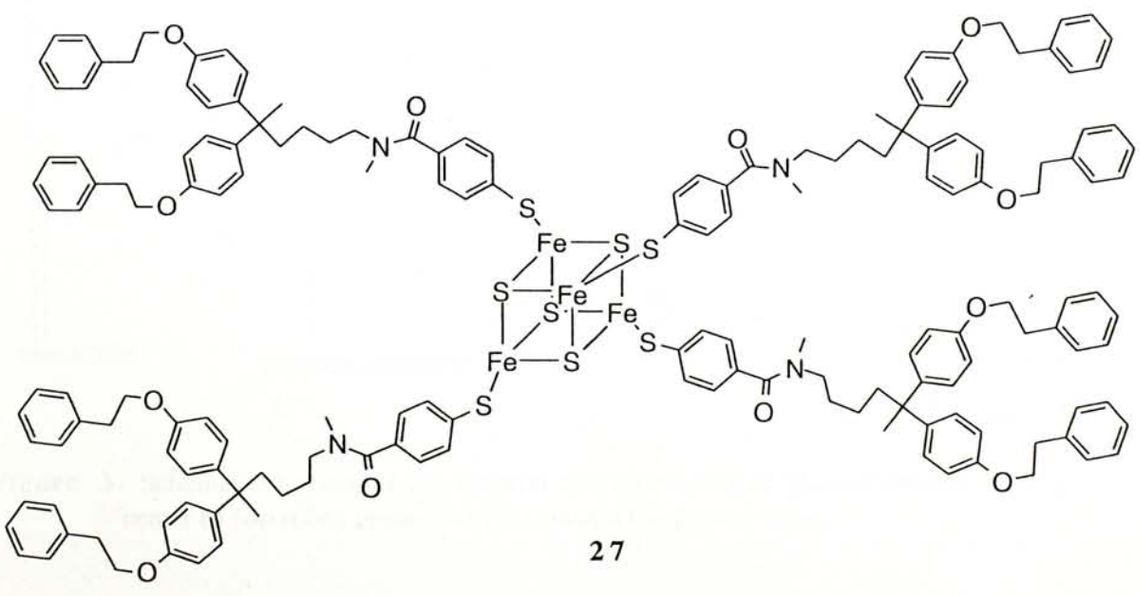

27

The decrease in reversibility of the redox behavior for the higher generation dendrimers is particular interesting in light of the study of the electron transfer properties of redox proteins.[19] It was suggested that the decrease in reversibility of the redox process was due to the insulating effect of the dendritic envelope.[11, 12] This is in agreement with the findings observed in the direct electrochemical studies of redox proteins such as cytochrome *c* that fast electron transfer could be realized when the protein could bind reversibly to the electrode surface and that the distance between the redox center and the electrode surface did not exceed a certain value.[20] Thus, the redox enzyme glucose oxidase was found to accept and transfer electrons *via* small oxidizable/reducible molecules but did not exchange electrons with simple metal electrode due to the remoteness of the flavin adenine dinucleotide-based redox centers from the electrode. Interestingly, upon chemical modification of the glucose oxidase with ferrocenyl moieties, the reversibility of the redox reaction between the enzyme and the electrode was enhanced.[21] The experimental outcome was rationalized by the facilitation of electron transfer through the electron relay center, as the distance between the electrode and the redox centers was now reduced in the presence of the ferrocenyl relay (Figure 3).

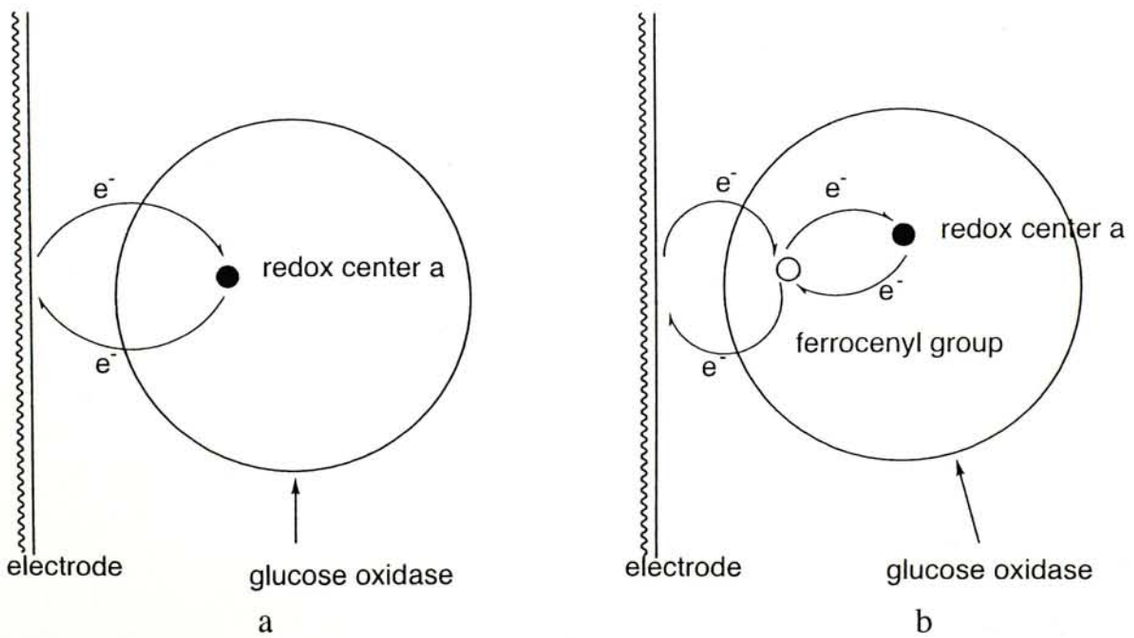

Figure 3. Schematic diagram of the electron transfer process of glucose oxidase having a) one redox center b) two redox centers which is interact with each other.

As our continued effort to the understanding of the electron transfer behavior of dendritic macromolecules, we wish to study the redox behavior of dendrimers with multiple, yet electrochemically different redox centers. In this thesis, we would like to prepare and conduct electrochemical studies on a series of metallodendrimers containing two kinds of redox centres, one with a Fe(II)–bis(terpy) center located at the dendrimer core and another ferrocenyl-based center located near the interior of the dendrimer. Particular emphasis will be placed on examining possible interactions between the redox centres, such as a shift of redox potential or a change of the reversibility of the redox processes. In the next chapter, we will describe the design and synthesis of our redox-active dendritic systems. The cyclic voltammetry results will also be disclosed.

Chapter II. Synthesis and Characterization

1. Structure of the electrochemically active dendrimers

The target electrochemically active dendrimers **28–31** involved in this study consist of two electrochemically different redox systems; an Fe(II)–bis(terpy) system located at the dendrimer central core and two electrochemically identical ferrocenyl systems located in symmetrical positions in the interior sector of the dendrimer. The polyether-based dendritic fragment reported earlier by us[22] was employed as the insulating shield and is connected to the redox active moieties by a 3,5-dihydroxyphenylethylene brancher. The electrochemical profile of the Fe(II)–bis(terpy) system has been well established and is known to consist of one Fe(II)-based oxidation and two ligand-based reduction processes.[11, 12] On the other hand, the ferrocenyl system is known to have a Fe(II)-based oxidation process.[8, 10] In order to evaluate the effect of the ferrocenyl redox groups on the redox properties of the central Fe(II)–bis(terpy) core, an analogous series of dendrimers **32–35** having a phenyl moiety in place of the ferrocene group was also prepared. Based on the previous results obtained from our laboratory, completely irreversible redox processes were noted when the polyether dendritic envelope had a generation of greater than three. Hence the G3 dendrimers would be the highest generation compounds synthesized in this project.

In this thesis, simplified structural diagrams are used to represent the structures of the dendrimers. The polyether-based dendritic fragment is drawn as a sector labeled with the generation number. For the text description, the notations $Gn_{(Fc)}$-X and $Gn_{(Ph)}$-X are used to describe the ferrocenyl- and the phenyl-appended dendrimers with the focal point group X, respectively.

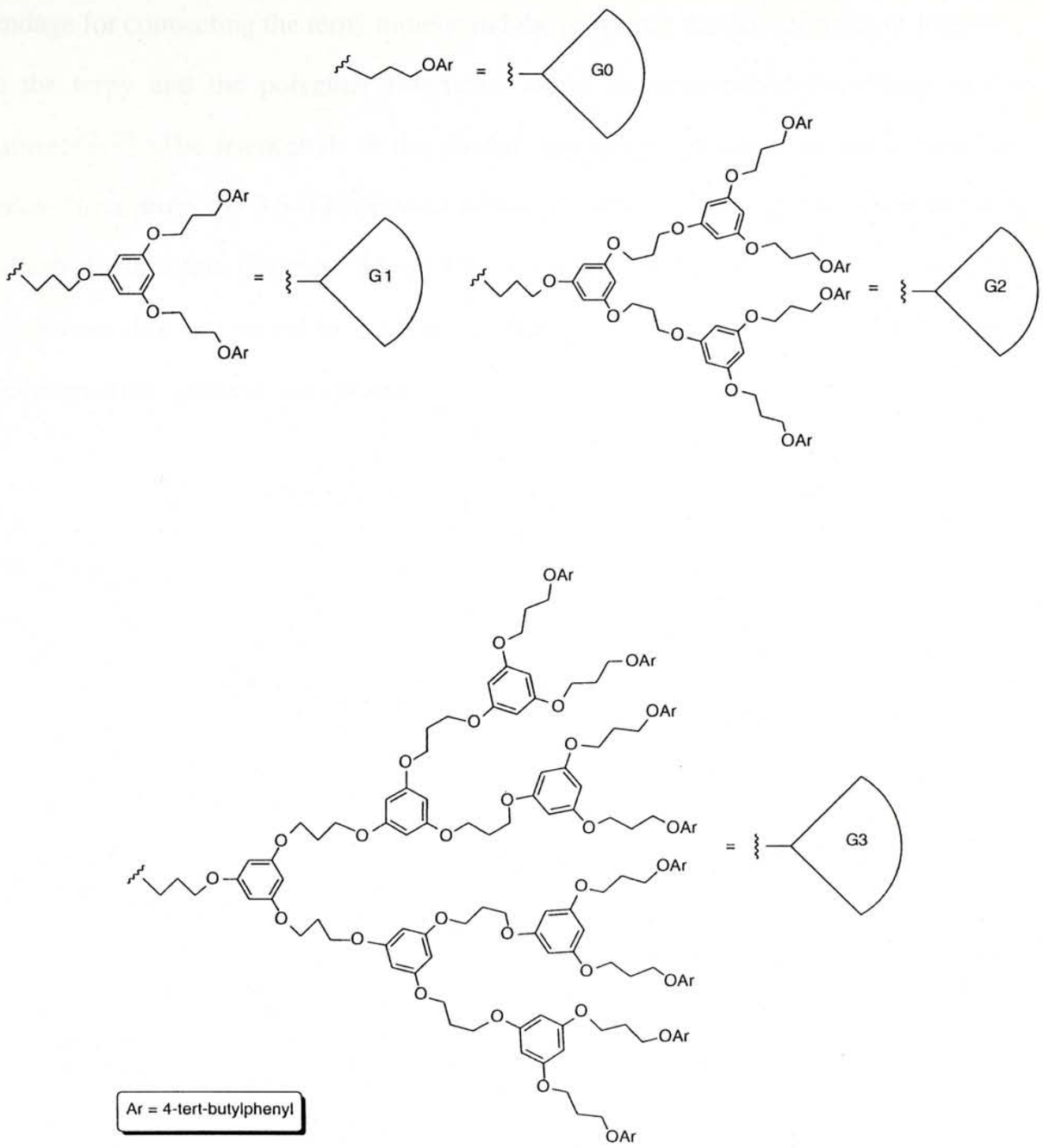

2. Retrosynthetic analysis

The retrosynthetic analysis to the metallodendrimers is shown in Scheme 1. The metallodendrimers could be prepared by metallation of the corresponding terpy ligands **36**—**43** with Fe(II) ion. The terpy ligands in turn could be assembled using a triply branched fragment having either the ferrocenyl **44** or the phenyl appendage **45** with two phenolic groups as anchors for the terpyridine unit and the polyether fragment. The key reaction involved the preparation of the bridging fragment bearing the appropriate

appendage for connecting the terpy moiety and the polyether dendritic fragment together. Both the terpy and the polyether fragments could be synthesized according to the literature.[22, 23] The ferrocenyl- or the phenyl-appendage, on the other hand, could be connected to a protected 3,5-dihydrobenzaldehyde derivative **46** *via* the Wittig reaction to furnish the bridging fragment **44** or **45**. Finally the terpy ligand and the polyether fragments are then connected to the bridging fragment *via* the phenolic linkages under Williamson ether synthesis conditions.

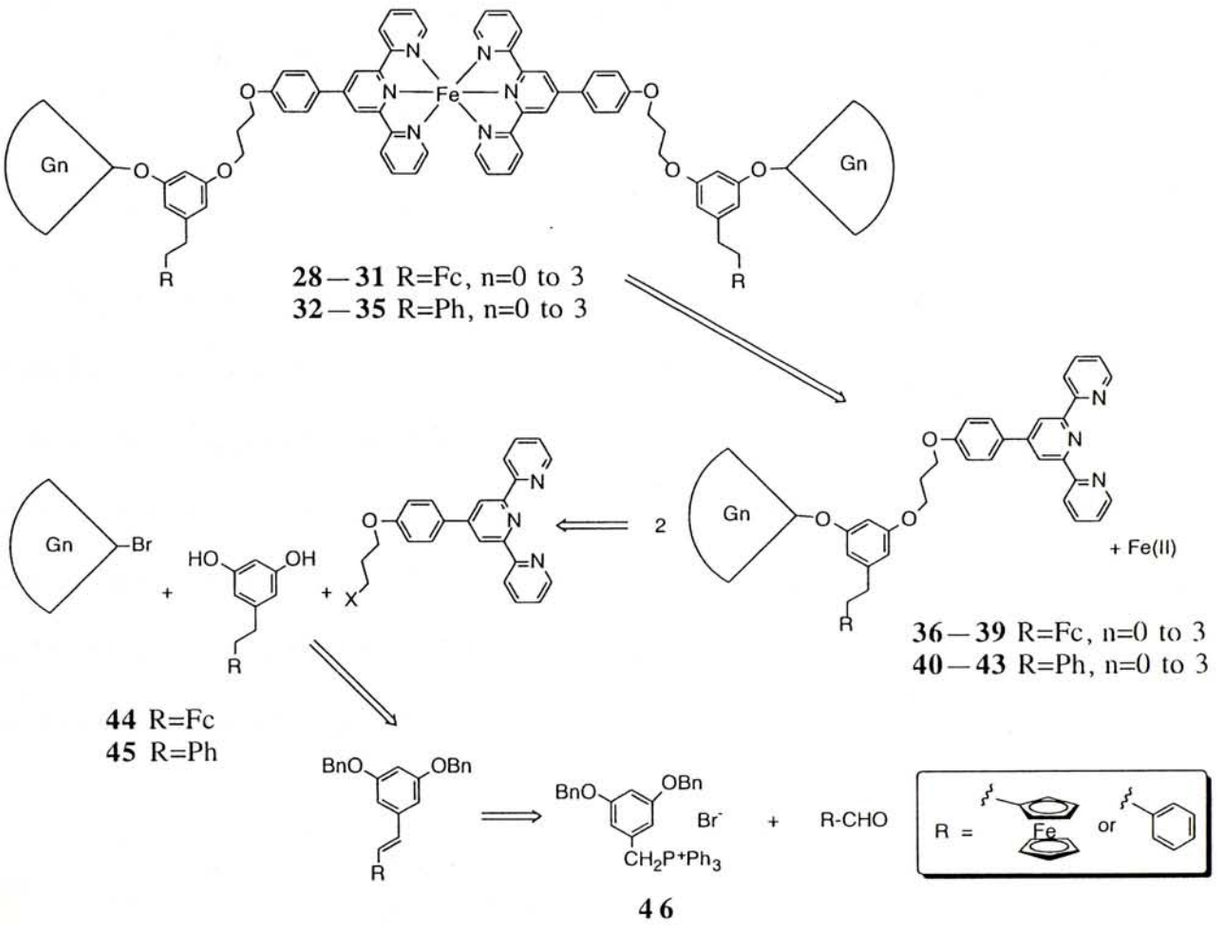

Scheme 1. Retrosynthetic scheme for the construction of metallodendrimers.

3. Synthesis

(i) Synthesis of the polyether dendritic sectors

The polyether dendritic sectors used in this study are the ones reported earlier by us.[22] A convergent synthetic method was used in their preparation as the number of reactions is restricted to a small number irrespective of dendrimer generation.[24, 25]

Therefore, completion of reactions in each step can be ensured and large excess reagents are not required even in the preparation of high generation dendritic sectors.

There are two reactions in the iterative synthesis cycle for the construction of the dendritic sectors. First, a bis-*O*-alkylation of the branching unit, 5-(3'-hydroxy-propoxy)-1,3-resorcinol **47** with a dendritic bromide, followed by functional group conversion of the hydroxyl group into the corresponding bromide (Scheme 2). The surface sector used is a 4-*tert*-butylphenoxy group .

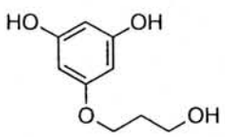

47

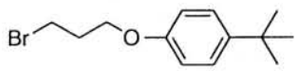

48

The dendritic sectors were synthesized as described below (Scheme 2). Treatment of the branching unit **47** with 2 mol equiv. of surface group **48** in the presence of 6 mol equiv. of potassium carbonate afforded the dendron G1-OH **49** in 72% yield as a white solid. After the bromination of the hydroxy group of **49** with triphenylphosphine and carbon tetrabromide, G1-Br **50** was obtained in 98% yield[22]. In the next reaction cycle, bis-*O*-alkylation of the branching unit **47** with 2 mol equiv of G1-Br **50** under similar conditions provided the G2-OH **51** in 60% yield as an oil. Subsequent bromination of

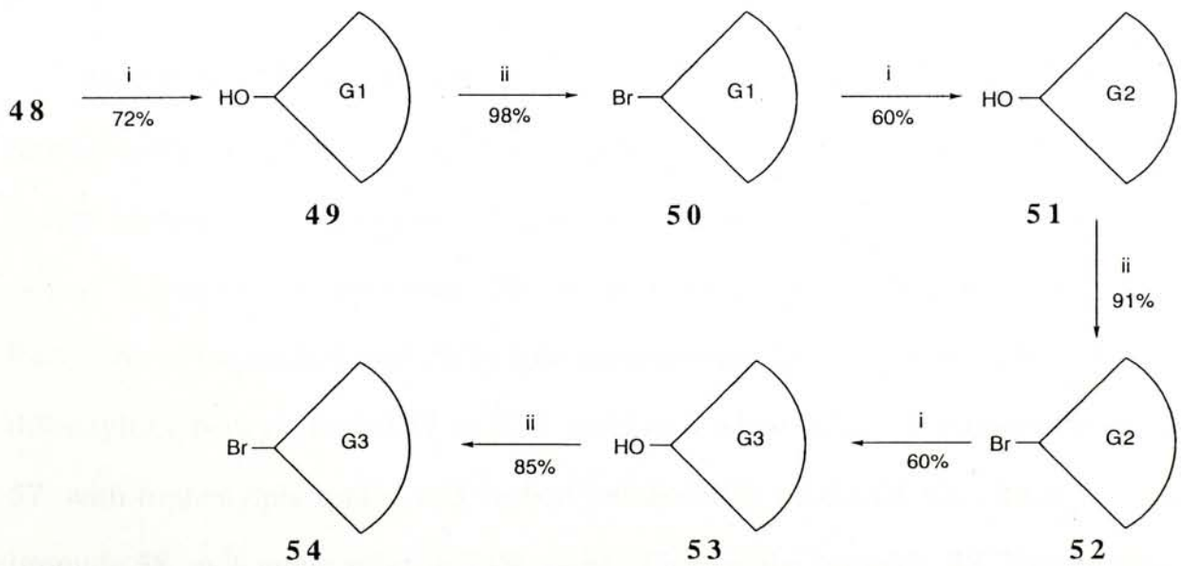

Scheme 2. *Reagents and Conditions*: i) **47**, K_2CO_3, acetone, 18-C-6, reflux, 24-60h; ii) CBr_4, PPh_3, THF.

G2-OH **51** gave the bromide G2-Br **52** in 91% yield. By repeating the same reaction sequence on G2-Br **52**, the dendrons G3-OH **53** and G3-Br **54** were obtained in 60% and 85% yield respectively. It was found that larger amount of triphenylphosphine and tetrabromomethane and higher concentration of the reactants were required to force the bromination reaction to completion as the dendrimer generation went up. This was due to the shielding effect on the focal point hydroxy group by the dendritic sector.

(ii) Synthesis of the bridging fragment

The bridging fragments containing two phenolic groups which will be used to connect to the terpy and the polyether dendritic fragments. Therefore they have to be protected beforehand prior to introduction of the ferrocenyl or the phenyl appendage. We chose the dibenzyl protected phosphonium salt **46** as the key intermediate for the synthesis of the two bridging fragments **44** and **45**. The benzyl protective groups could then be dismantled by hydrogenolysis.

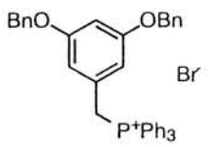

46

Methyl 3,5-dihydroxybenzoate **55**, prepared from acid-catalyzed esterification of commercially available 3,5-dihydroxybenzoic acid, was treated with 2 mol equiv. of benzyl bromide in the presence of potassium carbonate in refluxing acetone to give methyl 3,5-dibenzyloxybenzoate **56** in 70% yield as a white solid (Scheme 3). Reduction of the methyl ester **56** by lithium aluminum hydride in dry THF afforded 3,5-dibenzyloxy-benzyl alcohol **57** in 92% yield as a white solid. Treatment of compound **57** with triphenylphosphine and carbon tetrabromide produced 3,5-dibenzyloxybenzyl bromide **58** as a white solid in 74% yield. Finally, the bromide **58** was treated with triphenylphosphine in refluxing toluene for 12 h to give the desired phosphonium salt **46** in 81% yield.

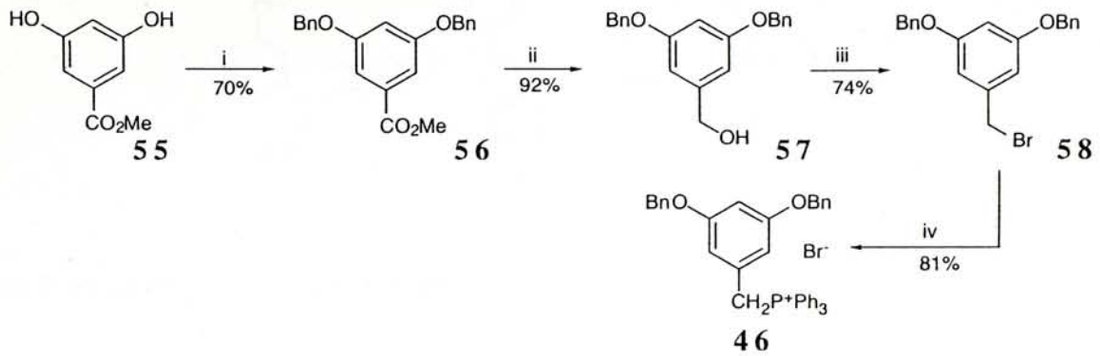

Scheme 3. *Reagents and Conditions:* i) BnBr, K_2CO_3, acetone, reflux; ii) $LiAlH_4$, THF, 0°C; iii) CBr_4, PPh_3, THF; iv) PPh_3, toluene, reflux.

Reaction of the phoshonium ylide, prepared *in situ* from the phosphonium salt **46** in the presence of sodium hydride, with ferrocenecarboxaldehyde **59**[26] in THF afforded the ferrocenyl olefin **60**, which could be purified by column chromatography and recrystallized from diethyl-ether (Scheme 4). The benzyl groups were then debenzylated by catalytic hydrogenation with 10% Pd on charcoal and the olefin was simultaneously saturated to afford the target bridging fragment **44** containing two phenolic groups and the electrochemically active ferrocenyl functionality.

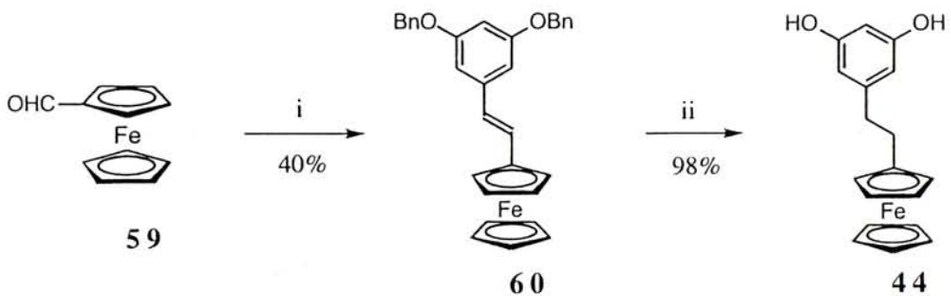

Scheme 4. *Reagents and conditions*: i) **46**, NaH, THF; ii) H_2, Pd/C, EtOH/ethyl acetate.

The other bridging fragment **45** containing the phenyl group was prepared in a similar manner. Hence, treatment of benzaldehyde **61** with the phosphonium ylide derived from **46** followed by the catalytic hydrogenation, produced the desired phenyl bridging fragment **45** as shown in Scheme 5.

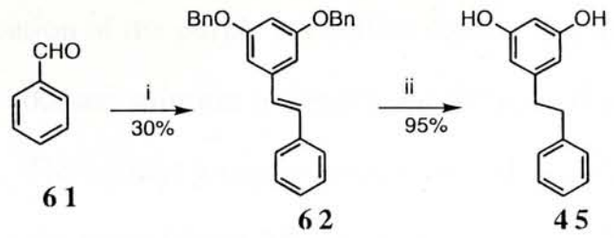

Scheme 5. *Reagents and conditions*: i) **46**, NaH, THF; ii) H_2, Pd/C, EtOH/ethyl acetate.

(iii) Preparation of the terpyridine ligand

The tridentate terpyridine ligand was synthesized from 4-hydroxybenzaldehyde according to the procedure from literature.[23] The phenolic group was firstly protected as the methyl ether **63** by treatment of 4-hydroxybenzaldehyde with methyl iodide and potassium carbonate (Scheme 6). Condensation of the protected aldehyde **63** with 2 mol equiv. of 2-acetylpyridine in the presence of excess ammonium acetate and acetamide gave two terpyridine isomers **64** and **65**.[27] The mixture was not separable at this stage but was reacted with $FeCl_2{\cdot}4H_2O$ in acetonitrile to give the purple iron(II) complex of isomer **64** only. Precipitation of the complex with NH_4PF_6 allowed

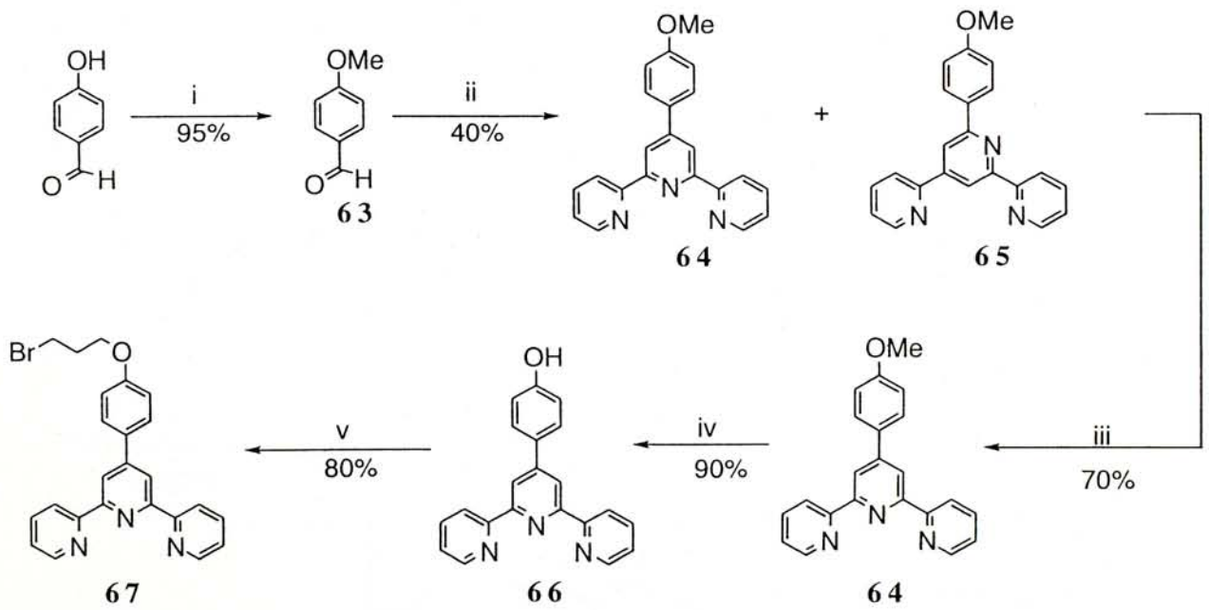

Scheme 6. *Reagents and conditions*: i) MeI, K_2CO_3, acetone; ii) 2-acetylpyridine, NH_4OAc, $AcNH_2$; iii) (1) $FeCl_2{\cdot}4H_2O$, MeOH, (2) H_2O_2, NaOH (aq), MeCN; iv) (1) HBr, acetic acid, 12h, (2) NaOH (aq); v) 1,3-dibromopropane, K_2CO_3, acetone, 18-C-6, 12h.

collection and purification of the purple crystalline solid. The iron(II) complex was then treated with H_2O_2 in alkaline solution to regenerate the terpyridine **64** as a yellow solid in 70% overall yield. The methyl group in compound **64** was then deprotected by HBr and acetic acid to give the terpy ligand **66**. Finally, mono-*O*-alkylation of **66** with 1,3-dibromopropane in the presence of 3 mol equiv. of K_2CO_3 in acetone afforded 4'-(4-(3-bromopropoxy)phenyl-2,2':6',2"-terpyridine **67** in 80% yield.

(iv) Preparation of the dendritic ligands

After securing the reliable routes for the various building fragments, we began to assemble the pieces together in order to obtain the various dendritic terpy ligands **36–43** (Scheme 8). To this end, the polyether dendritic fragments of the various generation (G0-Br to G3-Br) were first anchored to the ferrocenyl bridging fragment **44** in the presence of 3 mol equiv. of K_2CO_3 in acetone to produce the various phenols **68–71**, respectively, as yellow oil. Similar coupling reaction between the phenyl bridging fragment **45** to the various bromides (G0-Br to G3-Br) afforded the phenols **72–75**,

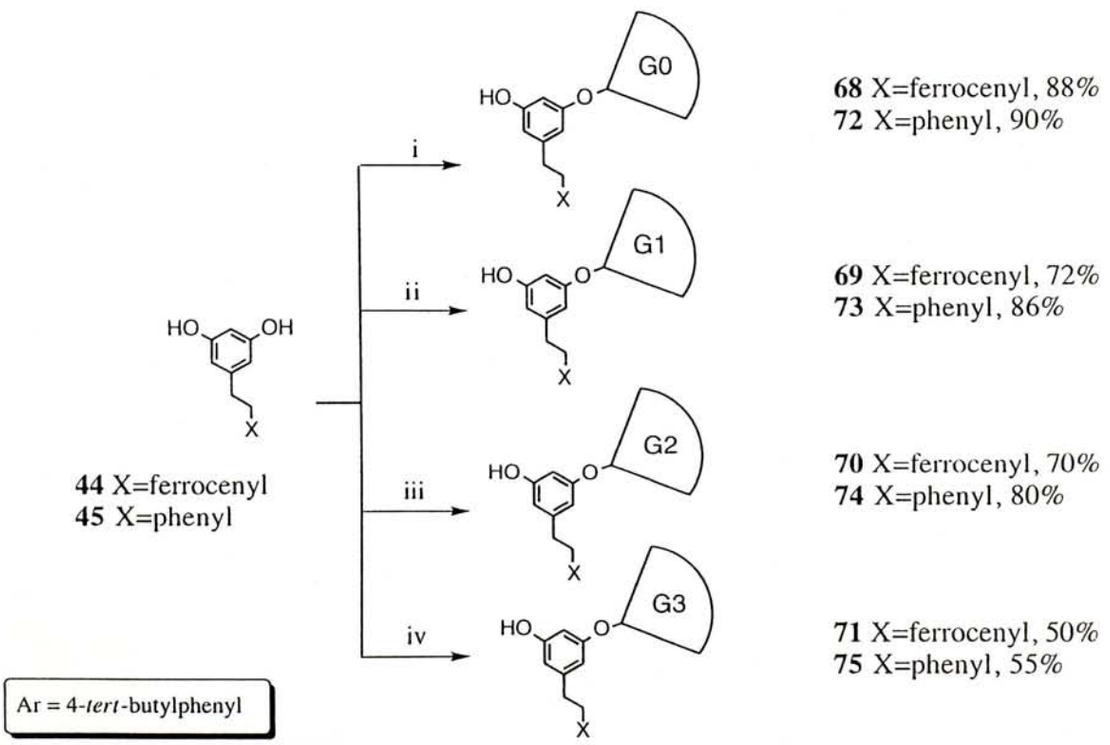

Scheme 7. *Reagents and Conditions:* i) G0-Br, K_2CO_3, acetone,18-C-6, reflux, 18h; ii) G1-Br, K_2CO_3, acetone,18-C-6, reflux, 24h; iii) G2-Br, K_2CO_3, acetone,18-C-6, reflux, 30h; iv) G3-Br, K_2CO_3, acetone,18-C-6, reflux, 48h

respectively as colorless oil. It was found that the coupling reaction became increasingly sluggish as the generation went up. The major side-product from the reactions was the bis-*O*-alkylation product. Fortunately, it could be easily separated by column chromatography (Scheme 7).

The monophenols **68–75** were then reacted with the terpy derivative **67** having the bromoalkyl side chain in the presence of 3 mol equiv. of K_2CO_3 in acetone to give the various dendritic ligands **36–43**, respectively (Scheme 8). Similar to the *O*-alkylation described in the previous section, the rate of coupling reaction rate declined as the generation went up. The products were then purified by column chromatography on alumina. For the ferrocenyl series, the products were found to be yellow oil while those of the phenyl series were obtained as colorless oil.

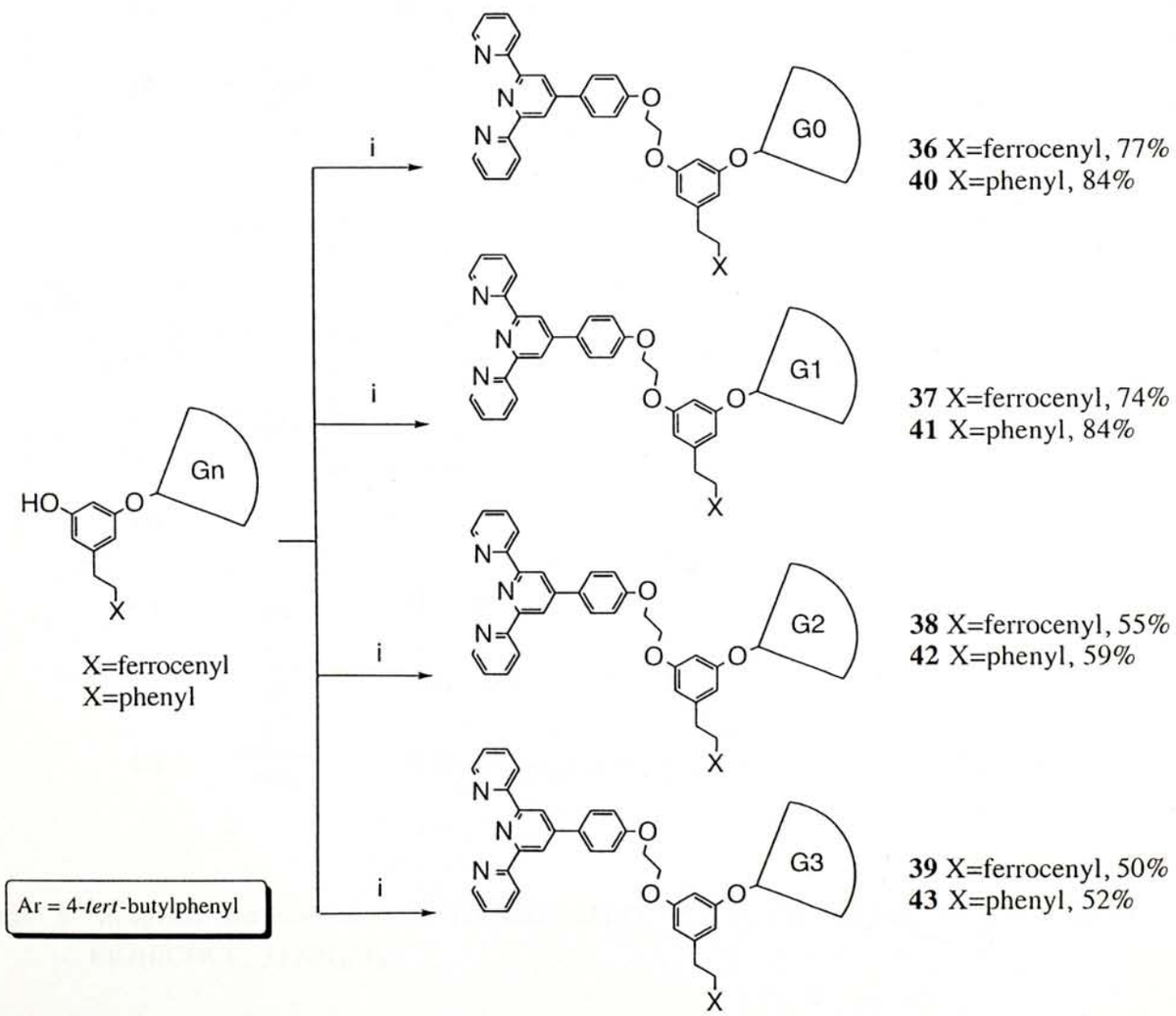

Scheme 8. *Reagents and Conditions:* i) **67**, K_2CO_3, acetone, 18-C-6, reflux, 18-36h.

(v) Preparation of dendritic metal complexes

The final operation in our synthetic sequence was the complexation of the dendritic ligands with iron(II) ion.[28] Hence, treatment of the ligand **36** with $FeCl_2 \cdot 4H_2O$ in refluxing methanol afforded a deep purple complex $[Fe(G0_{(Fc)})_2]^{2+}$, which was reacted with NH_4PF_6 to give $[Fe(G0_{(Fc)})_2](PF_6)_2$ **28** in 80% yield as a purple

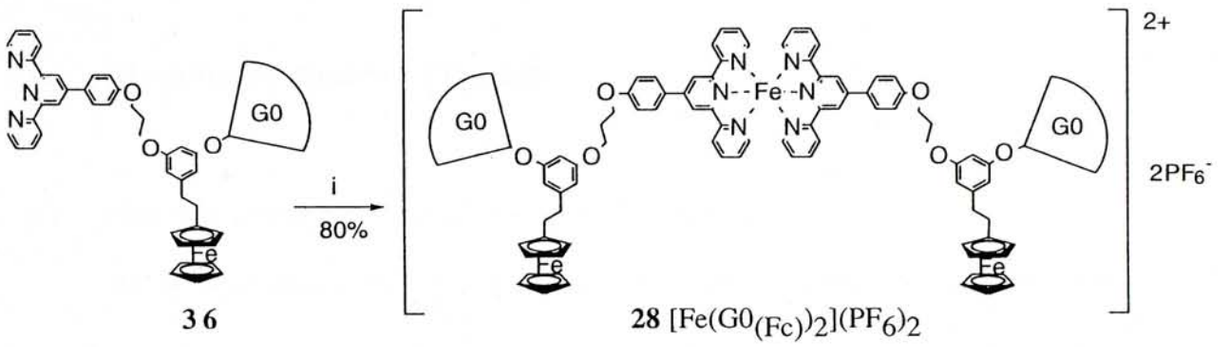

36 → **28** $[Fe(G0_{(Fc)})_2](PF_6)_2$

37 $\xrightarrow[80\%]{i}$ **29** $[Fe(G1_{(Fc)})_2](PF_6)_2$

38 $\xrightarrow[75\%]{ii}$ **30** $[Fe(G2_{(Fc)})_2](PF_6)_2$

39 $\xrightarrow[60\%]{ii}$ **31** $[Fe(G3_{(Fc)})_2](PF_6)_2$

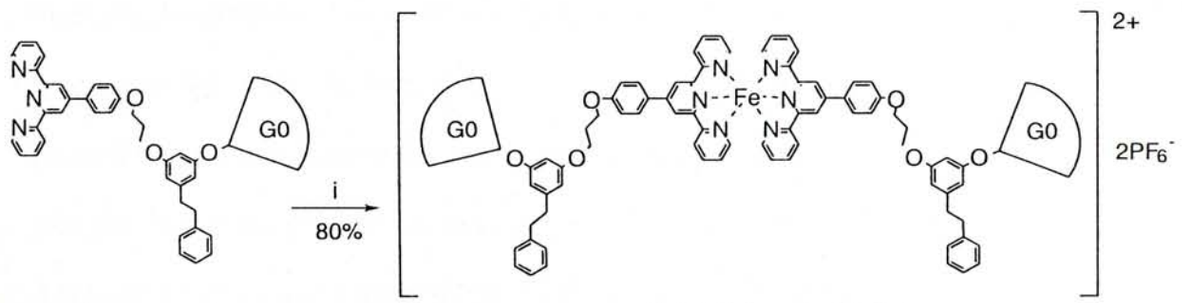

40 → **32** $[Fe(G0_{(Ph)})_2](PF_6)_2$

41 $\xrightarrow[78\%]{i}$ **33** $[Fe(G1_{(Ph)})_2](PF_6)_2$

42 $\xrightarrow[73\%]{ii}$ **34** $[Fe(G2_{(Ph)})_2](PF_6)_2$

43 $\xrightarrow[68\%]{ii}$ **35** $[Fe(G3_{(Ph)})_2](PF_6)_2$

Scheme 9. *Reagents and conditions*: i) (1) $FeCl_2 \cdot 4H_2O$, MeOH, (2) NH_4PF_6; ii) $FeCl_2 \cdot 4H_2O$, EtOH/$CHCl_3$, 2) NH_4PF_6.

crystalline solid (Scheme 9). Using the same procedure, the various metallodendrimers **28–35** were obtained. For dendritic ligands of the second and third generation that were insoluble in boiling methanol, a mixture of ethanol and chloroform was used as the reaction solvent to facilitate the metallation process. In this manner, the higher generation metallodendrimers could also obtained.

4. Structural characterization

(i) Nuclear magnetic resonance spectroscopy

All new dendritic fragments and ligands were characterized by ^{1}H- and ^{13}C-NMR spectroscopy. The structural characterization of the polyether dendritic fragments and the terpyridine ligands had been described previously.[22] Here we would concentrate our discussions on the spectral analysis of the bridging fragments, the target terpy ligands and the metallodendrimers.

Two main differences were noted between the ^{1}H-NMR spectra of the two bridging fragments. First, the 4 ethylene protons ^{1}H-signals of the ferrocenyl bridging fragments **44** were situated at δ 2.51–2.72, while the corresponding ^{1}H-signals of the phenyl bridging fragment **45** were situated at δ 2.71–2.90. The second difference was that the ^{1}H-signals of the protons at the Cp rings of **44** were much more upfield (δ from 4.03 – 4.12) than the phenyl proton ^{1}H-signals of the phenyl group of **45** (δ from 7.10 – 7.33). Moreover, the Cp-protons signals could be resolved into one singlet and two triplets, while the phenyl protons signals appeared as multiplet (Figure 4).

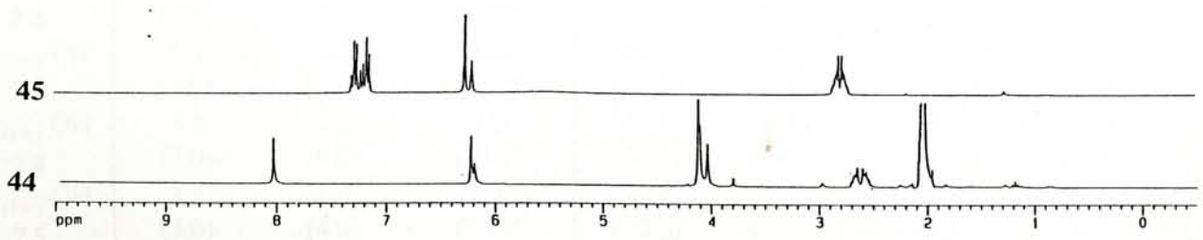

Figure 4. ^{1}H-NMR spectra of bridging fragments **44** and **45**.

Upon mono-*O*-alkylation of the ferrocenyl bridging fragment **44** with Gn-Br (n = 0 to 3), the three aromatic protons of the bridging 3,5-dihydroxyphenylethylene ring became non-equivalent and appeared as multiplets situated at δ 6.2–6.5. The singlet signal of the cyclopentadiene ring (Cp) still located at δ 4.11 while those of the mono-substituted Cp ring appeared as two triplets at δ 4.0 and 4.1 with a coupling constant of 2 Hz. The chemical shift values of this signal remained relatively constant throughout various generations while its intensity relative to the signals from protons of the surface group (*i.e.*, the *t*-Bu singlet at δ 1.2 or the two ArH doublets at δ 6.9 and δ 7.3) decreased with increasing generations. The ^{1}H-NMR signals arising from the polyether dendritic wedge could also be clearly identified at the expected regions. The relative integrations of the various signals arising from the polyether fragment to those of the bridging fragment were tabulated for both the ferrocenyl and phenyl substituted series (Table 1), and were in good agreement with the theoretical values.

Table 1. Chemical shift values and relative integration values of the various ^{1}H-NMR signals of the dendritic alcohols. Figures in brackets are the calculated values.

Compound	Bridging part			Polyether dendritic part			
	ArH	CH_2CH_2	Ph or Fc	Surface ^{t}Bu	Surface ArH	Brancher ArH	OCH_2
δ	6.4 - 6.2	2.8 - 2.5	7.4 - 7.1 4.1 - 4.0	1.3	7.4 – 6.8	6.2 - 6.1	4.2 - 4.1
$G0_{(Fc)}$-OH **68**	3.0 (3.0)	3.9 (4.0)	8.9 (9.0)	9.1 (9.0)	4.0 (4.0)	–	3.9 (4.0)
$G1_{(Fc)}$-OH **69**	3.1 (3.0)	4.2 (4.0)	9.5 (9.0)	18.8 (18.0)	8.1 (8.0)	3.0 (3.0)	11.9 (12.0)
$G2_{(Fc)}$-OH **70**	3.0 (3.0)	3.9 (4.0)	9.5 (9.0)	36.3 (36.0)	16.1 (16.0)	3.0 (3.0)	28.0 (28.0)
$G3_{(Fc)}$-OH **71**	3.0 (3.0)	4.2 (4.0)	9.5 (9.0)	72.6 (72.0)	32.0 (32.0)	3.0 (3.0)	59.8 (60.0)
$G0_{(Ph)}$-OH **72**	3.0 (3.0)	3.9 (4.0)	4.9 (5.0)*	9.2 (9.0)	3.9 (4.0)*	–	4.1 (4.0)
$G1_{(Ph)}$-OH **73**	3.1 (3.0)	4.2 (4.0)	5.4 (5.0)*	18.2 (18.0)	8.5 (8.0)*	3.0 (3.0)	12.1 (12.0)
$G2_{(Ph)}$-OH **74**	3.0 (3.0)	4.2 (4.0)	5.9 (5.0)*	36.5 (36.0)	17.0 (16.0)*	3.0 (3.0)	28.1 (28.0)
$G3_{(Ph)}$-OH **75**	3.1 (3.0)	4.1 (4.0)	6.1 (5.0)*	72.8 (72.0)	33.6 (32.0)*	3.0 (3.0)	60.6 (60.0)

*: The integration value included the ^{1}H-signal of $CHCl_3$ located at δ 7.26.

Attachment of the terpy moiety to the dendritic alcohols resulted in the immediate appearance of ^{1}H-NMR signals due to the terpy core (Table 2). Seven sets of proton signals were noted at δ 7.1 – 8.8 for both the two series. The label of the terpy protons are shown below:

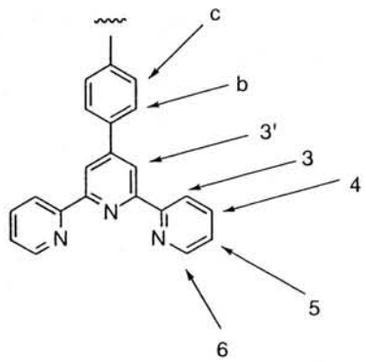

Table 2. Chemical shift of various terpy-protons. Figures in brackets are the multiplicities.

Compound	$H^{3'}$	H^3 and H^6	H^4	H^b	H^5	H^c
$G0_{(Fc)}$-terpy **36**	8.79 (s)	8.70 - 8.76 (m)	7.99 (dt)	7.90 (d)	7.46 (dt)	7.14 (d)
$G1_{(Fc)}$-terpy **37**	8.78 (s)	8.69 - 8.76 (m)	7.94 (dt)	7.83 (d)	7.41 (ddd)	7.10 (d)
$G2_{(Fc)}$-terpy **38**	8.79 (s)	8.69 - 8.75 (m)	7.95 (dt)	7.84 (d)	7.42 (dt)	7.10 (d)
$G3_{(Fc)}$-terpy **39**	8.79 (s)	8.69 - 8.73 (m)	7.94 (t)	7.84 (d)	7.46 (dt)	7.09 (d)
$G0_{(Ph)}$-terpy **40**	8.74 (s)	8.65 - 8.79 (m)	7.86 – 7.94 (m)*		7.37 (dd)	7.05 (d)
$G1_{(Ph)}$-terpy **41**	8.76 (s)	8.65 - 8.79 (m)	7.86 – 7.94 (m)*		7.38 (ddd)	7.06 (d)
$G2_{(Ph)}$-terpy **42**	8.76 (s)	8.65 - 8.79 (m)	7.86 – 7.95 (m)*		7.37 (ddd)	7.05 (d)
$G3_{(Ph)}$-terpy **43**	8.77 (s)	8.66 - 8.79 (m)	7.86 – 7.95 (m)*		7.38 (m)	7.05 (d)

*: The H^4 and H^b signals cannot be resolved due to overlapping with the Ph 1H-signals of the bridging fragment.

Upon complexation of the terpy ligands with Fe(II) ion, significant shifts of the ^{1}H-NMR signals on the terpy ring protons were noted. The stack plots of the ^{1}H-NMR spectra of the ferrocenyl and phenyl series metallodendrimers were shown in Figures 5 and 6. The relation integrations of the various regions agreed well with the theoretical values. Significant broadening of ^{1}H-NMR signals, however, were noted for the higher

generation G2 and G3 metallodendrimers in d^6-acetone, although sharp signals were still observed for the G0 and G1 metallodendrimers. Interestingly, the broadening of ^{1}H-NMR signals of the metallodendrimers was related to the solvent polarity. Hence, the signals of the highest generation G3 metallodendrimer were much sharper in d^6-DMSO than in d^6-acetone. We suggested that the broadening of ^{1}H-NMR signals in d^6-acetone was due to the formation of intermolecular aggregates, which was entropically more favorable in less polar solvents.

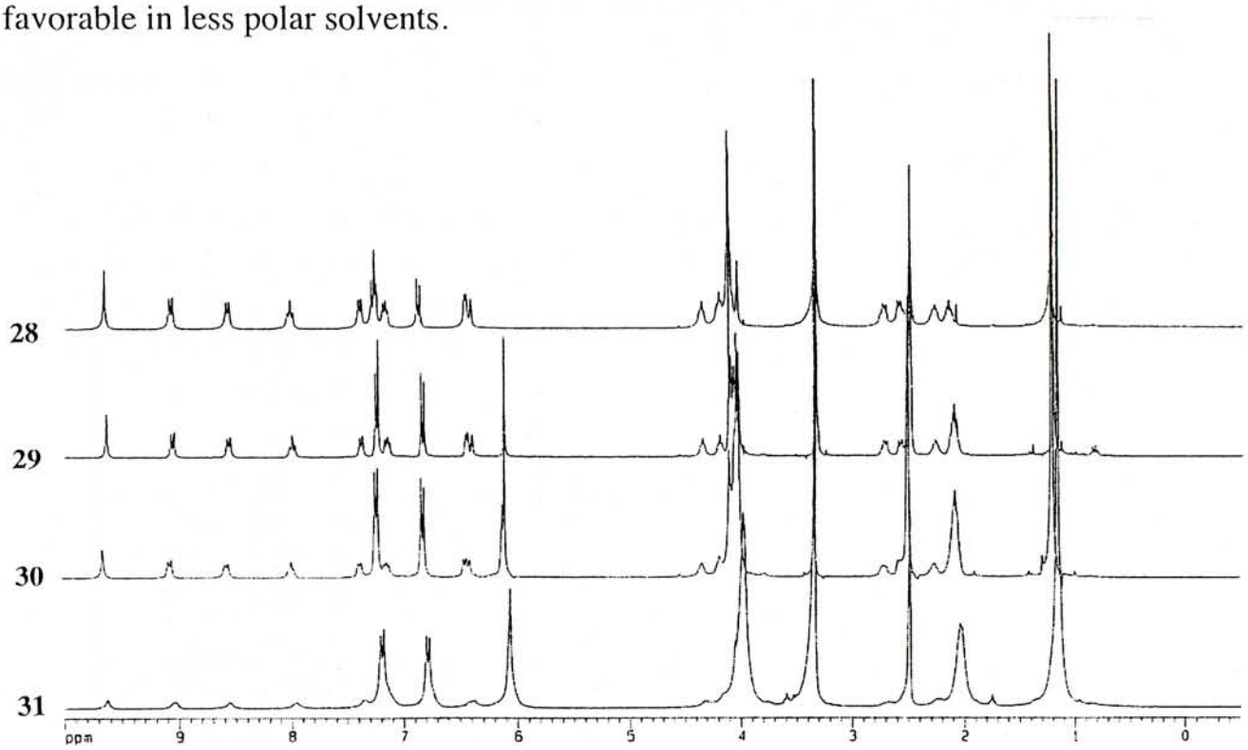

Figure 5. Stacked plot of the 1H-NMR spectra of the ferrocenyl series metallodendrimers **28**—**31**.

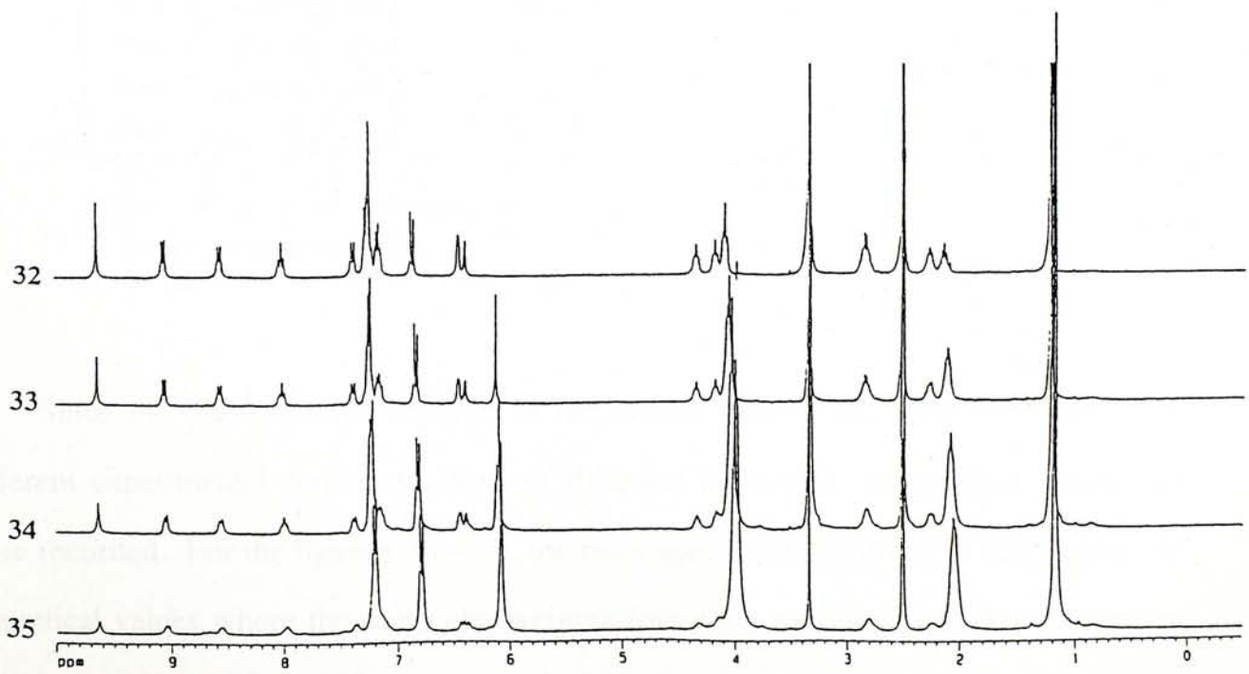

Figure 6. Stacked plot of the 1H-NMR spectra of the phenyl series metallodendrimers **32**—**35**.

(ii) Mass spectrometry analysis

Mass spectral analysis is an indispensable tool to determine the molecular weight of our compounds. Matrix-assisted laser desorption ionization (MADLI) technique turned out very useful in obtaining molecular ions of the dendrimers. Despite this, we were unable to obtain mass spectral data of some of the G3 dendrimers. Table 3 tabulated the results of the mass spectrometry data of the dendritic terpy ligands and the metallodendrimers.

Table 3. Mass spectral data of dendritic ligands and metallodendrimers.

Compound	Molecular peak observed	Theoretical value
$G0_{(Fc)}$-terpy **36**	878.3	878.3
$G1_{(Fc)}$-terpy **37**	1234.5	1233.5
$G2_{(Fc)}$-terpy **38**	1946.9*	1946.9
$G3_{(Fc)}$-terpy **39**	3371.9*	3371.7
$G0_{(Ph)}$-terpy **40**	770.4*	770.4
$G1_{(Ph)}$-terpy **41**	1126.6*	1126.6
$G2_{(Ph)}$-terpy **42**	1839.0*	1839.0
$G3_{(Ph)}$-terpy **43**	3264.0*	3263.8
$[Fe(G0_{(Fc)})_2](PF_6)_2$ **28**	905.3#	905.3
$[Fe(G1_{(Fc)})_2](PF_6)_2$ **29**	1262.5#	1262.5
$[Fe(G2_{(Fc)})_2](PF_6)_2$ **30**	— ✚	1973.8
$[Fe(G3_{(Fc)})_2](PF_6)_2$ **31**	3726.4♦	3725.8
$[Fe(G0_{(Ph)})_2](PF_6)_2$ **32**	1124.7♦	1124.5
$[Fe(G1_{(Ph)})_2](PF_6)_2$ **33**	1480.9♦	1480.7
$[Fe(G2_{(Ph)})_2](PF_6)_2$ **34**	2193.2♦	2193.1
$[Fe(G3_{(Ph)})_2](PF_6)_2$ **35**	3619.8♦	3619.9

*: $(M + H)^+$
#: $[M - 2PF_6]^{2+}$ doubly charged ion
✚: Molecular peak not found.
♦: [L + matrix (retinonic acid) + Fe – H]$^+$

Since the mass spectral analysis of the above compounds were obtained under different experimental conditions, ions of different molecular composition component were recorded. For the ligands **36**—**43**, the mass spectral data agreed strongly with the theoretical values where the molecular weights found are usually $(M + H)^+$. However, for the complexes **28** and **29**, the molecular ions obtained were the doubly charged ion

$\{Fe[Gn_{(Fc)}]_2\}^{2+}$. For the complexes **31 — 35**, the molecular ions observed were the corresponding terpy ligands which combined with one retinoic acid and an iron-ion.

(iii) Gel permeation analysis

In addition to mass spectral analysis, all dendritic ligands and complexes were characterized by gel permeation chromatography (GPC). Figures 7a and 7b showed the GPC chromatograms (UV detector) of the ferrocenyl ligands and the ferrocenyl containing metallodendrimers, respectively. While the profiles of the ligands were symmetrical, those of the metallodendrimers were broad and unsymmetrical. This could be due to the presence of metallodendrimer aggregates in THF. Metallodendrimers had been known to form aggregates in solvents of low polarity.[29] In fact, the ^{1}H-NMR signals of the G0 metallodendrimer in d_8-THF were broad, which was consistent with the presence of intermolecular aggregates. The GPC chromatograms of the phenyl series were shown in Figures 8a and 8b, and showed similar chromatographic profiles.

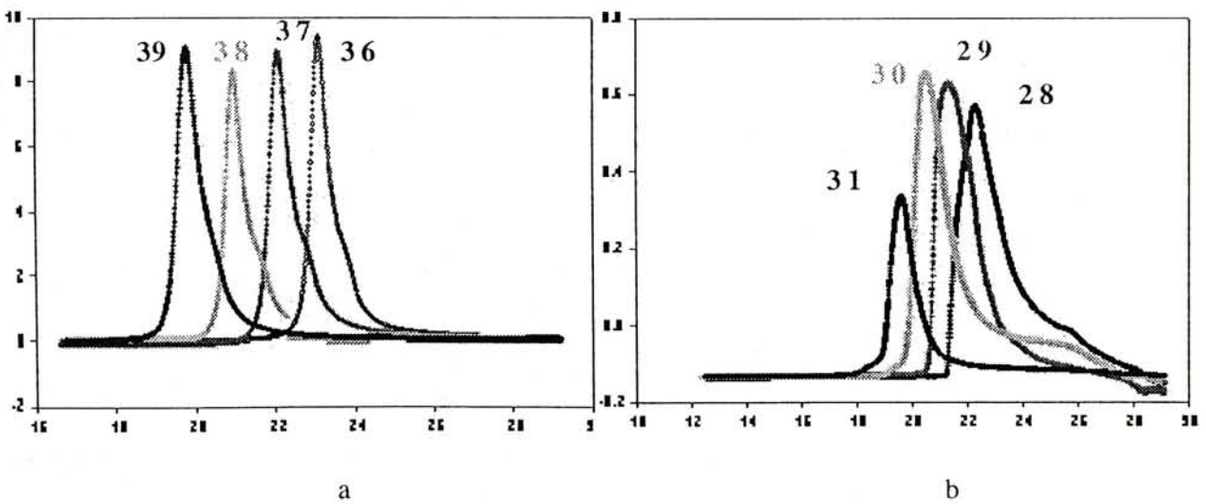

a b

Figure 7. GPC chromatograms for a) ferrocenyl ligands; b) ferrocenyl complexes.

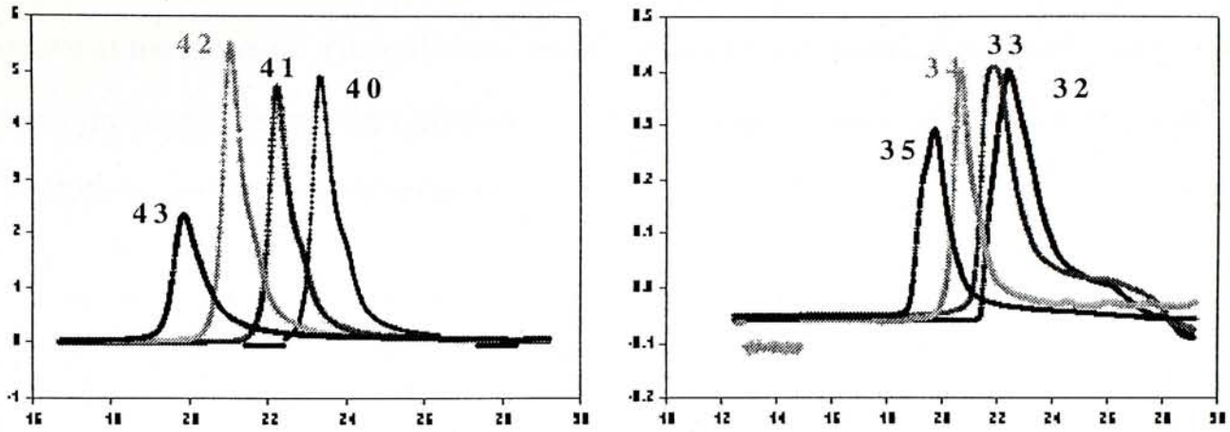

a b

Figure 8. GPC chromatograms for a) phenyl ligands; b) phenyl complexes.

The SEC estimated M_w of the dendritic species, based on polystyrenes as the internal standards, were tabulated (Table 4). It could be seen that the M_w values of the complexes **28**—**35** were consistently lower than the theoretical values, suggesting that metallodendrimers had highly compact structure. On the other hand, the G2 and G3

Table 4. Theoretical and calculated molecular weight of various ligands and complexes.

Compound	Retention time (min)	Calculated M_w	Theoretical M_w
$G0_{(Fc)}$-terpy **36**	23.104	696	877
$G1_{(Fc)}$-terpy **37**	22.145	1150	1233
$G2_{(Fc)}$-terpy **38**	20.889	2217	1946
$G3_{(Fc)}$-terpy **39**	19.720	4086	3373
$G0_{(Ph)}$-terpy **40**	23.333	618	769
$G1_{(Ph)}$-terpy **41**	22.187	1125	1126
$G2_{(Ph)}$-terpy **42**	20.995	2098	1838
$G3_{(Ph)}$-terpy **43**	19.789	3941	3263
$[Fe(G0_{(Fc)})_2](PF_6)_2$ **28**	22.256	1085	2100
$[Fe(G1_{(Fc)})_2](PF_6)_2$ **29**	21.330	1760	2813
$[Fe(G2_{(Fc)})_2](PF_6)_2$ **30**	20.571	2618	4238
$[Fe(G3_{(Fc)})_2](PF_6)_2$ **31**	19.608	4332	7087
$[Fe(G0_{(Ph)})_2](PF_6)_2$ **32**	22.393	1010	1885
$[Fe(G1_{(Ph)})_2](PF_6)_2$ **33**	21.267	1741	2597
$[Fe(G2_{(Ph)})_2](PF_6)_2$ **34**	20.611	2564	4022
$[Fe(G3_{(Ph)})_2](PF_6)_2$ **35**	19.665	4205	6872

terpy ligands appeared to have much higher M_w values, for reasons that are still unknown at the moment. Nevertheless, scatter plots of the theoretical molecular weight (in logarithm scale) against the retention time showed a good linear relationship for both the complexes and the ligands series (Figure 9).

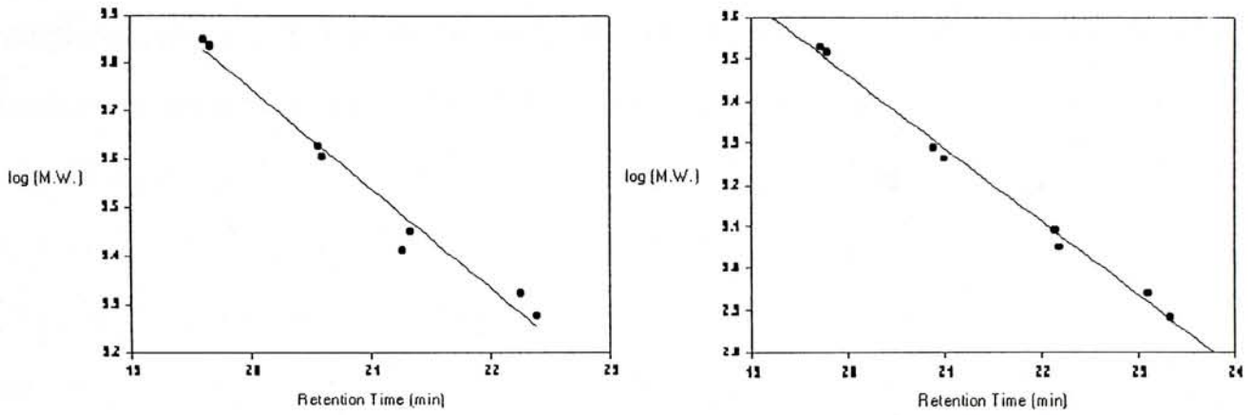

a b

Figure 9. Log(M.W.) against the retention time for the both series of: a); complexes b) ligands.

5. Conclusion

Two series of Fe(II)-containing metallodendrimers, one having a ferrocenyl bridging unit and the other a phenyl bridging unit, were prepared. These compounds were assembled by connecting a terpy ligand and a polyether dendritic fragment to the bridging unit by Williamson ether synthesis reactions. The structural identities of all compounds were characterized by ^{1}H- and ^{13}C-NMR spectroscopy and mass spectrometry. Their structural purities and molecular mass data were also evaluated by gel permeation chromatography. All the analytical results were consistent with the molecular structures of the metallodendrimers and the intermediates.

Chapter III. Physical and Electrochemical Properties

1. Physical appearance and solubility properties

The phenyl series of dendrimers, apart from those of the Fe(II)–bis(terpy) complexes, are colorless solids or glassy oils. On the other hand, the ferrocenyl series of dendrimers, apart from those of the Fe(II)–bis(terpy) complexes, exist as brown solids or oils. However, the Fe(II)–bis(terpy) complexes of both series appear as purple solids or powders, and give deep purple solutions in acetone, chloroform, THF and other polar solvents. The solubility properties of both the free dendritic ligands and the complexes are different from ordinary small ligands and their corresponding Fe(II)–bis(terpy) complexes reported in the literature. All higher generation dendritic ligands synthesized are extremely soluble in solvents such as ethyl acetate, acetone, dichloromethane and chloroform, but not in polar protic solvents such as alcohols. For the dendritic Fe(II)–bis(terpy) complexes, all of them are insoluble in alcoholic solvents such as methanol and ethanol yet they are extremely soluble in chlorinated solvents. This is because the introduction of a large number of the *t*-butylphenyl group on the dendrimer enhances the solubility of the resulting dendritic complexes in organic solvents.[30] Moreover, the hydrophobic environment surrounding the metal complexes may cause the counter anions (PF_6^-) to bind tightly near the central metal cation and form a tight ion pair which is surrounded by the dendritic envelope. The ionic nature of these supramolecules in solution is thus masked and leads to a dramatic change in their solubility behavior.

2. Cyclic voltammetry studies

One of the major objectives in this study is to investigate the electrochemical behavior of dendrimers having multiple redox centres. The electrochemical property of the dendrimers was studied by cyclic voltammetry technique. Cyclic voltammetry (CV) is potential-controlled "reversal" electrochemical experiment.[31] A cyclic potential sweep is applied to an electrode and the current response is observed. The electrochemical

reaction of interest takes place at the working electrode. Due to the electron transfer process, an electrical current is obtained at the working electrode. An auxiliary electrode is also present which is driven by the potentiostatic circuit in order to balance the electric current generated at the working electrode.[32]

Figure 10 shows the profile of a CV current response for a typical reduction process. During the forward potential sweep, the oxidized form is reduced; while on the reverse sweep, the reduced form near the electrode is reoxidized. In a single, reversible electron transfer process, the following characteristics are noted:

(1) The difference between the cathodic and anodic peak potentials is around 57—60 mV. However, it is rarely observed in actual experiment because of distortions due to solution resistance effects.

(2) The difference between the initial sweep peak and half-peak potentials of the forward sweep is about 56 mV/n.

(3) The square root of the scan rate should be proportional to the forward scan peak current .

(4) The shift ratio of the cathodic to anodic current should be equal to one.

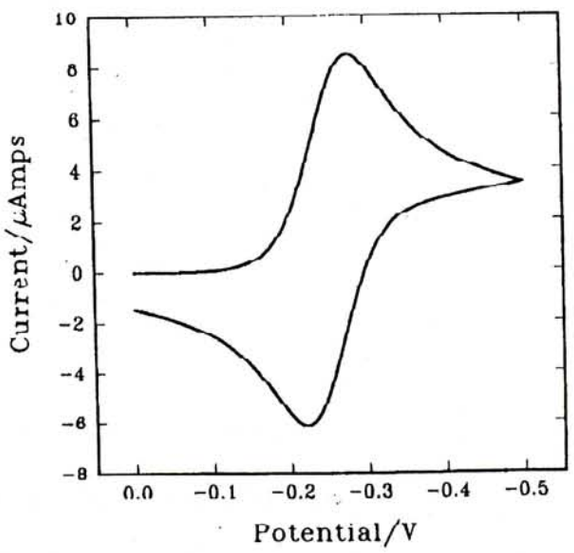

Figure 10. A typical CV current response for a redox active species.

If the rate of electron transfer is not rapid enough to maintain equilibrium concentrations of the redox couple species near the electrode surface, the peak wave will shift to more negative potentials in the case of reduction and to more positive potentials in the case of an oxidation. If the cathodic and the anodic peaks are well separated, in such cases an irreversible redox process is observed.

The electrochemical cell used in our study is shown in Figure 11. A glassy carbon working electrode, a silver wire reference electrode and a platinum wire auxiliary electrode were used. The CV experiment was conducted at the scan rate of 100 mV/s in freshly distilled dry CH_2Cl_2 with 0.2 M of tetrabutylammonium tetrafluoroborate (TBAT) as the electrolyte at room temperature. The sample was degassed to get rid of trace amount of oxygen prior to the experiment.

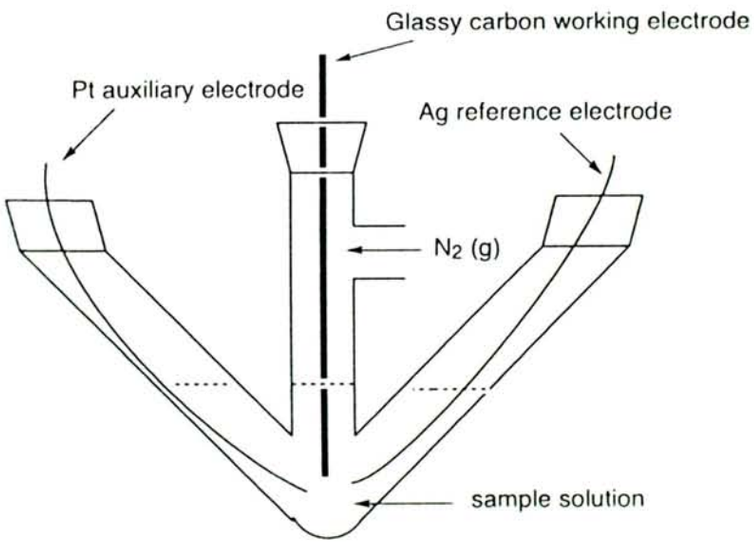

Figure 11. Experimental setup of CV studies.

The cyclic voltammograms of ferrocenyl-based $[Fe(Gn_{(Fc)})_2](PF_6)_2$ **28**—**31** and that of the phenyl-based $[Fe(Gn_{(Ph)})_2](PF_6)_2$ **32**—**35** metallodendrimers are shown (Figure 12—15). For both series of compounds, one oxidative wave corresponding to the Fe(II) to Fe(III) arising from the $Fe(terpy)_2$ moiety at about +1.0 V and two terpy-based reductive processes at −1.3 V and −1.5 V were noted (Table 5). For the ferrocenyl-based compounds, an additional oxidative wave corresponding to the

oxidation of Fe(II) to Fe(III) resulting from the ferrocenyl moiety at +0.3 V was also observed. These figures were similar in magnitude to those of $Fe(terpy)_2$ and mono-substituted $FeCp_2$ derivatives. As shown in Table 5, the redox potential values of the same redox process were essentially identical for the two different series, and were also close to values reported for our previous series of Fe(II)–bis(terpy) metallodendrimers **15** — **17** without the bridging fragment. Therefore the addition of either the phenyl or ferrocenyl appendage does not alter the redox properties of the Fe(II)–bis(terpy) centers.[12]

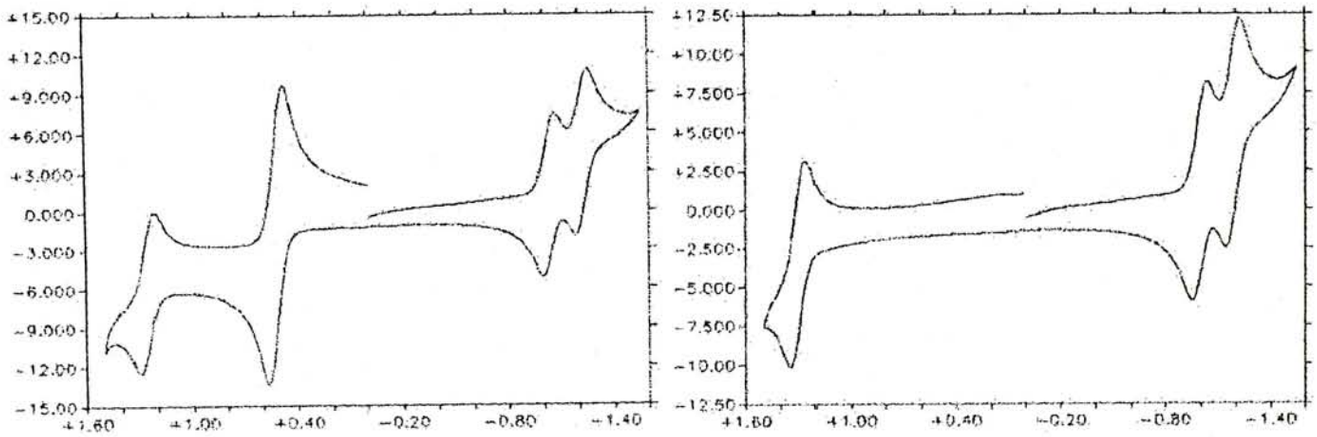

a b

Figure 12. Cyclic voltammograms of metallodendrimers a) **28**; b) **32**. (Scan rate = 100mV/s, solvent = dichloromethane, standard = ferrocenealdehyde, **59**)

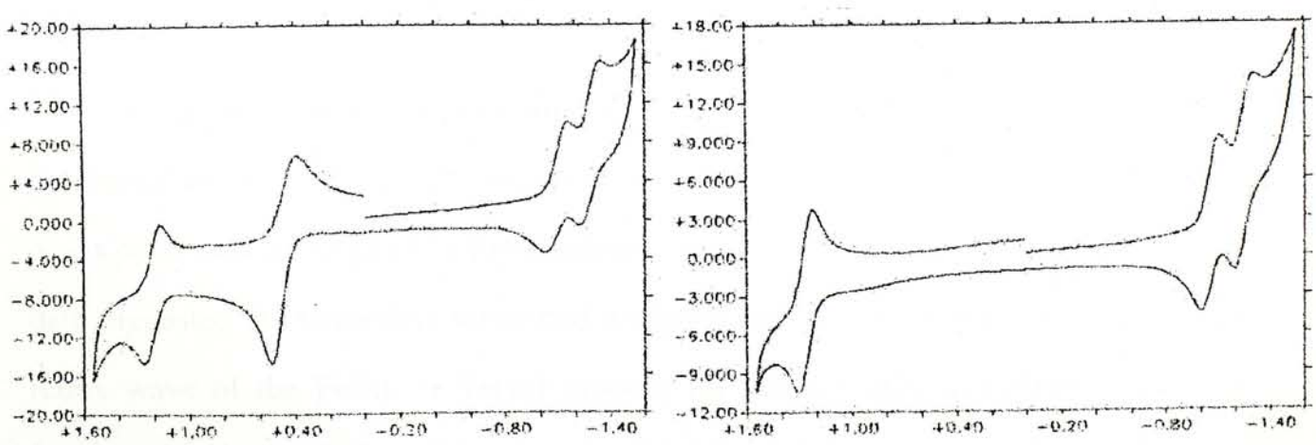

a b

Figure 13. Cyclic voltammograms of metallodendrimers a) **29**; b) **33**. (Scan rate = 100mV/s, solvent = dichloromethane, standard = ferrocenealdehyde, **59**)

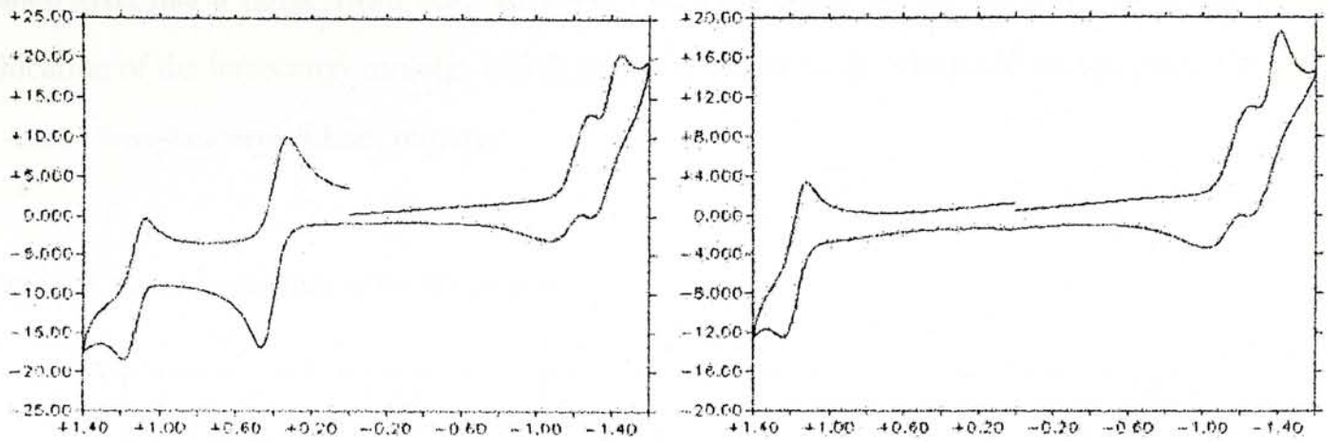

a b

Figure 14. Cyclic voltammograms of metallodendrimers a) **30**; b) **34**. (Scan rate = 100mV/s, solvent = dichloromethane, standard = ferrocenealdehyde, **59**)

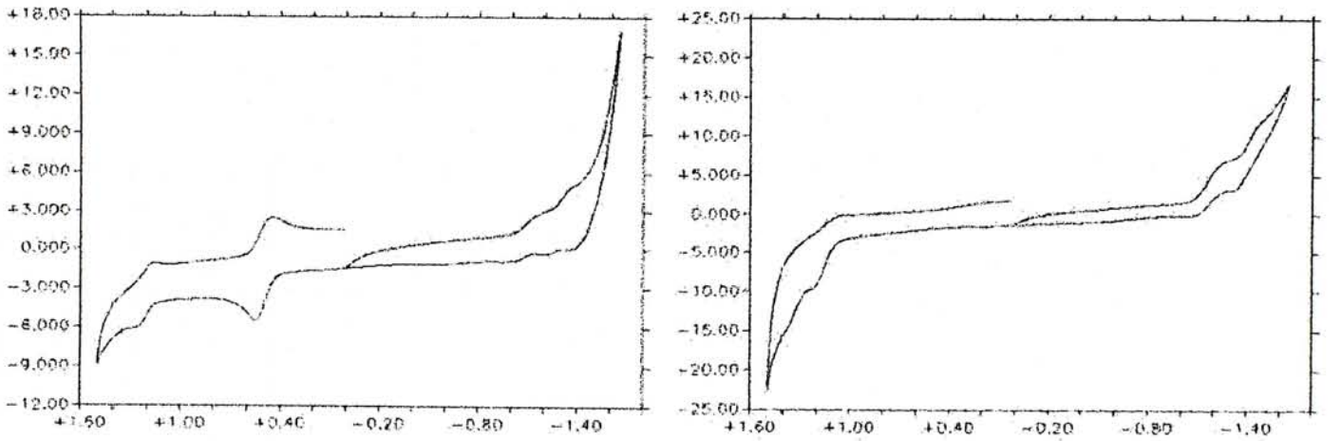

a b

Figure 15. Cyclic voltammograms of metallodendrimers a) **31**; b) **35**. (Scan rate = 100mV/s, solvent = dichloromethane, standard = ferrocenealdehyde, **59**)

In agreement with previous findings by others[33] and us, the peak separations increase gradually as the generation grows up. This is in accord with the notion that the redox processes are clogged by the insulating dendritic shell. A close examination of the data suggested the ferrocenyl series had a slightly better redox reversibility. Hence, the redox wave of the Fe(II) → Fe(III) process for the G3 was still observable for the ferrocenyl series while that of the phenyl series was completely irreversible and could not be observed. An additional interesting finding was that the reversibility of the ferrocenyl appendage belonging to the ferrocenyl series was only slightly affected by the dendritic

shell (ΔE has a range from 0.95 to 1.44 V). This could be due to the "off center" location of the ferrocenyl moiety, which makes it closer to the electrode surface than the "core" iron-bis(terpyridine) moiety.

Table 5. Experimental data of the CV studies.

	Ferrocenyl series			Phenyl series			Without bridging fragment	
	$E_{1/2}$ (V)	ΔE (mV)		$E_{1/2}$ (V)	ΔE (mV)		$E_{1/2}$ (V)	ΔE (mV)
G0	1.02	95	**G0**	–	–	**G0**	–	–
	0.29	82		1.03	88		1.03	80
	-1.26	67		-1.27	87		-1.27	80
	-1.45	72		-1.45	82		-1.38	70
G1	1.03	95	**G1**	–	–	**G1**	–	–
	0.29	100		1.03	86		1.02	130
	-1.31	120		-1.29	108		-1.29	110
	-1.46	108		-1.48	114		-1.48	120
G2	1.03	111	**G2**	–	–	**G2**	–	–
	0.29	139		1.04	127		1.02	200
	-1.28	221		-1.28	238		-1.29	140
	-1.44	221		-1.46	172		-1.47	130
G3	1.02	144	**G3**	–	–	**G3**	–	–
	0.30	101		_*	_*		_*	_*
	_*	_*		_*	_*		_*	_*
	_*	_*		_*	_*		_*	_*

*: Poorly resolved signal, no peak difference is reported.

Chapter IV. Summary

Two series of the iron-containing terpyridine-based electrochemically active dendrimers ferrocenyl or phenyl bridging group were synthesized. All these dendritic ligands and their complexes were characterized by the ^{1}H- and ^{13}C-NMR, elemental analysis, mass spectroscopy and gel permeation chromatography.

In cyclic voltammetry studies, we found that the introduction of an electrochemically active ferrocenyl group to the dendritic complexes does not affect the redox potential of the central Fe(II)—bis(terpy) core. The redox reversibility of the central Fe(II)—bis(terpyridine) moiety of both series decreased gradually with increasingly dendrimer generation. However, the redox process of "off center" ferrocenyl moiety belonging to the ferrocenyl series was only slightly affected by the dendritic shell, suggesting this unit was closer to the electrode surface than the "core" Fe(II)—bis(terpyridine) moiety.

Chapter V. Experimental

General. Melting points were measured on a Reichert Microscope apparatus and are uncorrected. ^{1}H-NMR (300 MHz) and ^{13}C-NMR (75.47MHz) spectra were recorded on a Brüker Advance DPX 300 spectrometer. All NMR measurements were carried out at room temperature. Chemical shifts are reported as parts per million in delta scale downfield from TMS. Coupling constant (*J*) are reported in hertz. Mass spectra were obtained on a Brüker APEX 47e FTMS spectrometer with liquid secondary-ion mass spectrometry (L-SIMS), electron spray ionization (ESI), fast atom bombardment (FAB) or atmospheric pressure chemical ionization (APCI) techniques. The reported molecular mass (*m/z*) values, unless otherwise stated, were the most abundant monoisotopic mass. Elemental analysis was carried out at either Shanghai Institute of Organic Chemistry, Academic Sinica, China or at MEDAC Ltd., Brunel Science Center, Surrey, United Kingdom. Cyclic voltammetry studies were carried out on a model BAS CV50W cyclic voltammeter; 0.2 M of tetrabutylammonium tetrafluoroborate (TBAT) was used as supporting electrolyte. Gel permeation chromatographic analyses (Styragel HR 3, HR 2 and HR 1 columns; 7.8 × 300 mm in series) were carried out in THF (freshly distilled from $CaCl_2$) on Waters 510 HPLC pump equipped with a Waters 486 tunable absorbance detector.

All non-aqueous reactions were carried out under dry nitrogen atmosphere with oven-dried (115 °C) glassware. The reactions were monitored by thin layer chromatography (TLC) performed on Merck precoated aluminum oxide $60F_{254}$ neutral plates or Merck precoated silica gel $60F_{254}$ plates, and compounds were visualized with a spray of 5 % w/v dodecamolybdophosphoric acid in ethanol with heating. Flash chromatography was carried out either on columns of Macherey Nagel silica gel 60 (230–400 mesh) or Merck neutral aluminum oxide 90 (70–200 mesh). Unless otherwise stated, all chemicals were purchased from commercial suppliers and used without further purification. All solvents were reagent grade. Dichloromethane was distilled from CaH_2 and stored over 4 Å molecular sieves.

Tetrahydrofuran (THF) was freshly distilled from sodium/benzophenone ketyl under nitrogen.

Methyl 3,5-dibenzyloxybenzoate (56). A mixture of methyl 3,5-dihydroxybenzoate (10.0 g, 50 mmol), benzyl bromide (14.8 mL, 124 mmol), potassium carbonate (27.6 g, 200 mmol) was stirred under nitrogen at 25 °C for 48 h. The mixture was then filtrated and the filtrate was concentrated on rotary evaporator. The residue was purified by flash chromatography on silica gel (hexane/EtOAc = 20/1) to afford the ester **56** as a white solid (15.7 g, 90 %), R_f 0.60 (hexane/EtOAc = 3/1); m.p. 67–68 °C; ^{1}H-NMR ($CDCl_3$) 3.92 (3H, s, CO_2CH_3), 5.08 (4H, s, OCH_2), 6.82 (1H, t, J = 2.4, ArH), 7.32 (2H, d, J = 2.4, ArH), 7.34–7.48 (10H, m, ArH); ^{13}C-NMR ($CDCl_3$) 52.2 (CH_3), 70.2 (OCH_2), 107.2, 108.3, 127.5, 128.1, 128.6, 132.0, 136.4, 159.7, 166.7 (CO_2); MS (L-SIMS, *m/z*) 349.1 ($M + H^+$, 100 %). Anal. Calcd for $C_{22}H_{20}O_4$: C, 75.85; H, 5.79. Found: C, 75.98; H, 5.81 %.

3,5-Dibenzyloxybenzyl alcohol (57). Lithium aluminum hydride powder (1.0 g, 27 mmol) was added to a stirred solution of the ester **56** (7.85g, 22.5 mmol) in THF at 0 °C. The reaction mixture was allowed to stir under nitrogen at 20 °C for another 2 h. The reaction was monitored by thin layer chromatography until all the starting material was consumed. The excess hydride was destroyed with ice-water. The product was extracted with ethyl acetate (3 × 100 mL) dried ($MgSO_4$) and filtered. After removal of the solvent on a rotary evaporator, the target product **57** was obtained as a white solid (6.64 g, 92 %), R_f 0.33 (hexane/EtOAc = 2/1); 79–82 °C; ^{1}H-NMR ($CDCl_3$) 1.60–1.90 (1H, br s, OH)4.63 (2H, s, CH_2OH), 5.04 (4H, s, OCH_2Ph), 6.56 (1H, t, J = 2.1, ArH), 6.63 (2H, d, J = 1.5, ArH), 7.27–7.46 (10H, m, ArH); ^{13}C-NMR ($CDCl_3$) 65.2 (C-OH), 70.0 (OCH_2Ph), 101.2, 105.7, 127.5, 128.0, 128.5, 136.8, 143.4, 160.1; MS (L-SIMS, *m/z*) 321.1 [$(M + H)^+$, 100 %]. Anal. Calcd for $C_{21}H_{20}O_3$: C, 78.73; H, 6.29. Found: C, 78.45; H, 6.30 %.

3,5-Dibenzyloxybenzyl bromide (58). A mixture of the benzyl alcohol **57** (20 g, 64 mmol), carbon tetrabromide (49 g, 150 mmol) and triphenylphosphine (39 g, 150 mmol) was stirred under nitrogen in THF at 20 °C for 4 hours. The reaction mixture was filtrated through celite and the filtrate was concentrated on rotary evaporator. The crude product was purified by flash chromatography on silica gel (hexane/EtOAc = 25/1) afforded the bromide **58** (23.2 g, 40 %) as a white solid, R_f 0.64 (hexane/EtOAc = 3/1); m.p. 84–86 °C; ^{1}H-NMR ($CDCl_3$) 4.42 (2H, s, CH_2Br), 5.04 (4H, s, OCH_2Ph), 6.57 (1H, t, J = 2.4, ArH), 6.66 (2H, d, J = 2.1, ArH), 7.30–7.48 (10H, m, ArH); ^{13}C-NMR ($CDCl_3$) 33.6 (*C*-Br), 70.1 (OCH_2), 102.1, 108.1, 127.5, 128.1, 128.6, 136.6, 139.7, 160.0; MS (L-SIMS, *m/z*) 385 [$(M + H)^+$, 100 %]. Anal. Calcd for $C_{21}H_{19}O_2Br$: C, 65.81;H, 5.00. Found: C, 65.97;H, 5.15 %.

3,5-Dibenzyloxybenzyltriphenylphosphonium bromide (46). A mixture of the bromide **58** (18 g, 47 mmol) and triphenylphosphine (19 g, 71 mmol) was heated to reflux in anhydrous toluene(200 mL) for 12 h. The desired phosphonium salt **46** was precipitated out from the solution as a white solid. The white phosphonium salt was then collected by suction filtration and air dried (25 g, 80 %); m.p. 220–222 °C; ^{1}H-NMR ($CDCl_3$) 5.10 (4H, s, OCH_2Ph), 5.32 (2H, d, J = 14.1, $ArCH_2P$), 6.49 (2H, t, J = 2.4, ArH), 6.90 (1H, d, J = 2.1, ArH), 7.52–7.68 (10H, m, ArH), 7.90–8.25 (15H, m, PhH); ^{13}C-NMR ($CDCl_3$) 31.0 (d, J = 47), 70.0, 103.0 (d, J = 4), 110.3 (d, J = 6), 118.1 (d, J = 86), 127.6, 127.9, 128.5, 129.2 (d, J = 9), 130.1 (d, J = 13), 134.4 (d, J = 10), 136.5, 159.8 (d, J = 3); MS (L-SIMS, *m/z*) 565.2 [$(M - Br)^+$, 90 %]. Anal. Calcd for $C_{39}H_{34}O_2PBr$: C, 72.56; H, 5.31. Found: C, 72.73; H, 5.33 %.

(*E*)-1-(3',5'-Dibenzyloxyphenyl)-2-ferrocenylethene (60). Sodium hydride (60 % dispersion in mineral oil, 0.1 g, 1.9 mmol) was added in small portions to a solution of the phosphonium salt **46** (1.2 g, 1.9 mmol) in THF (15 mL). After all the

hydride was added, ferrocenealdehyde **59**[26] (0.4 g, 1.9 mmol) was added. The reaction mixture was allowed to stir under nitrogen at 20 °C for 36 h. The reaction was monitored by thin layer chromatography until the starting material was completely reacted. The mixture was then filtrated and concentrated on a rotary evaporator. The crude product was purified by flash chromatography on silica gel (hexane/EtOAc = 35/1) to afford the ferrocenyl olefin **60** as an orange crystalline solid, which was recrystallized from diethyl ether (0.38 g, 40 %), R_f 0.53 (hexane/EtOAc = 10/1); m.p. 119–122 °C; ^{1}H-NMR (d^6-acetone) 4.13 (5H, s, CpH), 4.30 (2H, t, J = 1.8, CpH), 4.52 (2H, t, J = 1.8, CpH), 5.14 (4H, s, OCH_2Ph), 6.57 (1H, t, J = 2.1, ArH), 6.73 (1H, d, J = 16.2, *HC*=C*H*), 6.78 (2H, d, J = 2.1, ArH), 7.02 (1H, d, J = 16.2, *HC*=C*H*), 7.24–7.52(10H, m, PhH); ^{13}C-NMR (d^6-acetone) 67.7 (CpC), 68.8 (OCH_2Ph), 69.9 (CpC), 70.4(CpC), 84.1 (CpC), 101.5, 105.8, 126.6 (H*C*=CH), 128.4, 128.5 (HC=*C*H), 129.2, 138.4, 141.1, 161.2; MS (L-SIMS, *m/z*) 500.1 [$(M+H)^+$, 100 %]. Anal. Calcd for $C_{32}H_{28}O_2Fe$: C, 76.81; H, 5.64. Found: C, 76.93; H, 5.64 %.

1-(3',5'-Dihydroxylphenyl)-2-ferrocenylethane (44). A mixture of the olefin **60** (0.32 g, 0.64 mmol) and 10 % palladium on charcoal (32 mg) in ethanol/EtOAc mixture (4/1 v/v, 10 mL) was stirred under hydrogen at 20 °C for 3 h. The mixture was then filtered and concentrated on a rotary evaporator. The crude product was purified by flash chromatography on silica gel (hexane/EtOAc = 9/1) to afford the target compound **44** as a yellow oil (0.20 g, 95 %), R_f 0.50 (hexane/EtOAc = 1/1); ^{1}H-NMR (d^6-acetone) 2.51–2.72 (4H, m, H_2CCH_2Cp), 4.03 (2H, t, J = 7.5, CpH), 4.11 (2H, s, CpH), 4.12 (5H, s, CpH), 6.19 (1H, s, ArH), 6.22 (2H, s, ArH), 8.04 (2H, s, OH), ^{13}C-NMR (d^6-acetone) 32.1, 38.0, 67.8 (CpC), 68.8 (CpC), 69.2 (CpC), 89.7 (CpC), 101.0, 107.6, 145.4, 159.3 (*C*-OH); HRMS calcd for $C_{18}H_{18}O_2Fe$: 322.0656, found: 322.0661. Anal. Calcd for $C_{18}H_{18}O_2Fe$: C, 67.10; H, 5.63. Found: C, 67.69; H, 5.60 %.

(*E*)-1-(3',5'-Dibenzyloxyphenyl)-2-phenylethene (62). The phosphonium salt **46** (3.04 g, 4.7 mmol) was added into THF (30 mL), followed by addition of sodium hydride (60 % dispersion in mineral oil, 0.28 g, 7.1 mmol) into the suspension. After all the hydride was added, benzaldehyde **61** (0.48 g, 4.7 mmol) was added. The reaction mixture was allowed to stir under nitrogen at 20 °C for 36 h. The reaction was monitored by thin layer chromatography until the aldehyde was completely reacted. The mixture was then filtered and concentrated on a rotary evaporator. The crude product was purified by flash chromatography on silica gel (hexane/EtOAc = 35/1) to afford the olefin **62** as a white crystalline solid, which was recrystallized with diethyl ether (0.415 g, 23 %), R_f 0.53 (hexane/EtOAc = 10/1); m.p. 113–115 °C; ^{1}H-NMR ($CDCl_3$) 5.09 (4H, s, OCH_2Ph), 6.58 (1H, t, J = 2.1, ArH), 6.80 (2H, d, J = 2.1, ArH), 7.07 (2H, dd, J = 16.5, 4.2, *H*C=C*H*), 7.24–7.54 (15H, m, PhH); ^{13}C-NMR ($CDCl_3$) 70.1 (OCH_2Ph), 101.5 (H*C*=CH), 105.8 (HC=*C*H), 126.6, 127.6, 127.7, 128.0, 128.5, 128.6, 129.3, 136.8, 137.1, 139.4, 160.1; MS (L-SIMS, *m/z*) 392.2 (M^+, 100 %). Anal. Calcd for $C_{28}H_{24}O_2$: C, 85.68; H, 6.16. Found: C, 85.74; H, 6.18 %.

1-(3',5'-Dihydroxylphenyl)-2-phenylethane (45). A suspension of the olefin **62** (1.47 g, 3.75 mmol) and 10 % palladium on charcoal (0.15 g) in ethanol/EtOAc mixture (4/1 v/v, 20 mL) was stirred under hydrogen at 20 °C for 3 h. The mixture was then filtered and concentrated on a rotary evaporator. The crude product was purified by flash chromatography on silica gel (hexane/EtOAc = 9/1) to afford the phenyl olefin **45** as a pale yellow oil (0.78 g, 3.63 mmol), R_f 0.50 (hexane/EtOAc = 1/1); ^{1}H-NMR ($CDCl_3$) 2.71–2.90 (4H, m, H_2CCH_2), 6.21 (1H, s, ArH), 6.27 (2H, s, ArH), 7.10–7.33 (5H, m, PhH), ^{13}C-NMR ($CDCl_3$) 37.2 (H_2CCH_2), 37.6 (H_2CCH_2), 100.6, 108.3, 125.9, 128.3, 128.4, 141.5, 145.0, 156.3 (*C*–OH); HRMS calcd for $C_{14}H_{14}O_2$: 214.0994, found: 214.0986.

4'-(*p*-Hydroxy)phenyl-2,2':6',2"-terpyridine (66).[34] A mixture of 4'-(*p*-methoxy)phenyl-2,2':6',2"-terpyridine **64**[23] (2.0 g, 6.0 mmol), hydrogen bromide (20 mL) and acetic acid (20 mL) was heated at 130 °C for 5 h. An aqueous NaOH solution (20 %, 30 mL) was added to adjust the pH value of the reaction mixture to about 7 and the mixture was stirred for another 1 h. The precipitate was collected and washed with hexane to give the target compound **66** (1.8 g, 95 %) as a gray solid; R_f 0.23 (hexane/EtOAc = 5/2); m.p. 305–307 °C. lit. 285–290 °C; ^{1}H-NMR (d^6-DMSO) 3.3–3.5 (1H, br s, O*H*), 7.01 (2H, d, *J* = 8.7, H^c), 7.56 (2H, ddd, *J* = 1.8, 3.9, 6.6, H^5), 7.82 (2H, d, *J* = 8.7, H^b), 8.06 (2H, dt, *J* = 1.8, 7.8, H^4), 8.69 (2H, d, *J* = 7.8, H^3), 8.69 (2H, s, $H^{3'}$), 8.79 (2H, d, *J* = 6.0, H^6).

4'-(*p*-(3-Bromopropoxy)phenyl-2,2':6',2"-terpyridine (67). A mixture of 4'-(p-hydroxy)phenyl-2,2':6',2"-terpyridine **66** (1.24 g, 3.81 mmol), 1,3-dibromopropane (1.94 mL, 19.1 mmol) and powdered potassium carbonate (1.58 g, 11.4 mmol) in acetone (50 mL) was heated under reflux for 48 h. The reaction mixture was cooled and filtered. After concentration of the filtrate on a rotary evaporator, the crude product was distilled under reduced pressure to get rid of the excess 1,3-dibromopropane. Flash chromatography of the residue on alumna (hexane/EtOAc = 35/1) gave the bromide **67** as a white solid (1.29 g, 76 %), R_f 0.57 (hexane/EtOAc = 4/1); m.p. 161–162 °C; ^{1}H-NMR ($CDCl_3$) 2.37 (2H, quintet, *J* = 6.0, $CH_2CH_2CH_2$), 3.65 (2H, t, *J* = 6.3, CH_2Br), 4.19 (2H, t, *J* = 5.7, OCH_2), 7.04 (2H, d, *J* = 8.7, H^e), 7.36 (2H, ddd, *J* = 1.8, 3.9, 6.6, H^5), 7.83–7.92 (4H, m, H^b and H^4), 8.63–8.76 (6H, m, $H^{3'}$, H^3 and H^6); ^{13}C-NMR ($CDCl_3$) 29.9 ($CH_2CH_2CH_2$), 32.3 (CH_2Br), 65.4 (OCH_2), 114.8(C^c), 118.3($C^{3'}$), 121.4(C^3), 123.8(C^5), 128.6(C^b), 131.0(C^a), 136.9(C^4), 149.1(C^6), 149.7($C^{4'}$), 155.8(C^2), 156.3($C^{2'}$), 159.6(C^d); MS (L-SIMS, *m/z*) 446.1 [$(M + H)^+$, 100 %]. Anal. Calcd for $C_{24}H_{20}ON_3Br$: C, 64.58; H, 4.52; N, 9.41. Found: C, 64.77; H, 4.70; N, 9.12 %.

General procedure for the synthesis of ferrocenyl dendrons for $Gn_{(Fc)}$-OH (n = 0–3) 68, 69, 70, 71. A mixture of dendritic bromide Gn-Br (0.9 mol equiv.),

1-(3',5'-dihydroxylphenyl)-2-ferrocenylethane **44** (1 mol equiv.), potassium carbonate (3 mol equiv.) and 18-crown-6 (0.1 mol equiv.) was refluxed in acetone. The reaction time required was 18, 20, 24 and 36 h for G0 to G3 respectively. The reaction mixture was cooled and filtered. After concentration of the filtrate on a rotary evaporator, the crude product was purified as described in the following text.

$G0_{(Fc)}$-OH (68). Flash chromatography of the crude product on silica gel (hexane/EtOAc = 20/1) afforded the target compound **68** (72 %) as a yellow oil, R_f 0.34 (hexane/EtOAc = 5/1); ^{1}H-NMR (d^6-acetone) 1.28 (9H, s, ^{t}Bu), 2.20 (2H, quintet, J = 6.3, CCH_2C), 2.55–2.76 (4H, m, H_2CCH_2Cp), 4.02 (2H, t, J = 1.8, CpH), 4.09 (2H, t, J = 1.8, CpH,), 4.11 (5H, s, CpH), 4.13 (2H, t, J = 7.0, OCH_2), 4.15 (2H, t, J = 6.3, OCH_2), 6.28 (1H, t, J = 2.1, ArH), 6.33 (2H, t, J = 1.8, ArH), 6.88 (2H, d, J = 9.0, ArH), 7.31 (2H, d, J = 8.7, ArH), 8.19 (1H, s, OH); ^{13}C-NMR (d^6-acetone) 30.1 ($CH_2CH_2CH_2$), 31.8 (CH_3), 32.1, 34.5 (CMe_3), 38.2, 65.0 (OCH_2), 65.2 (OCH_2), 67.7 (CpC), 68.7 (CpC), 69.1 (CpC), 89.4 (CpC), 100.3, 106.7, 108.8, 114.7, 126.9, 143.7, 145.4, 157.6, 159.2, 161.0; MS (FAB, m/z) 513 (M^+, 100 %). Anal. Calcd for $C_{31}H_{36}O_3Fe$: C, 72.66; H, 7.08. Found: C, 72.94; H, 7.38 %.

$G1_{(Fc)}$-OH (69). Flash chromatography of the crude product on silica gel (hexane/EtOAc = 10/1) afforded the target compound **69** (88 %) as a yellow oil, R_f 0.39 (hexane/EtOAc = 4/1); ^{1}H-NMR (d^6-acetone) 1.27 (18H, s, ^{t}Bu), 2.09–2.27 (6H, m, CCH_2C), 2.55–2.76 (4H, m, H_2CCH_2Cp), 4.02 (2H, t, J = 1.8, CpH), 4.09 (2H, t, J = 1.8, CpH,), 4.11 (5H, s, CpH), 4.13 (10H, t, J = 7.0, OCH_2), 4.15 (2H, t, J = 6.3, OCH_2), 6.16 (3H, s, ArH), 6.14–6.20 (3H, m, ArH), 6.86 (4H, d, J = 9.0, ArH), 7.29 (4H, d, J = 8.7, ArH), 8.20 (1H, s, OH); ^{13}C-NMR (d^6-acetone) 29.9 ($CH_2CH_2CH_2$), 31.8 (CH_3), 32.1, 34.5 (CMe_3), 38.2, 64.9 (OCH_2), 65.0 (OCH_2), 65.2 (OCH_2), 67.7 (CpC), 68.7 (CpC), 69.1 (CpC), 89.4 (CpC), 94.8, 100.3, 106.7, 108.8, 114.7, 126.9,

143.7, 145.4, 157.6, 159.2, 161.0, 161.8; MS (L-SIMS, *m/z*) 868.4 (M^+, 100 %). Anal. Calcd for $C_{53}H_{64}O_7Fe$: C, 73.26; H, 7.42. Found: C, 73.00; H, 7.76 %.

$G2_{(Fc)}$-OH (70). Flash chromatography of the crude product on silica gel (hexane/EtOAc = 8/1) afforded the target compound **70** (70 %) as a yellow oil, R_f 0.48 (hexane/EtOAc = 2/1); ^{1}H-NMR (d^6-acetone) 1.26 (36H, s, ^{t}Bu), 2.10–2.25 (14H, m, CCH_2C), 2.53–2.76 (4H, m, H_2CCH_2Cp), 4.00 (2H, t, J = 1.8, CpH), 4.06(2H, t, J = 1.8, CpH), 4.08 (5H, s, CpH), 4.08–4.17 (28H, m, OCH_2), 6.15 (9H, s, ArH), 6.29 (1H, s, ArH), 6.32 (2H, s, ArH), 6.85 (8H, d, J = 9.0, ArH), 7.28 (8H, d, J = 8.7, ArH), 8.22 (1H, s, OH); ^{13}C-NMR (d^6-acetone) 30.0 ($CH_2CH_2CH_2$), 31.8 (CH_3), 32.1, 34.5 (CMe_3), 38.2, 64.9 (OCH_2), 65.0 (OCH_2), 65.2 (OCH_2), 67.7 (CpC), 68.7 (CpC), 69.1 (CpC), 89.4 (CpC), 94.8, 100.3, 106.7, 108.8, 114.8, 126.9, 143.8, 145.4, 157.6, 159.2, 161.0, 161.8; MS (L-SIMS, *m/z*) 1581.8 (M^+, 100 %). Anal. Calcd for $C_{97}H_{120}O_{15}Fe$: C, 73.65; H, 7.65. Found: C, 73.88; H, 7.94 %.

$G3_{(Fc)}$-OH (71). Flash chromatography of the crude product on silica gel (hexane/EtOAc = 4/1) afforded the target compound **71** (50 %) as a yellow oil, R_f 0.52 (hexane/EtOAc = 2/1); ^{1}H-NMR (d^6-acetone) 1.24 (72H, s, ^{t}Bu), 2.07–2.26 (30H, m, CCH_2C), 2.52–2.72 (4H, m, H_2CCH_2Cp), 4.02 (2H, t, J = 1.8, CpH), 3.80–4.25 (67H, m, CpH, OCH_2), 6.13 (21H, s, ArH), 6.27–6.36 (3H, m, ArH), 6.83 (16H, d, J = 9.0, ArH), 7.25 (16H, d, J = 8.7, ArH), 8.25 (1H, s, OH); ^{13}C-NMR (d^6-acetone) 30.0 ($CH_2CH_2CH_2$), 31.8 (CH_3), 32.1, 34.5 (CMe_3), 38.2, 65.0 (OCH_2), 65.1 (OCH_2), 65.2 (OCH_2), 67.7 (CpC), 68.7 (CpC), 69.1 (CpC), 89.4 (CpC), 94.8, 100.3, 106.7, 108.8, 114.7, 126.9, 143.7, 145.4, 157.6, 159.2, 161.0, 161.7; MS (L-SIMS, *m/z*) 3007.7 (M^+, 100 %). Anal. Calcd for $C_{185}H_{232}O_{31}Fe$: C, 73.88; H, 7.77. Found: C, 73.90; H, 8.19 %.

General procedure for the synthesis of phenyl dendrons $Gn_{(Ph)}$-OH (n = 0–3) 72, 73, 74, 75. A mixture of dendritic bromide Gn-Br (0.9 mol equiv.), 1-

(3',5'-dihydroxylphenyl)-2-phenylethane **45** (1 mol equiv.), potassium carbonate (3 mol equiv.) and 18-crown-6 (0.1 mol equiv.) was refluxed in acetone. The reaction time required was 18, 20, 24 and 36 h for G0 to G3 respectively. The reaction mixture was cooled and filtered. After concentration of the filtrate on a rotary evaporator, the crude product was purified as described in the following text.

$G0_{(Ph)}$-OH (72). Flash chromatography of the crude product on silica gel (hexane/EtOAc = 20/1) afforded the target compound **72** (90 %) as a colourless oil, R_f 0.23 (hexane/EtOAc = 6/1) ^{1}H-NMR ($CDCl_3$, OH not observed) 1.34 (9H, s, ^{t}Bu), 2.23 (2H, quintet, J = 6.0, CCH_2C), 2.79–2.95 (4H, m, H_2CCH_2Ph), 4.12 (2H, t, J = 6.0, OCH_2), 4.16 (2H, t, J = 6.0, OCH_2), 6.28 (2H, s, ArH), 6.37 (1H, s, ArH), 6.90 (2H, d, J = 8.7, ArH), 7.27–7.37 (7H, m, ArH, PhH); ^{13}C-NMR ($CDCl_3$) 29.2 ($CH_2CH_2CH_2$), 31.5 (CH_3), 34.0 (CMe_3), 37.5, 37.9, 64.3 (OCH_2), 64.4 (OCH_2), 99.6, 107.3, 108.0, 113.9, 125.9, 126.2, 128.3, 128.4, 141.6, 143.4, 144.5, 156.5, 156.5, 160.0; MS (L-SIMS, *m/z*) 404.2 (M^+, 100 %). Anal. Calcd for $C_{27}H_{32}O_3$: C, 80.16; H, 7.97. Found: C, 80.04; H, 8.20 %.

$G1_{(Ph)}$-OH (73). Flash chromatography of the crude product on silica gel (hexane/EtOAc = 10/1) afforded the target compound **73** (94 %) as a colourless oil, R_f 0.18 (hexane/EtOAc = 6/1); ^{1}H-NMR ($CDCl_3$, OH not observed) 1.31 (18H, s, ^{t}Bu), 2.23 (6H, quintet, J = 6.0, CCH_2C), 2.76–2.95 (4H, m, H_2CCH_2Ph), 4.04–4.20 (12H, m, OCH_2), 6.12 (3H, s, ArH), 6.26 (2H, s, ArH), 6.34 (1H, s, ArH), 6.86 (4H, d, J = 9.0, ArH), 7.14–7.34 (9H, m, ArH, PhH); ^{13}C-NMR ($CDCl_3$) 29.2 and 29.3 ($CH_2CH_2CH_2$), 31.5 (CH_3), 34.0 (CMe_3), 37.5, 37.9, 64.3 (OCH_2), 64.5 (OCH_2), 94.1, 99.6, 107.3, 108.0, 113.9, 125.9, 126.2, 128.3, 128.4, 141.6, 143.4, 144.5, 156.5, 160.1, 160.7; MS (MADLI-TOF, *m/z*) 783.7 [$(M + Na)^+$, 100 %]. Anal. Calcd for $C_{49}H_{60}O_7$: C, 77.34; H, 7.95. Found: C, 77.63; H, 8.16 %.

$G2_{(Ph)}$-OH (74). Flash chromatography of the crude product on silica gel (hexane/EtOAc = 8/1) afforded the target compound **74** (88 %) as a colourless oil, R_f 0.32 (hexane/EtOAc = 3/1); ^{1}H-NMR ($CDCl_3$, OH not observed) 1.29 (36H, s, ^{t}Bu), 2.21 (14H, quintet, J = 6.0, CCH_2C), 2.74–2.93 (4H, m, H_2CCH_2Ph), 4.04–4.19 (28H, m, OCH_2), 6.10 (9H, s, ArH), 6.24 (2H, s, ArH), 6.32 (1H, s, ArH), 6.85 (8H, d, J = 9.0, ArH), 7.12–7.34 (13H, m, ArH, PhH); ^{13}C-NMR ($CDCl_3$) 29.2 and 29.3 ($CH_2CH_2CH_2$), 31.5 (CH_3), 34.0 (CMe_3), 37.5, 37.9, 64.3 (OCH_2), 64.5 (OCH_2), 94.1, 99.6, 107.2, 108.0, 113.9, 125.9, 126.2, 128.3, 128.4, 141.6, 143.4, 144.5, 156.5, 160.0, 160.7; MS (L-SIMS, *m/z*) 1473.9 (M^+, 100 %). Anal. Calcd for $C_{93}H_{116}O_{15}$: C, 75.79; H, 7.93. Found: C, 75.71; H, 7.89 %.

$G3_{(Ph)}$-OH (75). Flash chromatography of the crude product on silica gel (hexane/EtOAc = 4/1) afforded the target compound **75** (55 %) as a colourless oil, R_f 0.50 (hexane/EtOAc = 2/1); ^{1}H-NMR ($CDCl_3$, OH not observed) 1.30 (72H, s, ^{t}Bu), 2.10–2.35 (30H, m, CCH_2C), 2.74–2.90 (4H, m, H_2CCH_2Ph), 4.05–4.23 (60H, m, OCH_2), 6.11 (21H, s, ArH), 6.23 (2H, br s, ArH), 6.32 (1H, br s, ArH), 6.85 (16H, d, J = 9.0, ArH), 7.13–7.33 (21H, m, ArH, PhH); ^{13}C-NMR ($CDCl_3$) 29.2 and 29.3 ($CH_2CH_2CH_2$), 31.5 (CH_3), 34.0 (CMe_3), 37.5, 37.9, 64.3 (OCH_2), 64.5 (OCH_2), 94.1, 99.6, 107.3, 108.0, 113.9, 125.9, 126.2, 128.3, 128.4, 141.6, 143.4, 144.5, 156.5, 160.1, 160.7; MS (MADLI-TOF, *m/z*) 2920.8 [$(M + Na)^+$, 100 %]. Anal. Calcd for $C_{181}H_{228}O_{31}$: C, 74.97; H, 7.93. Found: C, 74.88; H, 8.04 %.

General procedure for the synthesis of ferrocenyl terpy ligands for $Gn_{(Fc)}$-terpy (n = 0–3) 36, 37, 38, 39. A mixture of dendritic phenol $Gn_{(Fc)}$-OH (0.9 mol equiv.), 4'-(*p*-(3-bromopropoxy)phenyl-2,2':6',2"-terpyridine **67** (1 mol equiv.), potassium carbonate (3 mol equiv.) and 18-crown-6 (0.1 mol equiv.) was refluxed in acetone. The reaction time required was 20, 24, 36 and 48 h for n = 0 to 3 respectively. The

reaction mixture was cooled and filtered. After concentration of the filtrate on a rotary evaporator, the crude product was purified as described in the following text.

$G0_{(Fc)}$-terpy (36). Flash chromatography of the crude product on alumina (hexane/EtOAc = 30/1) afforded the target ligand **36** (77 %) as a yellow oil. An analytic sample was obtained by precipitate of the compound from acetone by the addition of hexane. R_f 0.57 (hexane/EtOAc = 10/1); ^{1}H-NMR (d^6-acetone) 1.25 (9H, s, ^{t}Bu), 2.19 (2H, quintet, J = 6.3, CCH_2C), 2.29 (2H, quintet, J = 6.3, CCH_2C), 2.55–2.78 (4H, m, H_2CCH_2Cp), 4.00 (2H, t, J = 1.8, CpH), 4.07 (2H, t, J = 1.8, CpH), 4.08 (5H, s, CpH), 4.13 (2H, t, J = 6.0, OCH_2), 4.15 (2H, t, J = 6.0, OCH_2), 4.20 (2H, t, J = 6.0, OCH_2), 4.29 (2H, t, J = 1.8, OCH_2), 6.38–6.45 (3H, m, ArH), 6.86 (2H, d, J = 8.7, ArH), 7.14 (2H, dt, J = 8.7, H^c), 7.29 (2H, d, J = 8.7, ArH), 7.46 (2H, dt, J = 1.2, 4.8, H^5), 7.90 (2H, d, J = 8.7, H^b), 7.99 (2H, dt, J = 1.5, 7.6, H^4), 8.70–8.76 (4H, m, H^3 and H^6), 8.79 (2H, s, H$^{3'}$); ^{13}C-NMR (d^6-acetone) 30.1 ($CH_2CH_2CH_2$), 31.8 (CMe_3), 32.2, 34.5 (CH_3),38.4, 65.0 (OCH_2), 65.1 (OCH_2), 65.4 (OCH_2), 67.8(CpC), 68.8(CpC), 69.1(CpC), 89.4 (CpC), 99.6, 108.0, 114.7, 116.1 (C^c), 118.5 (C$^{3'}$), 121.7 (C^3), 124.9 (C^5), 126.9, 129.1 (C^b), 131.3 (C^a), 137.8 (C^4), 143.8, 145.4, 150.1 (C^6), 150.4 (C$^{4'}$), 156.7 (C^2), 156.9 (C$^{2'}$), 157.6, 161.0, 161.1 (C^d); MS (L-SIMS, *m/z*) 878.3 [(M + H)$^+$, 100 %]. Anal. Calcd for $C_{55}H_{55}O_4N_3Fe$: C, 75.25; H, 6.31; N, 4.79. Found: C, 75.47; H, 6.37; N, 4.70 %.

$G1_{(Fc)}$-terpy (37). Flash chromatography of the crude product on alumina (hexane/EtOAc = 25/1) afforded the target ligand **37** (74 %) as a yellow oil, R_f 0.45 (hexane/EtOAc = 6/1); ^{1}H-NMR (d^6-acetone) 1.23 (18H, s, ^{t}Bu), 2.07–2.29 (8H, m, CCH_2C), 2.54–2.75 (4H, m, H_2CCH_2Cp), 3.97 (2H, t, J = 1.8, CpH), 4.03 (2H, t, J = 1.8, CpH), 4.05 (5H, s, CpH), 4.06–4.17 (14H, m, OCH_2), 4.20 (2H, t, J = 6.0, OCH_2), 6.14 (3H, s, ArH), 6.38–6.43 (3H, m, ArH), 6.82 (4H, d, J = 9.0, ArH), 7.10 (2H, d, J = 8.7, H^c), 7.25 (4H, d, J = 8.7, ArH), 7.41 (2H, ddd, J = 1.2, 4.8, 7.5, H^5), 7.83 (2H, d, J

= 9.0, H^b), 7.94 (2H, dt, *J* = 1.8, 7.5, H^4), 8.69–8.76 (4H, m, H^3 and H^6), 8.78 (2H, s, $H^{3'}$); ^{13}C-NMR (d^6-acetone) 30.0 ($CH_2CH_2CH_2$), 31.8 (CMe_3), 32.1, 34.5 (CH_3), 38.4, 65.0 (OCH_2), 65.1 (OCH_2), 65.2 (OCH_2), 65.4 (OCH_2), 67.8 (CpC), 68.7 (CpC), 69.1 (CpC), 89.3 (CpC), 94.8, 99.6, 108.0, 114.7, 116.0 (C^c), 118.5 ($C^{3'}$), 121.7 (C^3), 124.9 (C^5), 126.9, 129.1 (C^b), 131.3 (C^a), 137.8 (C^4), 143.7, 145.4, 150.1 (C^6), 150.3 ($C^{4'}$), 156.7 (C^2), 156.8 ($C^{2'}$), 157.6, 161.0 (C^d), 161.7; MS (MALDI-TOF, *m/z*) 1234.5 [(M + H)$^+$, 100 %]; Elemental analysis was not obtained because of self-decomposition of the compound.

$G2_{(Fc)}$-terpy (38). Flash chromatography of the crude product on alumina (hexane/EtOAc = 10/1) afforded the target ligand **38** (55 %) as a yellow oil, R_f 0.43 (hexane/EtOAc = 5/1); ^{1}H-NMR (d^6-acetone) 1.23 (36H, s, ^{t}Bu), 2.08–2.27 (16H, m, CCH_2C), 2.54–2.75 (4H, m, H_2CCH_2Cp), 3.97 (2H, t, *J* = 1.8, CpH), 4.05 (5H, s, CpH), 4.00–4.18 (37H, m, CpH, OCH_2), 4.21 (2H, t, *J* = 6.0, OCH_2), 6.12 (9H, s, ArH), 6.38–6.43 (3H, m, ArH), 6.82 (8H, d, *J* = 9.0, ArH), 7.10 (2H, d, *J* = 8.7, H^c), 7.25 (8H, d, *J* = 8.7, ArH), 7.42 (2H, dt, *J* = 1.2, 5.5, H^5), 7.84 (2H, d, *J* = 9.0, H^b), 7.95 (2H, dt, *J* = 1.5, 7.8, H^4), 8.69–8.75 (4H, m, H^3 and H^6), 8.79 (2H, s, $H^{3'}$); ^{13}C-NMR (d^6-acetone) 30.1 ($CH_2CH_2CH_2$), 31.8 (CMe_3), 32.1, 34.5 (CH_3), 38.4, 65.0 (OCH_2), 65.1 (OCH_2), 65.2 (OCH_2), 65.4 (OCH_2), 67.8 (CpC), 68.8 (CpC), 69.1 (CpC), 89.3 (CpC), 94.8, 99.7, 108.0, 114.8, 116.0 (C^c), 118.5 ($C^{3'}$), 121.7 (C^3), 124.9 (C^5), 126.9, 129.1 (C^b), 131.3 (C^a), 137.8 (C^4), 143.7, 145.4, 150.1 (C^6), 150.3 ($C^{4'}$), 156.7 (C^2), 156.8 ($C^{2'}$), 157.6, 161.0 (C^d), 161.7; MS (MADLI-TOF, *m/z*) 1946.9 [(M + H)$^+$, 100 %]; Elemental analysis was not obtained because of self-decomposition of the compound.

$G3_{(Fc)}$-terpy (39). Flash chromatography of the crude product on alumina (hexane/EtOAc = 5/1) afforded the target ligand **39** (54 %) as a yellow oil, R_f 0.36 (hexane/EtOAc = 2/1); ^{1}H-NMR (d^6-acetone) 1.24 (72H, s, ^{t}Bu), 2.07–2.22 (32H, m, CCH_2C), 2.51–2.73 (4H, m, H_2CCH_2Cp), 3.96 (2H, t, *J* = 1.8, CpH), 4.03 (5H, s,

CpH), 3.94–4.17 (64H, m, CpH, OCH_2), 4.20 (2H, t, J = 6.0, OCH_2), 6.12 (21H, br s, ArH), 6.39–6.43 (3H, m, ArH), 6.81 (16H, d, J = 8.7, ArH), 7.09 (2H, d, J = 8.7, H^c), 7.24 (16H, d, J = 8.7, ArH), 7.46 (2H, dt, J = 1.2, 5.4, H^5), 7.84 (2H, d, J = 8.7, H^b), 7.94 (2H, t, J = 7.8, H^4), 8.69–8.73 (4H, m, H^3 and H^6), 8.79 (2H, s, $H^{3'}$); ^{13}C-NMR (d^6-acetone) 30.1 ($CH_2CH_2CH_2$), 31.8 (CMe_3), 32.1, 34.5 (CH_3), 38.4, 65.0 (OCH_2), 65.1 (OCH_2), 65.2 (OCH_2), 65.4 (OCH_2), 67.8 (CpC), 68.8 (CpC), 69.2 (CpC), 89.3 (CpC), 94.8, 99.6, 108.0, 114.8, 116.0 (C^c), 118.5 ($C^{3'}$), 121.8 (C^3), 124.9 (C^5), 126.9, 129.1 (C^b), 131.3 (C^a), 137.8 (C^4), 143.7, 145.4, 150.1 (C^6), 150.3 ($C^{4'}$), 156.7 (C^2), 156.8 ($C^{2'}$), 157.6, 161.0 (C^d), 161.7; MS (MADLI-TOF, *m/z*) 3372.0 [$(M + H)^+$, 100 %]; Elemental analysis was not obtained because of self-decomposition of the compound.

General procedure for the synthesis of phenyl terpy ligands $Gn_{(Ph)}$-terpy (n = 0–3) 40, 41, 42, 43. A mixture of dendritic phenols $Gn_{(Ph)}$-OH (0.9 mol equiv.), 4'-(*p*-(3-bromopropoxy)phenyl-2,2':6',2"-terpyridine **67** (1 mol equiv.), potassium carbonate (3 mol equiv.) and 18-crown-6 (0.1 mol equiv.) was refluxed in acetone. The reaction time required was 20, 24, 36 and 48 h for n = 0 to 3 respectively. The reaction mixture was cooled and filtered. After concentration of the filtrate on a rotary evaporator, the crude product was purified as described in the following text.

$G0_{(Ph)}$-terpy (40). Flash chromatography of the crude product on alumina (hexane/EtOAc = 30/1) afforded the target ligand **40** (84 %) as a yellow oil, R_f 0.52 (hexane/EtOAc = 10/1); ^{1}H-NMR ($CDCl_3$) 1.30 (9H, s, ^{t}Bu), 2.18–2.34 (4H, m, CCH_2C), 2.79–2.96 (4H, m, H_2CCH_2Ph), 4.05–4.18 (6H, m, OCH_2), 4.23 (2H, t, J = 6.0, OCH_2), 6.37 (3H, s, ArH), 6.86 (2H, d, J = 9.0, ArH), 7.05 (2H, d, J = 8.7, H^c), 7.15–7.32 (7H, m, ArH and PhH), 7.37 (2H, dd, J = 4.8, 5.1, H^5), 7.86–7.94 (4H, m, H^b and H^4), 8.65–8.79 (4H, m, , H^3 and H^6), 8.74 (2H, s, $H^{3'}$); ^{13}C-NMR ($CDCl_3$) 29.3 ($CH_2CH_2CH_2$), 31.5 (CMe_3), 34.0 (CH_3), 37.7, 38.2, 64.3 (OCH_2), 64.4 (OCH_2), 64.6 (OCH_2), 99.0, 107.2, 113.9, 114.9 (C^c), 118.4 ($C^{3'}$), 121.5 (C^3), 123.8 (C^5), 125.9,

126.2, 128.3, 128.4, 128.5 (C^b), 130.5 (C^a), 137.2 (C^4), 141.7, 143.3, 144.2, 148.8 (C^6), 149.8 ($C^{4'}$), 155.5 (C^2), 156.0 ($C^{2'}$), 156.6, 159.9 (C^d), 159.9, 160.0; HRMS calcd for $C_{51}H_{51}O_4N_3$: 769.3879. Found: 770.3972. Anal. Calcd for $C_{51}H_{51}O_4N_3$: C, 79.56; H, 6.68; N, 5.46. Found: C, 79.02; H, 6.77; N, 5.25 %.

$G1_{(Ph)}$-terpy (41). Flash chromatography of the crude product on alumina (hexane/EtOAc = 20/1) afforded the target ligand **41** (84 %) as a yellow oil, R_f 0.61 (hexane/EtOAc = 5/1); ^{1}H-NMR ($CDCl_3$) 1.30 (18H, s, ^{t}Bu), 2.17–2.34 (8H, m, CCH_2C), 2.79–2.96 (4H, m, H_2CCH_2Ph), 4.05–4.18 (14H, m, OCH_2), 4.23 (2H, t, J = 6.0, OCH_2), 6.11 (3H, s, ArH), 6.37 (3H, s, ArH), 6.85 (4H, d, J = 8.7, ArH), 7.06 (2H, d, J = 8.7, H^c), 7.16–7.32 (9H, m, ArH and PhH), 7.38 (2H, ddd, J = 1.2, 4.8, 7.5, H^5), 7.86–7.94 (4H, m, H^b and H^4), 8.65–8.79 (4H, m, H^3 and H^6), 8.76 (2H, s, $H^{3'}$); ^{13}C-NMR ($CDCl_3$) 29.3 ($CH_2CH_2CH_2$), 31.5 (CMe_3), 34.0 (CH_3), 37.7, 38., 64.3 (OCH_2), 64.4 (OCH_2), 64.5 (OCH_2), 94.0, 99.0, 107.2, 113.9, 114.9 (C^c), 118.5 ($C^{3'}$), 121.6 (C^3), 123.9 (C^5), 125.9, 126., 128.3, 128.4, 128.6 (C^b), 130.4 (C^a), 137.4 (C^4), 141.7, 143.3, 144.2, 148.6 (C^6), 149.9 ($C^{4'}$), 155.3 (C^2), 155.9 ($C^{2'}$), 156.5, 159.9 (C^d), 156.0, 160.7; MS (L-SIMS, *m/z*) 1126.63 [$(M + H)^+$, 100 %]. Anal. Calcd for $C_{73}H_{79}O_8N_3$: C, 77.84; H, 7.07; N, 3.73. Found: C, 77.97; H, 6.91; N, 3.76 %.

$G2_{(Ph)}$-terpy (42). Flash chromatography of the crude product on alumina (hexane/EtOAc = 8/1) afforded the target ligand **42** (59 %) as a yellow oil, R_f 0.45 (hexane/EtOAc = 5/1); ^{1}H-NMR ($CDCl_3$) 1.29 (36H, s, ^{t}Bu), 2.17–2.34 (16H, m, CCH_2C), 2.79–2.96 (4H, m, H_2CCH_2Ph), 4.05–4.17 (30H, m, OCH_2), 4.22 (2H, t, J = 6.0, OCH_2), 6.10 (6H, s, ArH), 6.11 (3H, s, ArH), 6.37 (3H, s, ArH), 6.85 (8H, d, J = 8.7, ArH), 7.05 (2H, d, J = 8.7, H^c), 7.16–7.32 (13H, m, ArH and PhH), 7.37 (2H, ddd, J = 1.2, 4.8, 7.5, H^5), 7.86–7.95 (4H, m, H^b and H^4), 8.65–8.79 (4H, m, H^3 and H^6), 8.76 (2H, s, $H^{3'}$); ^{13}C-NMR ($CDCl_3$) 29.3 ($CH_2CH_2CH_2$), 31.5 (CMe_3), 34.0 (CH_3), 37.7, 38.2, 64.3 (OCH_2), 64.5 (OCH_2), 94.0, 99.0, 107.2, 113.9, 114.9 (C^c), 118.5 ($C^{3'}$),

121.5 (C^3), 123.9 (C^5), 125.9, 126.2, 128.3, 128.4, 128.5 (C^b), 130.5 (C^a), 137.3 (C^4), 141.7, 143.3, 144.2, 148.7 (C^6), 149.8 ($C^{4'}$), 155.4 (C^2), 156.0 ($C^{2'}$), 156.5, 159.9 (C^d), 160.7; MS (L-SIMS, *m/z*) 1840.1 [$(M + H)^+$, 100 %]. Anal. Calcd for $C_{117}H_{135}O_{16}N_3$: C, 76.40; H, 7.40; N, 2.28. Found: C, 76.11; H, 7.40; N, 1.96 %.

$G3_{(Ph)}$-terpy (43). Flash chromatography of the crude product on alumina (hexane/EtOAc = 4/1) afforded the target ligand **43** (54 %) as a yellow oil, R_f 0.52 (hexane/EtOAc = 2/1); ^{1}H-NMR ($CDCl_3$) 1.29 (72H, s, ^{t}Bu), 2.10–2.40 (32H, m, CCH_2C), 2.79–2.96 (4H, m, H_2CCH_2Ph), 4.01–4.25 (64H, m, OCH_2), 6.09 (21H, s, ArH), 6.36 (3H, br s, ArH), 6.84 (16H, d, J = 8.7, ArH), 7.05 (2H, d, J = 9.0, H^c), 7.16–7.35 (21H, m, ArH and PhH), 7.38 (2H, t, J = 4.2, H^5), 7.86–7.95 (4H, m, H^b and H^4), 8.66–8.79 (4H, m, H^3 and H^6), 8.77 (2H, s, $H^{3'}$); ^{13}C-NMR ($CDCl_3$) 29.3, 29.7 ($CH_2CH_2CH_2$), 31.5 (CMe_3), 34.0 (CH_3), 37.7, 38.2, 64.3 (OCH_2), 64.5 (OCH_2), 94.0, 99.0, 107., 113.9, 114.9 (C^c), 118.7 ($C^{3'}$), 121.8 (C^3), 124.0 (C^5), 125.9, 126.2, 128.3, 128.4, 128.6 (C^b), 130.3 (C^a), 137.7 (C^4), 141.7, 143.3, 144.2, 148.4 (C^6), 150.0 ($C^{4'}$), 155.0 (C^2), 155.6 ($C^{2'}$), 156.5, 160.0 (C^d), 160.7; MS (MADLI-TOF, *m/z*) 3264.0 [$(M + H)^+$, 100 %]. Anal. Calcd for $C_{205}H_{247}O_{32}N_3$: C, 75.41; H, 7.62; N, 1.29. Found: C, 75.44; H, 7.78; N, 1.20 %.

General procedure for the synthesis of Fe(II)–bis(terpy) complexes 28–35. $FeCl_2 \cdot 4H_2O$ (0.5 mol equiv.) was added to a boiling methanolic solution of the terpy ligand (1.0 mol equiv.) and a deep purple solution formed immediately. After the mixture had been refluxed for a further 2 h, a methanolic solution of NH_4PF_6 (1.0 mol equiv.) was added. The crude product was purified as described in the following text.

$[Fe(G0_{(Fc)})_2](PF_6)_2$ (28). The precipitate was filtered and washed with cold methanol to give $[Fe(G0_{(Fc)})_2](PF_6)_2$ as a deep purple crystalline solid (80 %). The residue was redissolved in dichloromethane and subjected to column chromatography on alumina

(hexane/EtOAc = 2/1 followed by $CHCl_3$/ethanol = 4/1) to give the target complex **28**, m.p. > 278 °C; ^{1}H-NMR (d^6-DMSO) 1.23 (18H, s, ^{t}Bu), 2.15–2.29 (4H, quintet, J = 6.0, CCH_2C), 2.28 (4H, t, J = 4.8, CCH_2C), 2.53–2.80 (8H, m, H_2CCH_2Cp), 4.05 (4H, t, J = 1.8, CpH), 4.07–4.17 (12H, m, CpH, OCH_2), 4.12 (10H, s, CpH), 4.21 (4H, t, J = 5.7, OCH_2), 4.36 (4H, t, J = 5.4, OCH_2), 6.41 (2H, s, ArH), 6.45 (2H, s, ArH), 6.47 (2H, s, ArH), 6.88 (4H, d, J = 8.7, ArH), 7.17 (4H, t, J = 6.0, H^5), 7.20–7.36 (8H, m, ArH, H^c), 7.40 (4H, d, J = 8.7, H^6), 8.02 (4H, t, J = 7.5, H^4), 8.57 (4H, d, J = 8.7, H^b), 9.06 (4H, d, J = 8.1, H^3), 9.64 (4H, s, $H^{3'}$); ^{13}C-NMR (d^6-acetone) 30.1 ($CH_2CH_2CH_2$), 31.8 (CMe_3), 32.2, 34.5 (CH_3), 38.4, 65.0 (OCH_2), 65.2 (OCH_2), 65.7 (OCH_2), 67.8 (CpC), 68.8 (CpC), 69.2 (CpC), 89.4 (CpC), 99.7, 108.0, 114.8, 116.4 (C^c), 121.4 ($C^{3'}$), 124.8 (C^3), 126.9, 128.4 (C^5), 129.3 (C^b), 130.2 (C^a), 139.6 (C^4), 143.8, 145.4, 150.9 (C^6), 154.1 ($C^{4'}$), 157.7, 159.3 (C^2), 161.0 ($C^{2'}$), 161.1 (C^d), 161.3, 162.3; MS (L-SIMS, m/z) 905.84 [$(M–2PF_6)^{2+}$, 50 %]. Anal. Calcd for $C_{110}H_{110}N_6O_8Fe_3P_2F_{12}$: C, 62.87; H, 5.28; N, 4.00. Found: C, 63.01; H, 5.45; N, 3.96 %.

$[Fe(G1_{(Fc)})_2](PF_6)_2$ (29). The precipitate was filtered and washed with cold methanol to give $[Fe(G1_{(Fc)})_2](PF_6)_2$ as a deep purple crystalline solid (80 %). The residue was redissolved in dichloromethane and subjected to column chromatography on alumina (hexane/EtOAc = 2/1 followed by $CHCl_3$/ethanol = 4/1) to give the target complex **29**, m.p. > 278 °C; ^{1}H-NMR (d^6-DMSO) 1.22 (36H, s, ^{t}Bu), 2.10 (12H, quintet, J = 6.0, CCH_2C), 2.18–2.35 (4H, m, CCH_2C), 2.53–2.79 (8H, m, H_2CCH_2Cp), 4.02–4.10 (32H, m, CpH, OCH_2), 4.12 (10H, s, CpH), 4.20 (4H, t, J = 6.0, OCH_2), 4.36 (4H, t, J = 5.4, OCH_2), 6.13 (6H, s, ArH), 6.41 (2H, s, ArH), 6.44 (2H, s, ArH), 6.84 (8H, d, J = 9.0, ArH), 7.16 (4H, t, J = 6.0, H^5), 7.21–7.31 (12H, m, ArH, H^c), 7.39 (4H, d, J = 8.7, H^6), 8.04 (4H, t, J = 7.2, H^4), 8.57 (4H, d, J = 8.4, H^b), 9.06 (4H, d, J = 8.1, H^3), 9.64 (4H, s, $H^{3'}$); ^{13}C-NMR (d^6-acetone) 30.1 ($CH_2CH_2CH_2$), 31.8 (CMe_3), 32.2, 34.5 (CH_3), 38.4, 65.0 (OCH_2), 65.1 (OCH_2), 65.3 (OCH_2), 65.8 (OCH_2), 67.8 (CpC), 68.8 (CpC), 69.2 (CpC), 89.4 (CpC), 94.9, 99.8, 107.8, 108.1, 114.8, 116.4 (C^c), 121.4 ($C^{3'}$), 124.8 (C^3),

126.9, 128.4 (C^5), 129.3 (C^b), 130.2 (C^a), 139.7 (C^4), 143.8, 145.6, 150.9 (C^6), 154.1 ($C^{4'}$), 157.7, 159.4 (C^2), 161.0 ($C^{2'}$), 161.1 (C^d), 161.4, 161.8, 162.4; MS (L-SIMS, *m/z*) 1262.47 [$(M-2PF_6)^{2+}$, 100 %]. Anal. Calcd for $C_{154}H_{166}N_6O_{16}Fe_3P_2F_{12}$: C, 65.72; H, 5.94; N, 2.99. Found: C, 65.98; H, 6.06; N, 2.95 %.

$[Fe(G2_{(Fc)})_2](PF_6)_2$ (30). The precipitate was filtered and washed with cold methanol to give $[Fe(G2_{(Fc)})_2](PF_6)_2$ as a deep purple crystalline solid (75 %). The residue was redissolved in dichloromethane and subjected to column chromatography on alumina (hexane/EtOAc = 1/1 followed by $CHCl_3$/ethanol = 4/1) to give the target complex **30**, m.p. > 278 °C; ^{1}H-NMR (d^6-DMSO) 1.20 (72H, s, ^{t}Bu), 2.08 (28H, br s, CCH_2C), 2.27 (4H, br s, CCH_2C), 2.54–2.78 (8H, m, H_2CCH_2Cp), 3.93–4.20 (78H, m, CpH, OCH_2), 4.35 (4H, br s, OCH_2), 6.10 and 6.12 (18H, s, ArH), 6.40 (2H, s, ArH), 6.43 (2H, s, ArH), 6.45 (2H, s, ArH), 6.82 (16H, d, J = 8.7, ArH), 7.14(4H, t, J = 6.6, H^5), 7.23 (16H, d, J = 8.7, ArH), 7.19–7.30 (4H, m, H^c), 7.38 (4H, d, J =7.8, H^6), 7.98 (4H, t, J = 6.9, H^4), 8.57 (4H, d, J = 7.8, H^b), 9.05 (4H, d, J = 8.1, H^3), 9.64 (4H, s, $H^{3'}$); ^{13}C-NMR (d^6-acetone) 30.1 ($CH_2CH_2CH_2$), 31.8 (CMe_3), 32.2, 34.5 (CH_3), 38.3, 65.0 (OCH_2), 65.1 (OCH_2), 65.2 (OCH_2), 65.8 (OCH_2), 67.8 (CpC), 68–70 (board signal for CpC), 94.8, 99.8, 108.1, 114.8, 116.5 (C^c), 121.5 ($C^{3'}$), 124.9 (C^3), 126.9, 128.5 (C^5), 129.3 (C^b), 130.3 (C^a), 139.8 (C^4), 143.8, 145.5, 150.9 (C^6), 154.2 ($C^{4'}$), 157.6, 159.3 (C^2), 161.0 ($C^{2'}$), 161.0 (C^d), 161.3, 161.8, 162.4. Anal. Calcd for $C_{242}H_{278}N_6O_{32}Fe_3P_2F_{12}$: C, 68.55; H, 6.61; N, 1.98. Found: C, 68.09; H, 6.62; N, 1.92 %.

$[Fe(G3_{(Fc)})_2](PF_6)_2$ (31). The reaction mixture was cooled to 25 °C and the purple product stuck to the reaction vessel, the colourless supernatant was decanted and the residue was washed with cold ethanol. The residue was then purified by flash chromatography on alumina (hexane/EtOAc = 1/1 followed by $CHCl_3$/ethanol = 4/1) to give $[Fe(G3_{(Fc)})_2](PF_6)_2$ as a deep purple crystalline solid (60 %) after precipitation with ethanol from chloroform, m.p. > 278 °C; ^{1}H-NMR (d^6-DMSO) 1.18 (144H, s, ^{t}Bu), 1.90–2.40

(64H, br s, CCH_2C), 2.41–2.80 (8H, m, H_2CCH_2Cp), 3.70–4.26 (142H, m, CpH, OCH_2), 4.26–4.40 (4H, br s, OCH_2), 6.07 (42H, s, ArH), 6.30–6.50 (6H, m, ArH), 6.79 (32H, d, J = 8.4, ArH), 7.02–7.31 (40H, d, J = 8.7, H^5, H^c and ArH), 7.31–7.45 (4H, d, J = 7.8, H^6), 7.81–8.10 (4H, m, H^4), 8.45–8.70 (4H, m, H^b), 8.90–9.9.15 (4H, m, H^3), 9.63 (4H, s, $H^{3'}$); ^{13}C-NMR (d^6-acetone) 30.1 ($OCH_2CH_2CH_2O$), 31.8 (CMe_3), 32.1, 34.4 (CH_3), 38.4, 65.0 (OCH_2), 65.2 (OCH_2), 65.8 (OCH_2), 67.9 (CpC), 68.9 (CpC), 69.3 (CpC), 89.4 (CpC), 94.8, 99.7, 107.9, 114.7, 116.5 (C^c), 121.5 ($C^{3'}$), 125.0 (C^3), 126.9, 128.5 (C^5), 129.2 (C^b), 130.4 (C^a), 139.8 (C^4), 143.7, 145.4, 150.9 (C^6), 154.3 ($C^{4'}$), 157.5, 159.2 (C^2), 161.0 (C^d), 161.2, 161.7, 162.3; MS (MADLI-TOF, m/z) 3372.4 {[M-Fe-2PF_6+H]$^+$, 50 %}.

$[Fe(G0_{(Ph)})_2](PF_6)_2$ (32). The precipitate was filtered and washed with cold methanol to give $[Fe(G0_{(Ph)})_2](PF_6)_2$ as a deep purple crystalline solid (80 %). The residue was redissolved in dichloromethane and subjected to column chromatography on alumina (hexane/EtOAc = 2/1 followed by $CHCl_3$/ethanol = 4/1) to give the target complex **32**, m.p. > 278 °C; ^{1}H-NMR (d^6-DMSO) 1.23 (18H, s, ^{t}Bu), 2.14 (4H, quintet, J = 6.0, CCH_2C), 2.27 (4H, t, J = 5.4, CCH_2C), 2.74–2.96 (8H, m, H_2CCH_2Ph), 4.09 (8H, t, J = 5.1, OCH_2), 4.18 (4H, t, J = 6.0, OCH_2), 4.35 (4H, t, J = 6.0, OCH_2), 6.40 (2H, br s, ArH), 6.46 (4H, br s, ArH), 6.87 (4H, d, J = 8.7, ArH), 7.17 (4H, t, J = 6.6, H^5), 7.17–7.33 (18H, m, PhH, ArH and H^c), 7.39 (4H, d, J = 8.7, H^6,), 8.02 (4H, t, J = 7.2, H^4), 8.57 (4H, d, J = 8.7, H^b), 9.06 (4H, d, J = 8.1, H^3), 9.64 (4H, s, $H^{3'}$); ^{13}C-NMR (d^6-acetone) 30.1 ($OCH_2CH_2CH_2O$), 31.8 (CMe_3), 34.5 (CH_3), 38.3, 38.8, 65.0 (OCH_2), 65.1 (OCH_2), 65.7 (OCH_2), 99.8, 108.0, 114.8, 116.4 (C^c), 121.5 ($C^{3'}$), 124.8 (C^3), 126.6 (C^5), 126.9, 128.4, 129.0, 129.3, 129.3 (C^b), 130.3 (C^a), 139.7 (C^4), 142.7, 143.8, 145.0, 150.9 (C^6), 154.1 ($C^{4'}$), 157.6, 159.3 (C^2), 161.0 ($C^{2'}$), 161.0 (C^d), 161.3, 162.3; MS (MADLI-TOF, m/z) 1124.7 {[L+Fe+retenoic acid-H]$^+$, 100 %}. Anal. Calcd for $C_{102}H_{102}N_6O_8FeP_2F_{12}$: C, 64.97; H, 5.45; N, 4.46. Found: C, 64.79; H, 5.58; N, 4.46 %.

$[Fe(G1_{(Ph)})_2](PF_6)_2$ (33). The precipitate was filtered and washed with cold methanol to give $[Fe(G1_{(Ph)})_2](PF_6)_2$ as a deep purple crystalline solid (78 %). The residue was redissolved in dichloromethane and subjected to column chromatography on alumina (hexane/EtOAc = 2/1 followed by $CHCl_3$/ethanol = 4/1) to give the target complex **33**, m.p. > 278 °C; ^{1}H-NMR (d^6-DMSO) 1.25 (36H, s, ^{t}Bu), 2.11–2.39 (12H, m, CCH_2C), 2.34 (4H, t, J = 6.0, CCH_2C), 2.85–2.96 (8H, m, H_2CCH_2Ph), 4.09–4.20 (24H, m, OCH_2), 4.23 (4H, t, J = 6.0, OCH_2), 4.41 (4H, t, J = 6.0, OCH_2), 6.16 (6H, s, ArH), 6.43 (2H, d, J = 2.1, ArH), 6.48 (4H, d, J = 1.8, ArH), 6.85 (8H, d, J = 9.0, ArH), 7.12–7.33 (22H, m, PhH , ArH and H^5), 7.38 (4H, t, J = 8.4, H^c), 7.56 (4H, d, J = 5.4, H^6), 8.04 (4H, t, J = 7.2, H^4), 8.45 (4H, d, J = 7.8, H^b), 9.00 (4H, d, J = 7.2, H^3), 9.59 (4H, s, $H^{3'}$); ^{13}C-NMR (d^6-acetone) 30.1 ($OCH_2CH_2CH_2O$), 31.8 (CMe_3), 34.5 (CH_3), 38.3, 38.8, 65.0 (OCH_2), 65.1 (OCH_2), 65.7 (OCH_2), 94.8, 99.9, 108.0, 108.1, 114.8, 116.4 (C^c), 121.4 ($C^{3'}$), 124.8 (C^3), 126.7 (C^5), 126.9, 128.4, 129.1, 129.3 (C^b), 130.2 (C^a), 139.7 (C^4), 142.7, 143.8, 145.1, 150.9 (C^6), 154.1 ($C^{4'}$), 157.6, 159.3 (C^2), 161.0 ($C^{2'}$), 161.1 (C^d), 161.3, 161.8, 162.4; MS (MADLI-TOF, m/z) 1480.9 [(L + Fe + retinoic acid - H^+, 100 %]. Anal. Calcd for $C_{146}H_{158}N_6O_{16}FeP_2F_{12}$: C, 67.48; H, 6.13; N, 3.23. Found: C, 67.10; H, 6.06; N, 3.25 %.

$[Fe(G2_{(Ph)})_2](PF_6)_2$ (34). The precipitate was filtered and washed with cold methanol to give $[Fe(G2_{(Ph)})_2](PF_6)_2$ as a deep purple crystalline solid (73 %). The residue was redissolved in dichloromethane and subjected to column chromatography on alumina (hexane/EtOAc = 1/1 followed by $CHCl_3$/ethanol = 4/1) to give the target complex **34**, m.p. > 278 °C; ^{1}H-NMR (d^6-DMSO) 1.26 (72H, s, ^{t}Bu), 2.18–2.28 (16H, m, CCH_2C), 2.34 (16H, t, J = 6.0, CCH_2C), 2.85–2.96 (8H, m, H_2CCH_2Ph), 4.17 (56H, dt, J = 1.8, 6.2, OCH_2), 4.27 (4H, t, J = 6.0, OCH_2), 4.41 (4H, t, J = 6.0, OCH_2), 6.16 (18H, s, ArH), 6.43 (2H, d, J = 2.1, ArH), 6.49 (4H, d, J = 2.1, ArH), 6.88 (16H, d, J = 8.7, ArH), 7.12–7.26 (30H, m, ArH, PhH and H^5), 7.38 (4H, t, J = 7.8, H^c), 7.56 (4H, d,

J = 4.2, H^6), 8.05 (4H, br s, H^4), 8.45 (4H, d, J = 9.0, H^b), 9.00 (4H, d, J = 6.3, H^3), 9.58 (4H, s, $H^{3'}$); ^{13}C-NMR (d^6-acetone) 30.1 ($OCH_2CH_2CH_2O$), 31.8 (CMe_3), 34.5 (CH_3), 38.3, 38.8, 65.0 (OCH_2), 65.2 (OCH_2), 65.8 (OCH_2), 94.8, 99.9, 108.0, 108.1, 114.8, 116.4 (C^c), 121.5 ($C^{3'}$), 125.0 (C^3), 126.7 (C^5), 126.,, 128.4, 129.0, 129.3 (C^b), 130.3 (C^a), 139.7 (C^4), 142.7, 143.8, 145.1, 150.9 (C^6), 154.1 ($C^{4'}$), 157.6, 159.3 (C^2), 161.0 ($C^{2'}$), 161.0 (C^d), 161.3, 161.8, 162.4; MS (MADLI-TOF, m/z) 2193.2 [(L + Fe + retinoic acid - H^+, 100 %]. Anal. Calcd for $C_{234}H_{270}N_6O_{32}FeP_2F_{12}$: C, 69.84; H, 6.76; N, 2.09. Found: C, 69.50; H, 6.67; N, 2.06 %.

$[Fe(G3_{(Ph)})_2](PF_6)_2$ (35). The reaction mixture was cooled to 25 °C and the purple product stuck to the reaction vessel, the colourless supernatant was decanted and the residue was washed with cold ethanol. The residue was then purified by flash chromatography on alumina (hexane/EtOAc = 1/1 followed by $CHCl_3$/ethanol = 4/1) to give $[Fe(G3_{(Ph)})_2](PF_6)_2$ as a deep purple crystalline solid (79 %) after precipitation with ethanol from chloroform, m.p. > 278 °C; ^{1}H-NMR (d^6-DMSO) 1.18 (144H, s, ^{t}Bu), 2.01–2.32 (64H, m, CCH_2C), 2.70–2.80 (8H, m, H_2CCH_2Ph), 3.76–4.38 (124H, m, OCH_2), 4.32 (4H, br s, OCH_2), 6.07 (42H, s, ArH), 6.35–6.47 (6H, m, ArH), 6.79 (32H, d, J = 8.7, ArH), 7.00–7.30 (18H, m, PhH, H^c and H^5), 7.20 (32H, d, J = 8.7, ArH), 7.37 (4H, d, J = 7.2, H^6), 7.97 (4H, br s, H^4), 8.54 (4H, d, J = 9.0, H^b), 9.04 (4H, d, J = 6.9, H^3), 9.63 (4H, s, $H^{3'}$); ^{13}C-NMR (d^6-acetone) 30.1 ($OCH_2CH_2CH_2O$), 31.8 (CMe_3), 34.5 (CH_3), 38.3, 38.8, 65.0, 65.2, 65.7 (OCH_2), 94.8, 99.9, 108.0, 114.7, 116.4 (C^c), 121.4 ($C^{3'}$), 124.9 (C^3), 126.6 (C^5), 126.9, 128.4, 129.1, 129.2 (C^b), 130.3 (C^a), 139.6 (C^4), 142.6, 143.8, 145.0, 150.8 (C^6), 154.0 ($C^{4'}$), 157.6, 159.2 (C^2), 160.9 ($C^{2'}$ and C^d), 161.2, 161.7, 162.3; MS (MADLI-TOF, m/z) 3619.8 [(L + Fe + retinoic acid - H^+, 100 %]. Anal. Calcd for $C_{410}H_{494}N_6O_{64}FeP_2F_{12}$: C, 71.62; H, 7.24; N, 1.22. Found: C, 71.52; H, 7.39; N, 1.34 %.

Cyclic voltammetry studies. Cyclic voltammetry was performed on a self-made electrochemical cell equipped with three electrodes (see figure 11): a platinum disc working electrode purchased from Bioanalytical Systems Inc., IN, USA, a silver wire reference electrode, and a platinum wire auxiliary electrode. Experiments were carried out at ~20 °C in dried dichloromethane solutions containing 0.2 M tetrabutylammonium tetrafluoroborate (TBAT) as the supporting electrolyte. Both the sample and the electrolyte were dried in oven for one day prior to use. The solutions were purged with nitrogen for 10 min prior to measurement and the sweep rate was 100 mV/s. The potentials were then calibrated with ferrocenealdehyde serving as the internal standard ($E_{1/2}$ = 0.636 V in dichloromethane).

References

(1) Tomalia, D. A.; Naylor, A. M.; Goddard III, W. A. *Angew. Chem. Int. Ed. Engl.* **1990**, *29*, 138—175.

(2) Fisher, M.; Vögtle, F. *Angew. Chem. Int. Ed. Engl.* **1999**, *38*, 884—905.

(3) Boulas, P. L.; Gómez-Kaifer, M.; Echegoyen, L. *Acc. Chem. Int. Ed. Engl.* **1998**, *37*, 216—247.

(4) Takada, K.; Díaz, D. J.; Abruña, H. D.; Cuadrado, I.; Casado, C.; Alonso, B.; Moran M.; Losada, J. *J. Am. Chem. Soc.* **1997**, *119*, 10763—10773.

(5) Castro, R.; Cuadrado, I.; Alonso, B.; Casodo, C. M.; Moran, M.; Kaifer, A. E. *J. Am. Chem. Soc.* **1997**, *119*, 5760—5761.

(6) Fillaut, J.-L.; Astruc, D. *J. Chem. Soc., Chem. Commun.* **1993**, 1320—1322.

(7) Newkome, G. R.; Cardullo, F.; Constable, E. C.; Moorefield, C. N.; Cargill Thompson, A. M. W. *J. Chem. Soc., Chem. Commun.* **1993**, 925—927.

(8) Cardona, C. M.; Kaifer, A.E. *J. Am. Chem. Soc.* **1998**, *120*, 4023—5024.

(9) Rowe, G. K.; Creager, S. E. *Langmuir* **1991**, *7*, 2307—2312.

(10) Cardona, C. M.; McCarley, T. D.; Kaifer, A. E. *J. Org. Chem.* **2000**, *65*, 1857—1864.

(11) Newkome, G. R.; Guther, R.; Moorefield, C. N.; Cardullo, F.; Echegoyen, L.; Pérez-Cordero, E.; Luftmann, H. *Angew. Chem. Int. Ed. Engl.* **1995**, *34*, 2023—2026.

(12) Chow, H. F.; Chan, Y. K.; Chan, T. W. D.; Kwok, W. M. R. *Chem. Eur. J.* **1996**, *2*, 1085—1091.

(13) Kimura, M.; Shiba, T.; Muto, T.; Hanabusa, K.; Shirai, H. *Chem. Commun.* **2000**, 11—12.

(14) Smith, D. K.; Diederich, F. *Chem. Eur. J.* **1998**, *4*, 1353—1361.

(15) Dandliker, P. T.; Diederich, F.; Gross, M.; Knobler, C. B.; Louati, A.; Sanford, E. M. *Angew. Chem.* **1994**, *33*, 1739—1742.

(16) Dandliker, P. J.; Diederich, F.; Gisselbrecht, J.-P.; Louati, A.; Gross, M. *Angew. Chem. Int. Ed. Engl.* **1995**, *34*, 2725—2728.

(17) Weyermann, P.; Gisselbrecht, J.-P.; Boudon, C.; Diederich, F.; Gross, M. *Angew. Chem. Int. Ed. Engl.* **1999**, *38*, 3215—329.

(18) Gorman, G. B.; Parkhurst, B. L.; Su, W. Y.; Chen, K. Y. *J. Am. Chem. Soc.* **1997**, *119*, 1141—1142.

(19) Armstrong, F. A.; Hill, H. A. O.; Walton, N. J. *Acc. Chem. Res.* **1988**, *21*, 407—413.

(20) Hill, H. A. O. *Pure & Appl. Chem.* **1987**, *59*, 742—748.

(21) Degani, Y.; Heller, A. *J. Phys. Chem.* **1987**, *91*, 1285—1289.

(22) Chow, H. F.; Wang, Z. Y.; Lau, Y. F. *Tetrahedron* **1998**, *54*, 13813—13824.

(23) Collin, J. P.; Guillerez, S.; Sauvage, J. P.; Barigelletti, F.; Cola, L. D.; Flamigni, L.; Balzani, V. *Inorg. Chem.* **1991**, *30*, 4230—4238.

(24) Fréchet, J. M. J.; Hawher, C. J. *J. Am. Chem. Soc.* **1990**, *112*, 7638—7647.

(25) Chow, H. F.; Mong, K. K. T.; Nongrum, M. F.; Wan, C. W. *Tetrahedron*, **1998**, *54*, 8543—8660.

(26) Mueller-Westerhoff, U. T.; Yang, Z.; Ingram, G. *Organomet. Chem.* **1993**, *463*, 163—167.

(27) Constable, E. C.; Ward, M. D.; Corr, S. *Inorg. Chim. Acta* **1988**, *141*, 201—203.

(28) Constable, E. C.; Thompson, A. M. W. C. *J. Am. Chem. Soc., Dalton Trans.* **1992**, 2947—2950.

(29) Kawher, C. J.; Wooley, J. M.; FrÇchet, J. M. J. *J. Am. Chem. Soc.* **1993**, *115*, 4375—4376.

(30) Constable, E. C.; Harverson, P.; Smith, D. R.; Whall, L. A. *Tetrahedron* **1994**, *50*, 7799—7806.

(31) Fry, A.; Britton, W. E. *"Laboratory Techniques in Electroanalytical Chemistry"*, 1st ed.; Marcel Dekker: New York, 1984, Chapter 13.

(32) Gosser, D. K. "*Cyclic Voltammetry: simulation and analysis of reaction mechanisms*"; VCH Publishers, Inc.: New York, 1994; p27—69.

(33) Alvarez, J.; Kaifer, A. E., *Organometallics* **1999**, *18*, 5733—5734.

(34) Saphni, W.; Calzaferri, G. *Helv. Chim. Acta* **1984**, *67*, 450—454.

Spectra

		Page
(1)	^{1}H NMR spectrum of $[Fe(G0_{(Fc)})_2](PF_6)_2$ **28**	66
(2)	^{13}C NMR spectrum of $[Fe(G0_{(Fc)})_2](PF_6)_2$ **28**	67
(3)	^{1}H NMR spectrum of $[Fe(G1_{(Fc)})_2](PF_6)_2$ **29**	68
(4)	^{13}C NMR spectrum of $[Fe(G1_{(Fc)})_2](PF_6)_2$ **29**	69
(5)	^{1}H NMR spectrum of $[Fe(G2_{(Fc)})_2](PF_6)_2$ **30**	70
(6)	^{13}C NMR spectrum of $[Fe(G2_{(Fc)})_2](PF_6)_2$ **30**	71
(7)	^{1}H NMR spectrum of $[Fe(G3_{(Fc)})_2](PF_6)_2$ **31**	72
(8)	^{13}C NMR spectrum of $[Fe(G3_{(Fc)})_2](PF_6)_2$ **31**	73
(9)	^{1}H NMR spectrum of $[Fe(G0_{(Ph)})_2](PF_6)_2$ **32**	74
(10)	^{13}C NMR spectrum of $[Fe(G0_{(Ph)})_2](PF_6)_2$ **32**	75
(11)	^{1}H NMR spectrum of $[Fe(G1_{(Ph)})_2](PF_6)_2$ **33**	76
(12)	^{13}C NMR spectrum of $[Fe(G1_{(Ph)})_2](PF_6)_2$ **33**	77
(13)	^{1}H NMR spectrum of $[Fe(G2_{(Ph)})_2](PF_6)_2$ **34**	78
(14)	^{13}C NMR spectrum of $[Fe(G2_{(Ph)})_2](PF_6)_2$ **34**	79
(15)	^{1}H NMR spectrum of $[Fe(G3_{(Ph)})_2](PF_6)_2$ **35**	80
(16)	^{13}C NMR spectrum of $[Fe(G3_{(Ph)})_2](PF_6)_2$ **35**	81

[Fe(G0(Fc))2](PF6)2 28
ppm
Integral
9.638
9.073
9.046
8.584
8.555
8.047
8.022
7.997
7.410
7.381
7.296
7.266
7.250
7.192
7.169
7.149
6.889
6.860
6.469
6.451
6.413
4.363
4.226
4.207
4.186
4.131
4.122
4.116
4.110
4.086
4.051
4.045
4.040
3.343
2.738
2.726
2.709
2.610
2.593
2.580
2.505
2.500
2.494
2.279
2.171
2.151
2.131
2.083
1.440
1.233
1.137
1.022
4.000
4.027
4.091
4.058
4.074
8.117
4.063
4.087
4.102
2.041
4.073
4.540
10.511
11.902
4.104
18.616
4.056
4.088
4.056
4.078

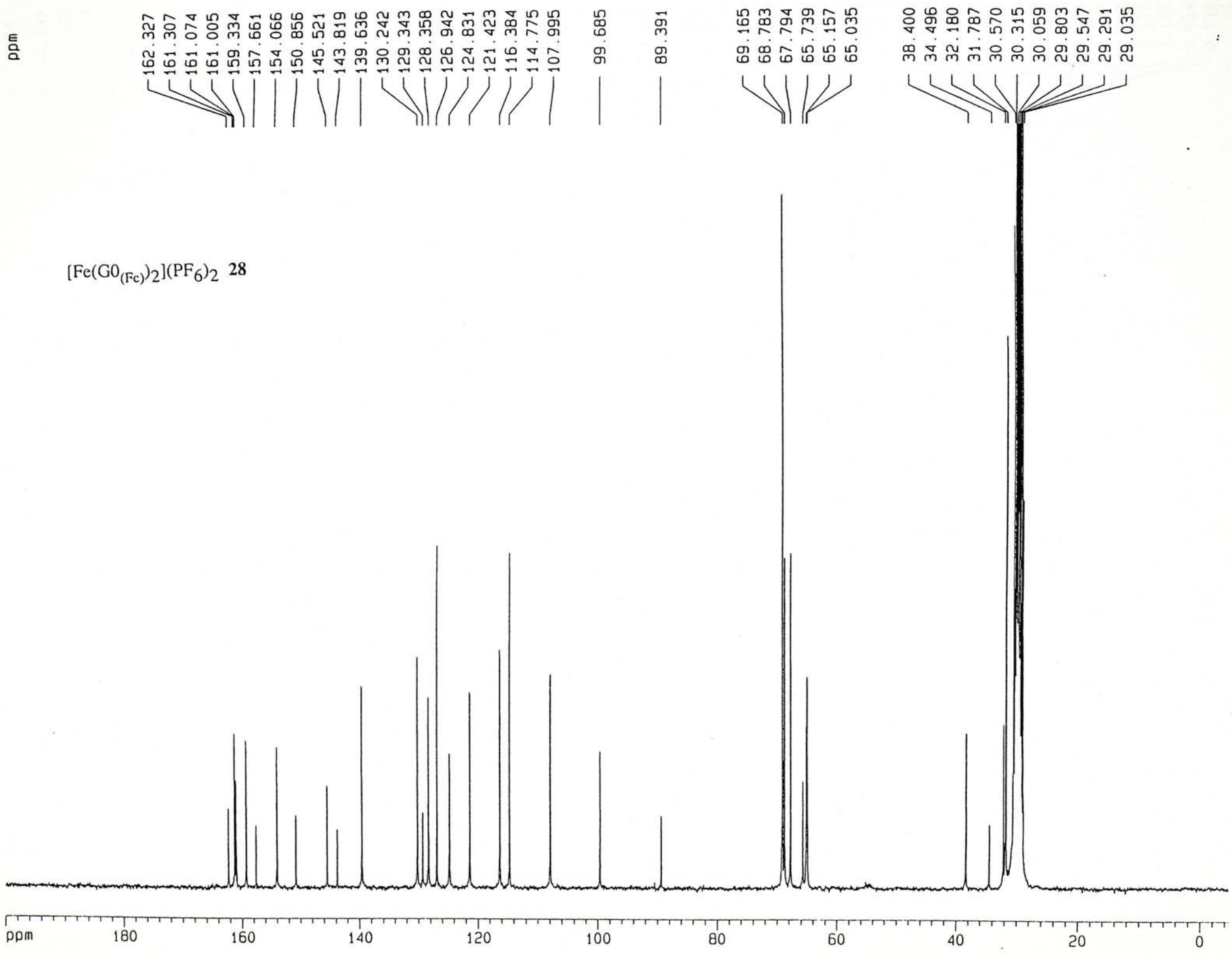

$[Fe(G0_{(Fc)})_2](PF_6)_2$ **28**

$[Fe(G1_{(Fc)})_2](PF_6)_2$ **29**

$[Fe(G1_{(Fc)})_2](PF_6)_2$ **29**

[Fe(G2(Fc))2](PF6)2 30
ppm
Integral
9.638
9.068
9.041
8.581
8.555
7.996
7.973
7.393
7.367
7.248
7.219
7.165
7.143
7.122
6.835
6.806
6.453
6.429
6.400
6.189
6.122
6.101
4.540
4.345
4.187
4.099
4.053
4.034
3.911
3.789
3.427
3.339
2.721
2.583
2.556
2.500
2.267
2.076
1.908
1.410
1.384
1.292
1.204
1.096
0.993
4.000
4.080
3.986
4.048
4.034
19.829
4.172
16.113
6.088
18.163
4.110
4.587
73.406
72.965
4.073
4.459
4.102
28.194

$[Fe(G2_{(Fc)})2](PF_6)_2$ **30**

$[Fe(G3_{(Fc)})2](PF_6)_2$ 31

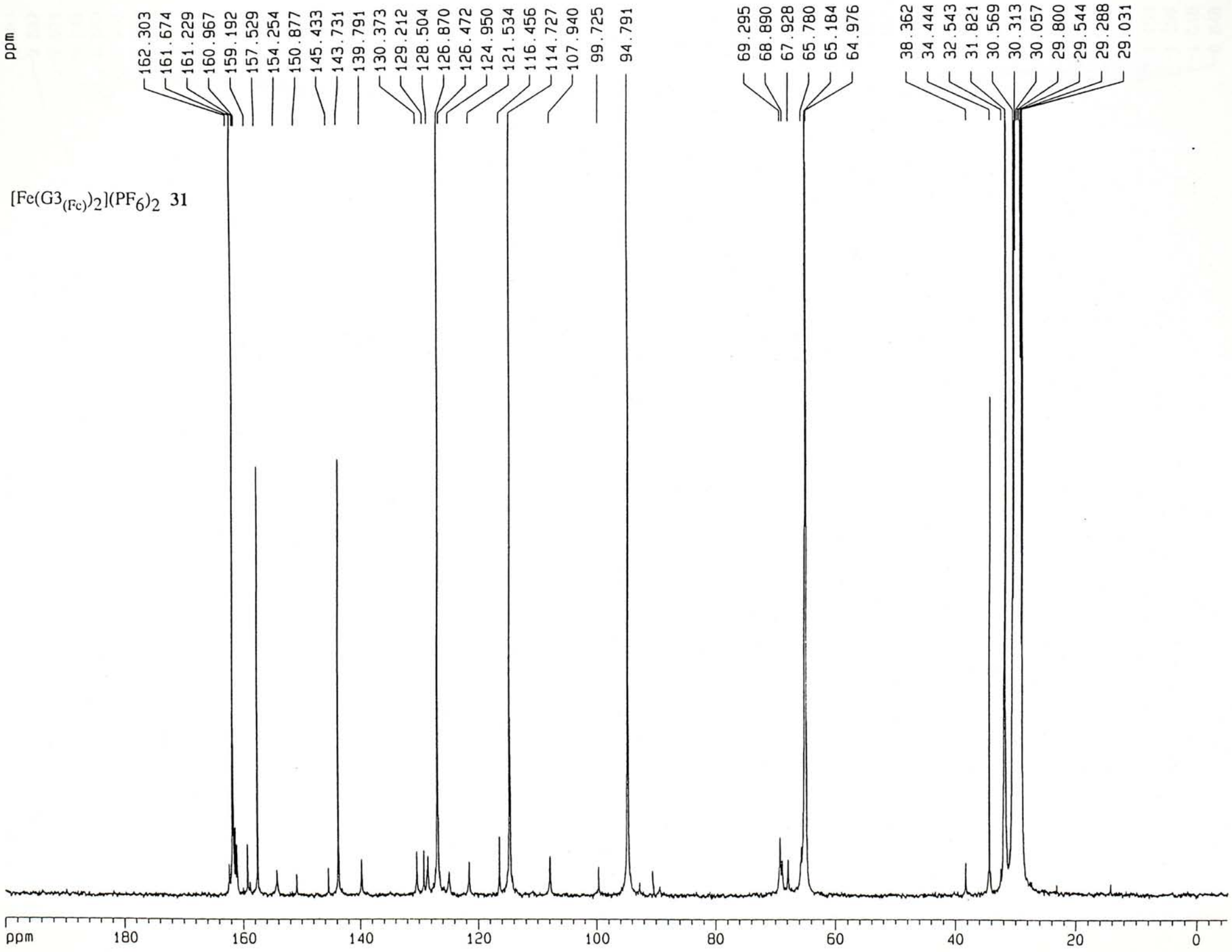

$[Fe(G3_{(Fc)})_2](PF_6)_2$ **31**

[Fe(G0(Ph))2](PF6)2 32
ppm
9.637
9.073
9.046
8.582
8.553
8.020
7.996
7.407
7.378
7.302
7.294
7.286
7.265
7.255
7.250
7.229
7.192
7.170
7.148
6.886
6.857
6.466
6.456
6.409
6.402
4.350
4.203
4.183
4.163
4.115
4.094
4.077
3.341
3.318
2.862
2.849
2.829
2.815
2.511
2.505
2.500
2.494
2.488
2.282
2.265
2.247
2.158
2.137
2.117
1.436
1.408
1.229
1.159
1.056
1.018
0.848
Integral
4.000
4.082
4.033
4.049
4.057
18.291
4.097
4.070
4.085
2.050
4.025
4.099
8.142
18.239
4.050
4.091
8.080
ppm

$[Fe(G0_{(Ph)})_2](PF_6)_2$ **32**

ppm
9.637
9.069
9.041
8.580
8.552
8.036
8.010
7.986
7.403
7.375
7.266
7.242
7.183
7.162
7.140
7.056
7.049
7.030
6.854
6.825
6.465
6.452
6.398
6.128
4.346
4.179
4.159
4.078
4.059
4.040
3.988
3.340
3.318
3.254
2.844
2.825
2.783
2.726
2.505
2.500
2.494
2.262
2.243
2.119
2.100
2.084
1.531
1.493
1.422
1.392
1.327
1.214
1.037
1.003
0.948
0.848
[Fe(G1(Ph))2](PF6)2 33
Integral
4.061
4.002
4.081
4.023
4.048
26.125
8.091
4.037
2.079
6.000
4.024
4.079
24.354
3.956
4.007
12.193
36.640
ppm
0
1
2
3
4
5
6
7
8
9

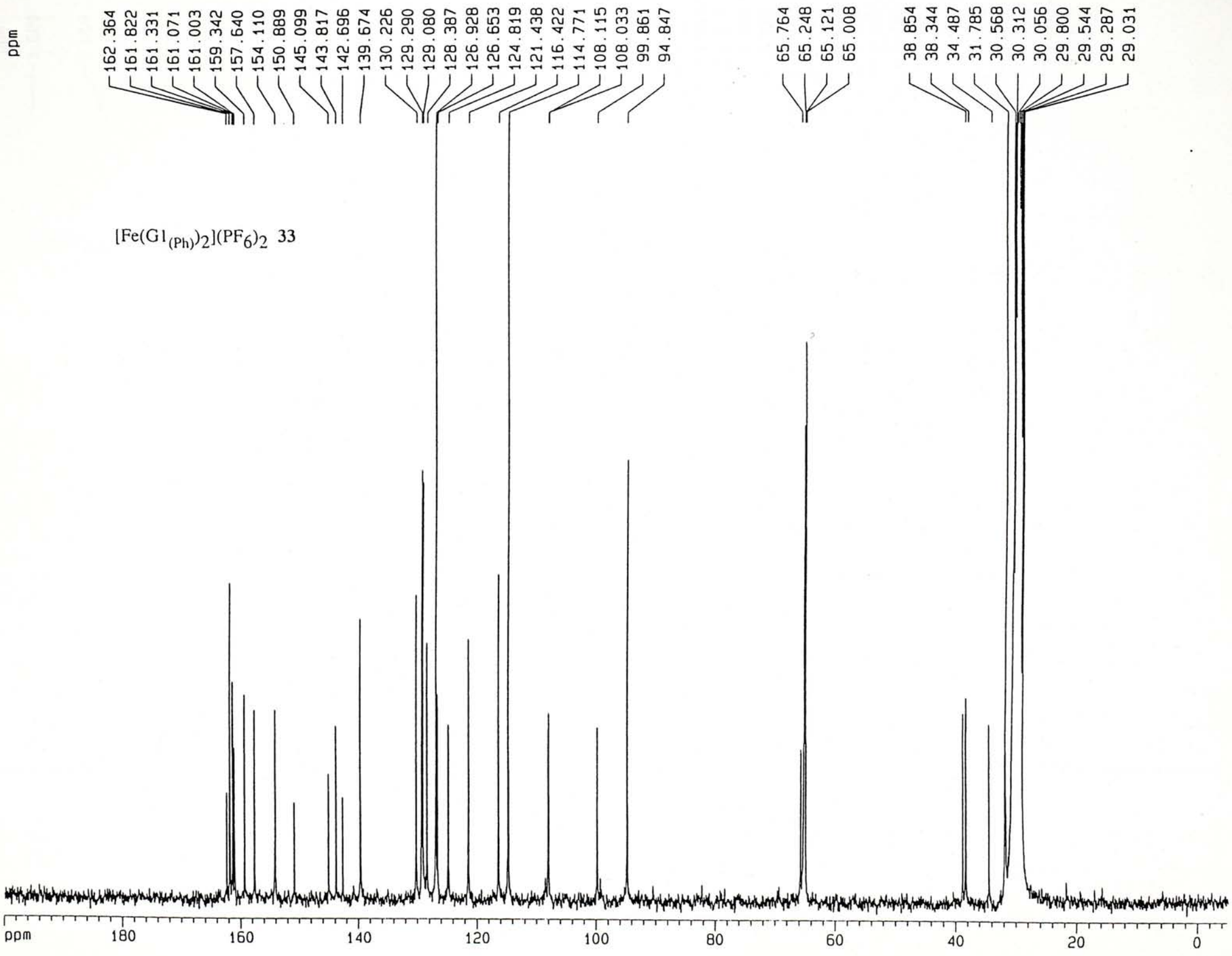
ppm
162.364
161.822
161.331
161.071
161.003
159.342
157.640
154.110
150.889
145.099
143.817
142.696
139.674
130.226
129.290
129.080
128.387
126.928
126.653
124.819
121.438
116.422
114.771
108.115
108.033
99.861
94.847
65.764
65.248
65.121
65.008
38.854
38.344
34.487
31.785
30.568
30.312
30.056
29.800
29.544
29.287
29.031
[Fe(G1(Ph))2](PF6)2 33
ppm
180
160
140
120
100
80
60
40
20
0

[Fe(G2(Ph))2](PF6)2 34
ppm
Integral
9.629
9.059
9.030
8.571
8.564
8.546
7.993
7.969
7.390
7.365
7.246
7.218
7.163
7.148
6.832
6.804
6.456
6.436
6.386
6.119
6.097
4.336
4.166
4.031
3.991
3.517
3.430
3.338
3.229
2.830
2.813
2.733
2.500
2.253
2.232
2.072
1.409
1.294
1.201
0.991
0.849
4.000
4.089
4.046
4.038
4.055
30.451
4.876
16.429
4.131
2.069
18.719
4.108
5.663
57.528
8.181
4.597
28.501
74.346

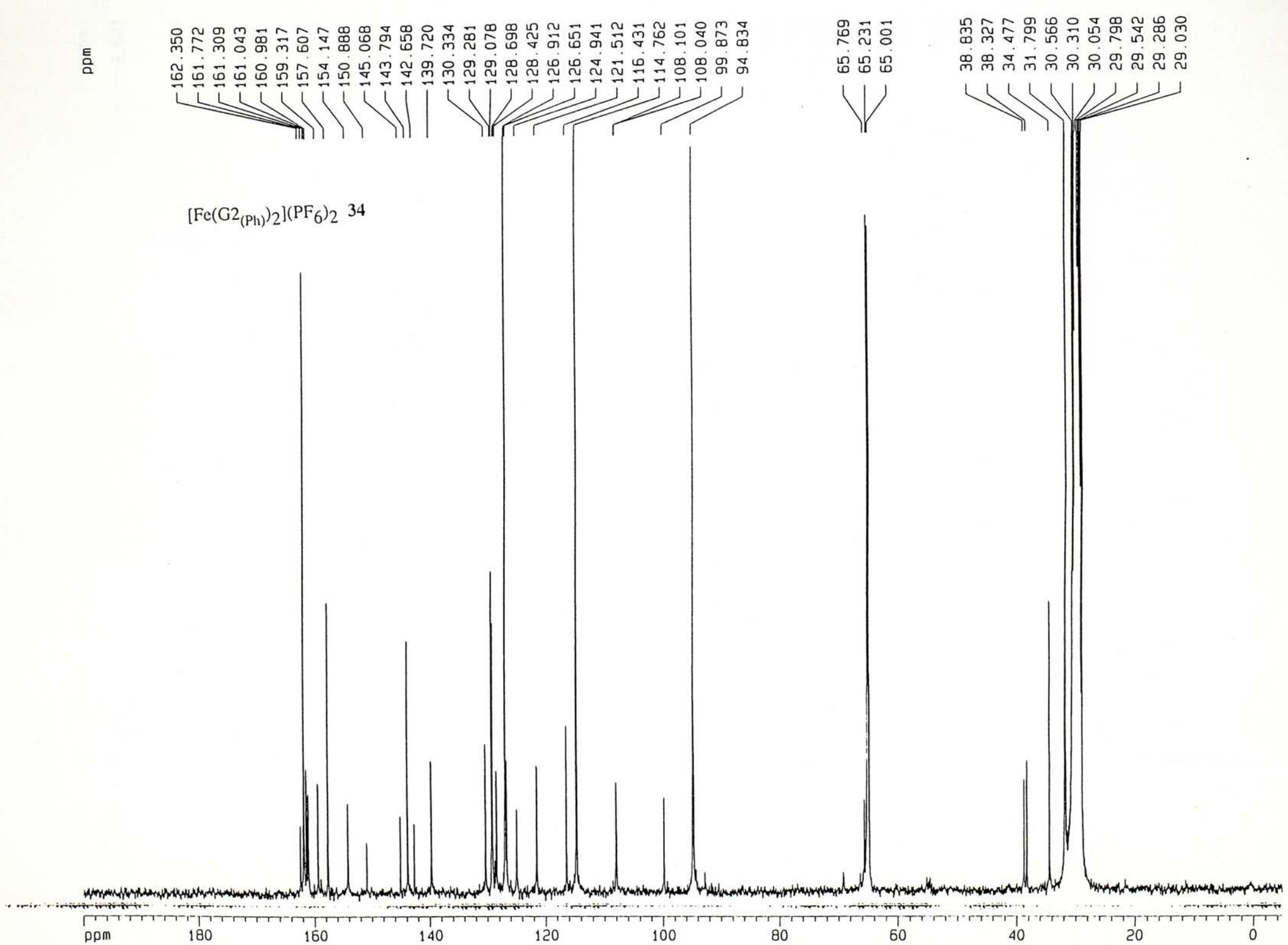
ppm
162.350
161.772
161.309
161.043
160.981
159.317
157.607
154.147
150.888
145.068
143.794
142.658
139.720
130.334
129.281
129.078
128.698
128.425
126.912
126.651
124.941
121.512
116.431
114.762
108.101
108.040
99.873
94.834
65.769
65.231
65.001
38.835
38.327
34.477
31.799
30.566
30.310
30.054
29.798
29.542
29.286
29.030
[Fe(G2(Ph))2](PF6)2 34
ppm
180
160
140
120
100
80
60
40
20
0

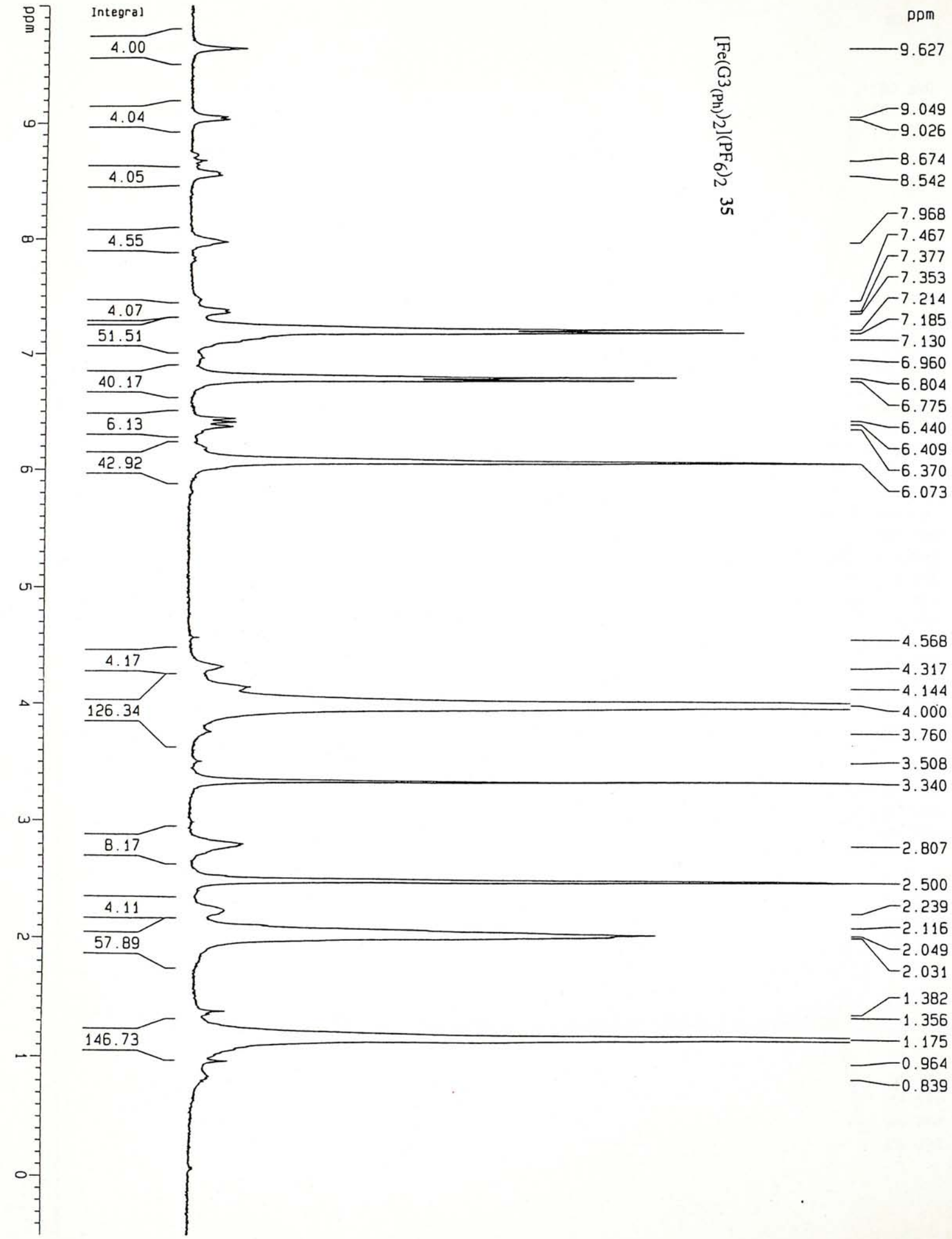
[Fe(G3(Ph))2](PF6)2 35
Integral
4.00
4.04
4.05
4.55
4.07
51.51
40.17
6.13
42.92
4.17
126.34
8.17
4.11
57.89
146.73
ppm
9.627
9.049
9.026
8.674
8.542
7.968
7.467
7.377
7.353
7.214
7.185
7.130
6.960
6.804
6.775
6.440
6.409
6.370
6.073
4.568
4.317
4.144
4.000
3.760
3.508
3.340
2.807
2.500
2.239
2.116
2.049
2.031
1.382
1.356
1.175
0.964
0.839

ppm
[Fe(G3(Ph))2](PF6)2 35
162.309
161.716
161.230
160.942
159.219
157.559
153.963
150.838
150.046
145.035
143.755
142.611
139.614
130.275
129.249
129.063
128.695
128.339
127.254
126.886
126.637
126.486
124.892
121.355
116.367
115.994
115.094
114.736
108.025
99.853
94.801
65.712
65.189
64.973
38.800
38.289
34.463
32.533
31.816
30.566
30.310
30.053
29.797
29.541
29.284
29.028
ppm
0
20
40
60
80
100
120
140
160
180